Republic of Iraq
Ministry of Higher Education and Scientific Research
University of Babylon-
College of Engineering
Civil Engineering Department

Mechanical and Durability Properties of Low Carbon Concrete Containing Ground Granulated Blast Furnace Slag

A Thesis

Submitted to the College of Engineering, University of Babylon in Partial Fulfillment of the Requirements for the Master Degree in Engineering / Civil Engineering / Construction Materials

By

Shahad Sabah Abdullah Jabir

Supervised By

Prof. Dr. Abbas Salim Abbas AL-Ameeri
Prof. Dr. Suhaila Ghazi Mattar

2023 A.D. 1445 A.H.

بسم الله الرحمن الرحيم

{ قَالُواْ سُبْحَٰنَكَ لَا عِلْمَ لَنَآ إِلَّا مَا عَلَّمْتَنَآ ۖ
إِنَّكَ أَنتَ ٱلْعَلِيمُ ٱلْحَكِيمُ }

صدق الله العلي العظيم

سورة البقرة

DEDICATION

This thesis is dedicated to:

My great parents, who leads me through the valley of darkness with light of hope and never stop giving of themselves in countless ways,

My beloved brothers and sisters; the symbol of love and giving,

My dearest husband, who encourage and support me,

My beautiful little daughter

Shahad Sabah Abdullah

SUPERVISOR'S CERTIFICATE

I certify that the preparation of this thesis entitled " ***Mechanical and Durability Properties of Low Carbon Concrete Containing Ground Granulated Blast Furnace Slag*** *"* was done by " Shahad Sabah Abdullah " under my supervision at the department of Civil Engineering, College of Engineering, University of Babylon, as a partial fulfilment of the requirements for the degree of Master of Science in Civil Engineering (Construction Materials).

SUPERVISOR

Signature:

Name: Prof. Dr. Abbas Salim Abbas AL-Ameeri

Date: / / 2023

Signature: *S Mattar*

Name: Prof. Dr. Suhaila Ghazi Mattar

Date: / / 2023

ACKNOWLEDGEMENTS

At first, all thanks to Allah, the most gracious, the most merciful, who gave me the ability and desire to achieve this study.

I would especially like to express my deep appreciation and sincere gratitude to ***Prof. Dr. Abbas Salim Abbas AL-Ameeri and Prof. Dr. Suhaila Ghazi Mattar*** for their supervision, invaluable guidance and assistance throughout the work described in this thesis. They consistently allowed this thesis to be my own work, but steered me in the right direction whenever they thought I needed it. I have the full luck and honour of being under their supervision, for their continuous encouragement and invaluable guidance throughout this thesis.

Great acknowledgement and appreciation to the head and staff of Civil Engineering Department.

I would like also to express my special appreciation to ***staff of construction materials laboratory at the Civil Engineering Department*** for presenting all the facilities to finish this work.

Appreciation is devoted to ***my family***, especially ***my father, my mother and my husband*** for their encouragement and prayers during all my study and to my brothers and my sister for their support.

Finally, special thanks go to ***my Friends***, for their encouragement and unlimited support at all times.

Shahad Sabah Abdul

Abstract

Global warming is a serious issue that threatens the world and future human life, and the construction sector is a major source of carbon emissions, with cement manufacture constituting a significant contribution. Thus, Low Carbon Concrete (LCC) is a solution for reducing the emission of carbon from the whole process of manufacture.

Lowering the building's embodied carbon dioxide equivalent (eCO_2) is a critical response to global and national carbon reduction targets. Globally, the construction industry is developing tools, databases, and methodologies for quantifying eCO_2 in buildings and developing strategies for its reduction. The building sector consumes around 40% of global energy and emits 30% of human greenhouse gas (GHG) emissions.

The compressive strength, splitting, ultrasonic pulse velocity, and drying shrinkage of low carbon concrete mixes, aged (28,56 and 90) days, were examined in this study to evaluate the effect of ground granulate blast furnace slug (GGBS) replacement on physical and mechanical properties of concrete. Water absorption, porosity, chloride penetration depth, chloride transfer, chloride concentration test, and rebar corrosion were also investigated to assess the durability of these types of concrete and to identify the correlation between chloride ion penetration resistance, corrosion resistance, and optimal strength concrete mixtures.

For this study, fifteen mixed patterns were selected and cast into 100-mm cubes, Ø100x200-mm for splitting strength, Ø100x50-mm short cylinder for chloride migration test, and 100×100×400-mm prism moulds, and 10-mm diameter rebar was embedded into the concrete prisms for the accelerated corrosion test.

The findings of these experimental tests reveal that the mixture with strength 35 MPa has the minimum embodied carbon dioxide (eCO_2) /compressive strength when compared to other mixtures. Also, the result showed a decrease in the slump

of the concrete mixes with the increase of the GGBS content, it's about 13%for mixes C(25, 30 and 35)MPa and nearly about 16% for mixes C(40 and 55)MPa when the GGBS percentage is 25%, but when the replacement percentage is 50% the reduction is about 27% for mixes C(25, 30 and 35)MPa and about 44% for mix C(40) and 38% for mix C(55) compared to reference mixes .

In general, increasing the percentage of GGBS led to improvement in the most of the properties except for drying shrinkage, where the drying shrinkage test recorded the highest value for high-strength mixtures with the increase in the percentage of GGBS.

While the durability properties, including water absorption, porosity, chloride transfer, chloride penetration depth, chloride concentration with depth, and corrosion of reinforcing steel, behaved unevenly. The result indicated that resistance of chloride penetration increased with strength and GGBS percentage, it was approximately 50% and 70% when 25% and 50% GGBS was used, repressively. However, this was not the case for all samples, since 35MPa samples with 50% GGBS were shown to have the same resistance to chloride penetration of 55MPa samples with the same GGBS replacement. The corrosion resistance typically rises with the strength and GGBS percentage. This was not the case for all samples, the 35 MPa samples with 25% GGBS were shown to be more impermeable, i.e. to sustain resistance better, than the 55 MPa samples with the same GGBS percentage. This research concluded that achieving good durability is not only by increasing the strength of concrete, but it is possible to obtain high durability by increasing the effectiveness of GGBS with cement by achieving a high structure and resistance to the penetration of hostile elements such as chlorides.

List of Contents

List of Tables

List of Figures

List of Figures

List of Figures

List of Abbreviations and Symbols	
ACI	*American Concrete Institute*
ASR	*alkali-silica reaction*
ASTM	*American Society for Testing and Materials*
BRE	*Building Research Establishment*
BS	*British Standard*
CaO	*calcium oxide*
CH	*calcium hydroxide*
cm	*Centimetre*
Cl^-	*Chloride ion*
Cl/OH	*chloride/hydroxide ratio*
CP	*Cathodic protection*
CSH	*calcium silicate hydrates*
°C	*Celsius temperature*
C/S	*CaO/SiO2*
D_{nssm}	*Diffusion coefficient for non-steady state migration*
EE	*embodied energy*
EC2	*The Euro-code*
eCO_2	*Embodied carbon dioxide*
et al.	*and others*
etc.	*to the end*
f_{cr}	*Ultimate compressive strength*
Fe	*iron atoms*
$FeCl_2$	*Ferrous chloride*
Fe_2O_3	*ferric oxide*
$Fe(OH)_2$	*ferrous hydroxides*
$Fe(OH)_3$	*Ferric hydroxide*
FTIA	*Finnish Transport Infrastructure Agency*
GGBS	*Ground granulate blast furnace slug*
GHG	*Greenhouse gases*
GJ	*gigajoules*
HCl	*hydrochloric acid*
hrs.	*hours*
HRWR	*High Range Water Reducing*
i.e.	*in other word*
IOSR	*International Organization of Scientific Research*

List of Abbreviations and Symbols	
IQS	*The Iraqi standards*
ITZ	*interfacial transition zone*
K	*Thermal Conductivity*
Kg	*kilogram*
kN	*Kilo Newton*
Kpa	*Kilo pare*
L	*Litter*
LCC	*Low carbon concrete*
m	*Meter*
µm	*Micro meter*
max.	*Maximum*
MgSO4	*magnesium sulfate*
mm	*Millimeter*
MPa	*Mega Pascal (MN/m2)*
Mt	*megatons*
NaCl	*sodium chloride*
No.	*Number*
oCO_2	*Operation carbon dioxide*
OH^-	*hydroxyl ions*
p	*Fracture load*
PFA	*pulverized fuel ash*
OPC	*Ordinary Portland cement*
r	*Disc radius*
RCS	*Reinforced concrete structures*
s	*second*
SCMs	*Supplementary Cementitious Materials*
SiO2	*silicon dioxide*
SP	*Super plasticizer*
SRPC	*Sulfate Resisting Portland Cement*
SSD	*Saturated Surface Dry*
TCS	*Third Cement Series*
UPV	*Ultra sonic pulse velocity*
V	*Voltage*
w/cm	*Water-Cementitious material ratio*

CHAPTER ONE

INTRODUCTION

CHAPTER ONE

Introduction

1.1 General

Concrete is the most widely used construction material in the world, with around six billion tons manufactured each year (**Kumar Karri et al., 2015)**.

Except water, concrete is the most consumed materials in the world. Because of its widespread usage, even little reductions in greenhouse gas emissions per ton of made concrete can have a major global impact. Due to the increased environmental consciousness among building material consumers, reliable estimations of greenhouse gas (GHG) emission footprints of various construction materials are becoming increasingly relevant. When selecting a material for a specific structure, a life cycle evaluation of competing construction materials (e.g., steel and concrete) can be performed **(Jönsson et al., 1998)**.

Concrete's fundamental elements are cement, water, coarse aggregates, and fine aggregates. The extraction of aggregates has significant consequences for land use **(Schuurmans et al., 2005)**. Yet, Portland cement is the largest source of greenhouse gas emissions in the concrete manufacturing process. According to reports, the cement sector accounts for 5% of worldwide anthropogenic CO_2 emissions **(Mahasenan & Humphreys, 2002)**. As a result, the emissions due to Portland cement have often considered the main focus when researchers assess the greenhouse gas emissions of concrete. The increase in these emissions one of them, CO_2 due to cement production and other construction materials, has considerable impact on the climate system in terms of the increase of temperature and reduction of relative humidity in Earth's atmosphere **(IPCC, 2014)**.

1.2 Problem Definition

Cement, unlike the other elements, is not found in nature and should be obtained through a manufacturing process. In 2018, cement production was approached to 4.1 billion metric tonnes, China production was 57.8% of the total amount **(Chang & Goldfarb, 2019; U.S. et al., 2019)**. Global demand from developing countries is expected to grow up to 4.83 billion metric tonnes by 2030 **(Statista, 2018;Chen et al., 2022)**. As a result, the concrete is considered to be the most used material in the world after water.

Several nations currently have legislation in place that establishes objectives for reducing carbon emissions. This is owing to the high energy intensity of the processes involved in the manufacture of Portland cement (PC), as 900 kilograms of embodied carbon dioxide (eCO_2) is released for every 1000 kg of cement produced **(Zhou et al., 2012)**.

OPC is one of the most common binders that used in concrete production, and current manufacture methods involve using high levels of clinker, a kilned and quenched materials that require high energy input during production, resulting in GHG emissions, as well as material derived CO_2 emissions through processes due to the chemical reaction that converts limestone to lime and clay disintegration to silica and alumina **(Neville, 2011)**. One significant advantage of growing usage of alternative types of cementitious materials is to reduce GHG emissions **(Miller et al., 2018)**.

Corrosion of steel reinforcement is one of the major causes affecting the long-term performance of reinforced-concrete structures **(El Maaddawy & Soudki, 2003)**. In general, chloride-induced corrosion of reinforcing steel in concrete is separated into two stages: initiation and propagation. Corrosion initiation refers to the depassivation of reinforcing steel caused by the presence of chloride ions or carbonation of concrete **(Tuutti, 1982)**. The combined

diffusion processes of chloride and moisture through porous concrete cover are primarily responsible for corrosion **(Cheung et al., 2009)**, while the corrosion propagation stage may entail far more sophisticated operations such as electrochemical response and rust expansion triggered concrete cover cracking, spalling, and delamination **(Martın-Pérez, 1999)**.

Chloride ingress into concrete maybe occur only if the concrete pores are completely or partially filled with water. Permeation, capillary suction, and diffusion are the ways to contribute penetration via capillary pores or fissures **(Hilsdorf & Kropp, 1995; Basheer et al.,2001)**. The concrete cover, which is the layer of concrete that separates the steel rebar's from the external environment, is a critical in resisting chloride ingress for a certain period of time (so-called service lifetime), after which the critical chloride concentration is reached at the rebar level, triggering corrosion of the steel.

Steel corrosion in concrete is an electrochemical process that involves anodic iron dissolution and, in general, cathodic oxygen reduction **(Hausmann, 1967; Stratmann & Müller, 1994).** The water/proton ratio can also be reduced depending on the availability of oxygen and the pH near the steel surface **(Hansson, 1984)**. Finally, for electron transmission, an electrical connection between the anode and the cathode is required, as is an electrolytic environment for ion transfer in solution as shown in **Figure (1.1).**

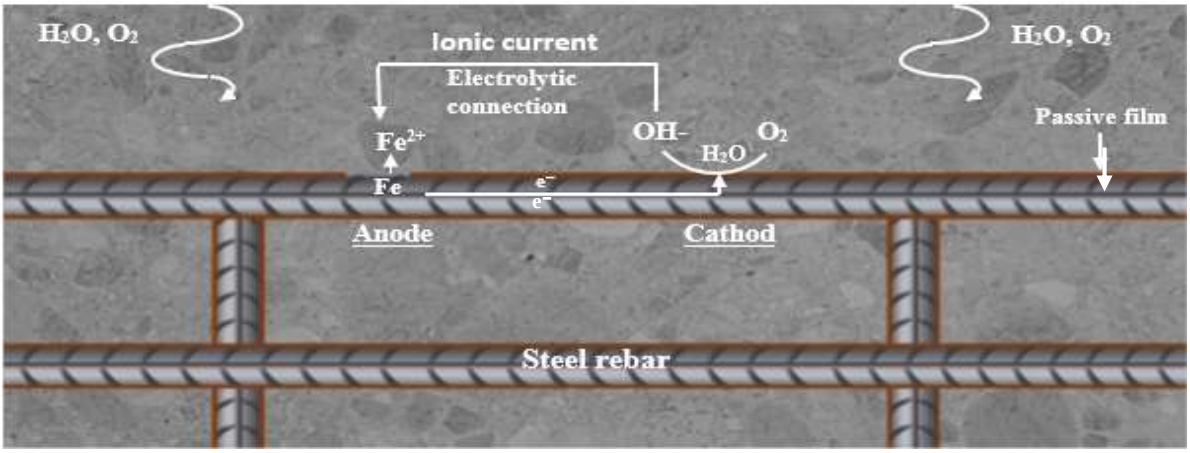

Figure (1.1): - Schematic representation of the steel corrosion in concrete (Rodrigues et al., 2021).

Due to corrosion in steel rebar, there is volumetric expansion of corrosion products may reach to 6 times of original volume of steel rebar. This increase in volume of embedded rebar gradually exerts internal pressure on the surrounding concrete as reinforcement corrosion commences and propagates, causing longitudinal cracking and even breaking of the concrete cover **(Zou et al., 2014)**. After that, and because aggressive agents have better access, reinforcement corrosion may be hastened, resulting in premature failure and a reduced service life of RC structures **(Zhang et al., 2017)**.

1.3 Significance of the Research

There are several strategies to minimize eCO_2 related with concrete manufacture, such as using more efficient equipment, alternative fuels, and carbon capture and storage **(WBCSD, 2009; Habert *et al.*, 2010)** , one of the most prevalent means to reduce emissions is to reduce the demand for Ordinary Portland Cement (OPC).

For decades, the construction industry has been seeking for alternative binding materials/mineral admixtures to completely or partially replace OPC in order to lessen its negative environmental impact. Mineral admixtures or supplementary cementitious materials (SCMs) such as pulverized fuel ash (PFA)

and ground granulated blast furnace slag (GGBS) are increasingly being used in concrete because they can improve concrete durability and quality while also lower the negative environmental impact of PC in terms of carbon emissions and energy consumption **(Lothenbach et al., 2011)**.

Global eCO_2 emissions would be lowered if cement were replaced with alternative recyclable materials. A 50% substitution of cement for alternative cementitious materials would reduce CO_2 emissions by more than 1 billion tonnes. This is comparable to deleting around one-quarter of the world's autos **(Malhotra, 2004)**.

On the other hand, to minimize the quick deterioration of concrete under harsh climatic conditions, high-quality and long-lasting concrete is necessary. Alternative cementing materials' favorable impacts should be evaluated in this context. Natural cementitious materials or recyclable materials, such as GGBS, have recently received considerable attention as a possible partial replacement by cement. SCMs, such as GGBS, are employed in concrete, not only is the porosity reduced, but the pores become finer, and the change in mineralogy of the cement hydrates results in a reduction in chloride ion mobility **(Li & Roy, 1986)**.

Global production of ground granulated blast-furnace slag is expected to reach 280 million tonnes in 2025, with China's production to total around will be 153 million tonnes **(Fan et al., 2018; Sanjuán et al., 2022)**. China was the largest slag user in 2020, but its share is predicted to fall from 62% to 55% by 2025 due to reduction of steel output in this country **(Huang et al., 2018)**.

The initial protection provided by SCMs-containing concretes against chloride penetration varies depending on the material, curing time, and age of the concrete when exposed to the chloride environment. PFA and GGBS, for example, require appropriate quantities of calcium hydroxide to be released as a result of Portland cement hydration **(Mehta, 1983)**. In comparison to OPC

concrete, SCMs-containing concretes had a very limited chloride penetration beyond **(Basheer et al., 2002)**.

The behavior of concrete buildings in the maritime environment has revealed that reinforcement corrosion caused by chloride attack is the primary source of discomfort. It is a global issue with major economic implications, and it is currently one of the primary study areas in concrete buildings. Despite substantial effort and development in understanding the factors impacting chloride penetration and the corrosion process over the previous two decades, quantitative modeling of these mechanisms has only just begun **(Costa & Appleton, 1999)**.

In the conventional diffusion method **(Dhir & Byars, 1993; Li et al., 1999)**, in obtaining the steady-state chloride flow over the material, it takes a long time for chloride ions to permeate the concrete. Tests for chloride transfer have been developed. By accelerating the rate of chloride entrance with the applied electric field, the chloride diffusion coefficient in the test period is substantially shorter than in natural diffusion experiments. In the chloride transfer procedure, the Nordtest technique may characterize concrete during electrically induced migration in transitory settings **(NT Build 492, 1999)**.

Reinforced concrete structures may be built to survive for more than a century. Corrosion may occur gradually over the life of a structure and might take years to reveal harm. According to **(Penttala, 2009)**, following the commencement of reinforcement corrosion, the surface might degrade for up to 10 years. As a result, numerous methods have been developed to accelerate the corrosion process. In this study, the impressed current approach will be used as an accelerated corrosion test to exam the effect of concrete properties on the corrosion resistance of steel bar.

Purnell and Black revealed that altering independent mix design elements can reduce embodied carbon dioxide even more. It was determined that using crushed aggregates, a lowered w/b ratio, and a superplasticizer in place of CEM 1 results in a lower CO_2/MPa at the stipulated mean strength range of 50-70 MPa. The results show that mix design may be adjusted to produce less carbon for a given mean strength objective **(Purnell & Black, 2012)**.

1.4 Aims and Objectives

The aims and objectives of the research are based on experimental program and theoretical calculation to find the durable mixture with lower embodied carbon dioxide by using different percentage of GGBS in concrete mixture. Therefore, objectives of study can be achieved by:

- Computing the eCO_2 of various design mixtures, including the usage of 25% and 50% GGBS.
- Investigating the effect of GGBS replacement percentage in concrete mixture with different grade of strength on chloride penetration to find the optimum mixture that achieve least level of carbon dioxide emissions.
- The impacts of chlorides on corrosion in the concrete structure by simulating the marine environment using high concentration of chloride and an accelerated electrochemical corrosion experiment.
- Selecting the best concrete mixture results in the lowest CO_2 emissions while also providing the best durability.

1.5 Layout of the Thesis

This study is based on five chapters as follows:

Chapter 1: A comprehensive summary and background on properties of concrete mixture with SCMs replacement in terms of embodied carbon dioxide in these mixtures, as well as chloride attack to concrete structure are reviewed in

this chapter. Furthermore, the research's aims and objectives are stated. The aim of the introductory chapter is to plan the scope of the current research and to offer a brief explanation of this thesis.

Chapter 2: The theoretical basis of the embodied CO_2 of materials employed in concrete mixture are reviewed. As well as the experimental and theoretical findings of the concrete using SCMs are presented.

Chapter 3: The experimental program is devoted. all investigational works are designated in detail in this chapter, including information of the materials used, the mechanical properties of SCMs concrete as well as the examinations that tested to investigate the properties concrete with SCMs such as physical, mechanical and durability.

Chapter 4: The results and analysis of concrete with and without GGBS are investigated for different examinations, which also recognized and examined the best case of replacement of GGBS percentage to find the least chloride penetration depth in this chapter.

Chapter 5: Based on the present research, the results and recommendations for further work were recorded to be guide line to researchers in future.

CHAPTER TWO

LITERARURE REVIEW

CHAPTER TWO

Literature Review

2.1 Introduction

This chapter aims to explore various aspects related to the ingredients of concrete, their sustainability, and the analysis of their environmental impact through embodied carbon dioxide (eCO_2). The review delves into the raw materials, supplementary cementitious materials (SCMs), chemical admixtures, and their significance in concrete production. Additionally, it examines the concept of eCO_2 and its utilization as a measure for assessing the environmental influence of concrete. Furthermore, the review investigates different mix design approaches and highlights the differences between them. Finally, it elucidates the motivations behind conducting this study.

2.2 Concrete Constituents

2.2.1 Cement

Cement is an important component of concrete and it is used to bind components such as fine and coarse aggregate. Cement is responsible for the majority of the embodied carbon dioxide (eCO_2) and embodied energy (EE) produced by concrete, including 7 megatons (Mt) of CO_2 in 2010 **(Griffin et al., 2014)**, as 0.93 kilograms of CO_2 is produced per kilogram of cement clinker **(Shanks et al., 2019)**, while 3.1 gigajoules (GJ) of energy is consumed per tonne of cement clinker **(Habert, 2013)**. As a result, a mixture with a greater cement content is likely to have a higher eCO_2 than a mixture with a lower cement content, but increased cement content also leads to improved concrete strength and a bigger EE since a higher cement content requires more energy. The main

factor causing cement to have a significant eCO_2 is the use of high temperature to produce it, usually around 1450 °C required to burn fossil fuels in order to heat the kiln calcining the limestone, clay, and shale (see **Figure 2.1**).That results in roughly 50% of the CO_2, with the remaining 44% of CO_2 emissions from the production of cement clinker from calcining limestone **(Shanks et al., 2019)** as shown in **Equation (2-1)**.

$$CaCO_3 \rightarrow CaO + CO_2 \uparrow \qquad \textbf{(2-1)}$$

Molecular weight $\quad 100 \quad \rightarrow \quad 56 + \ 44$

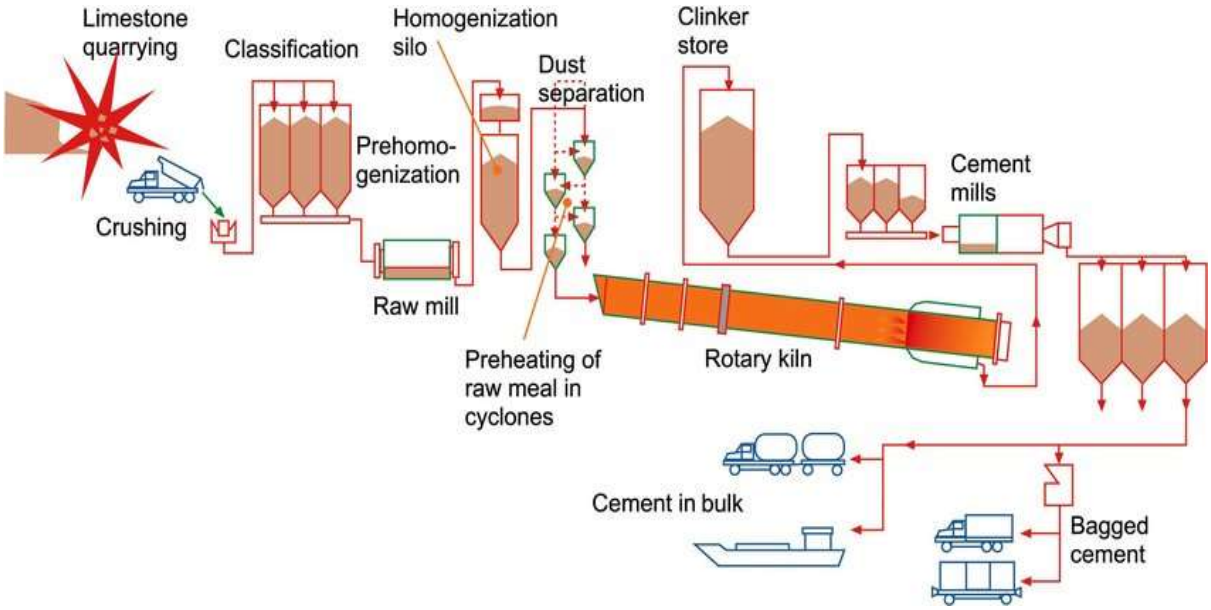

Figure (2.1): - Manufacture of cement clinker in rotary kiln (Zevenhoven et al., 2002)

2.2.2 Aggregate

Aggregate in concrete refers to both coarse aggregate, which is commonly gravel, and fine aggregate, which is usually sand, and accounts for 70–85% of the mass of concrete and 13–20% of CO_2 emissions from concrete **(Aginam, Chidolue & Nwakire, 2013)**. While **Flower and Sanjayan (2007)** claimed that fine aggregate generates 30–40% of the CO_2 created per tonne of coarse aggregate, coarse material frequently requires crushing for use in concrete.

The aggregate type, size, and source are thought to have an effect on the strength, durability, and workability of concrete. There is substantial debate about whether crushed or uncrushed aggregate produces the best concrete qualities. Uncrushed aggregate, according to Hachani, improved workability due to the rounded shape of the particles, resulting in a lower water content for the same cement quantity and thus increased concrete strength **(Hachani et al. 2017)**. Teychenne proposed that despite the angular structure of the particles and the lower workability of crushed aggregate, it resulted in stronger concrete due to improved particle interlocking **(Teychenne et al., 1997)**. The aggregate type and source had an influence on concrete durability **(Dhir et al., 2003)**. The increase of the aggregate size from 9.5mm to 19.0mm greatly boosts the mean compressive strength of the concrete cubes while simultaneously enhancing workability **(Vilane & Sabelo, 2016).** The fine aggregate and coarse aggregate composition of a concrete mixture influence its strength, durability, and workability. The fix of water/cement (w/c) ratio and increase both coarse and fine aggregate content reduced concrete workability , however it had no effect on compressive strength, whether the aggregate proportion was more than 0.6 or less than 0.4**(Okonkwo & Arinze Emmanuel, 2018)**.

2.2.3 Water

Water is a key ingredient of concrete and it accounts about 7-10% of its mass **(Hewlett, 1999)**. It is responsible for the workability of concrete as well as the hydration of cement, both of which are required to provide adequate strength and durability **(Long et al., 2009)**. The water/cement ratio is directly connected with concrete workability, and that a greater w/c ratio leads to enhanced concrete workability **(Bhattarai et al., 2019)**. The w/c ratio is the ratio of water content to cement content (or cementitious material content in the case of different cementitious materials such as supplementary cementitious materials, SCMs) and

it is important for the qualities of hardened concrete; a lower w/c ratio is thought to produce higher strength and durability, as shown in **Figure (2.2)**.

Water utilization contributed the least CO_2 emissions per cubic meter of concrete. Previous similar studies looked at excluded these components, which generate less than one-half of a percent of CO_2 emissions per cubic meter. The analysis of emissions linked with water usage found that they may be considered inconsequential**(Sanal et al., 2016)**.

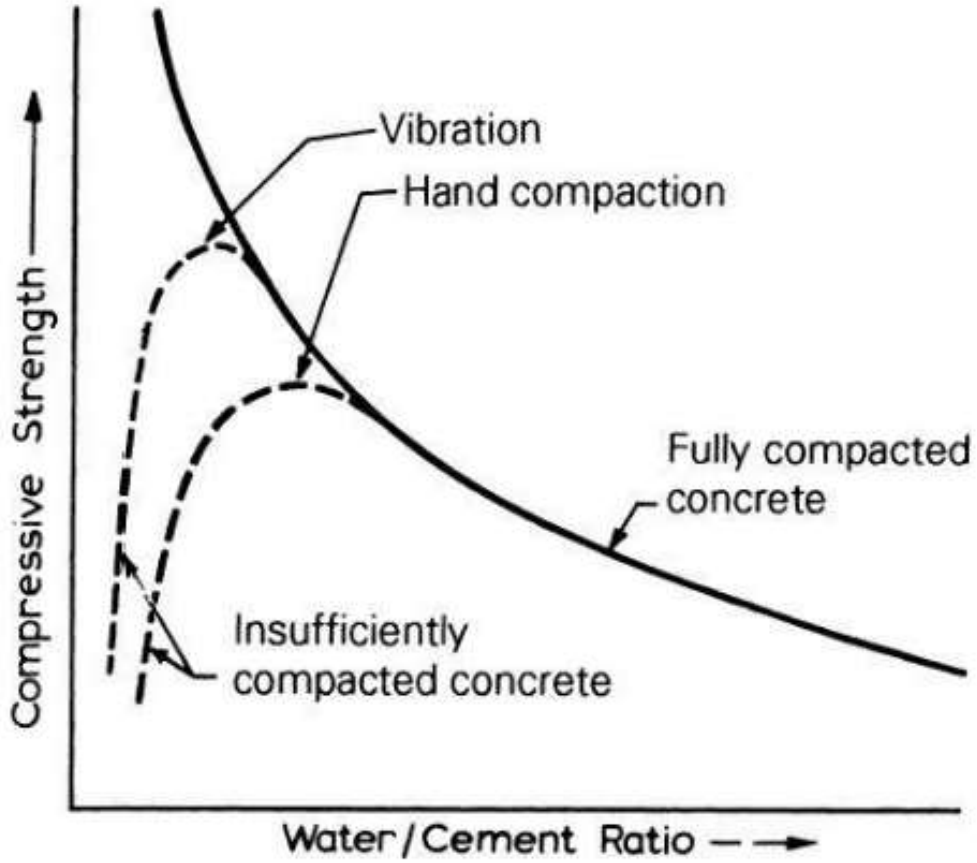

Figure (2.2): - Relationship between water to cement ratio and compressive strength (Neville, 2011)

2.2.4 Supplementary Cementitious Materials (SCMs)

Supplementary cementitious material (SCMs) are pozzolanic materials can be used alone, with OPC, or in combinations. SCMs, when combined with OPC and water, may improve the characteristics of concrete due to pozzolanic or hydraulic activity, or both. Pozzolanic materials require calcium hydroxide (CH), which is provided by the hydrating cement, whereas hydraulic materials harden with water. Ground-granulated blast furnace slag (GGBS), pulverized fuel ash (PFA), natural pozzolans (calcined clay and metakaolin), and silica fume are all common supplementary cementitious materials utilised in the concrete industry. Using SCMs often reduces the impact of the cement industry on the environment.

2.2.4.1 Pulverized Fuel Ash (PFA)

Pulverized fuel ash (PFA) is indeed a type of fly ash generated as a byproduct of coal combustion in power plants. With a global production of approximately 700-1000 Mt per year, PFA has been extensively researched for its potential as a cement clinker replacement and its impact on the embodied carbon dioxide (eCO_2) emissions of concrete **(Zhang et al., 2019)**. Research studies have shown promising results regarding the use of fly ash, including PFA, as a partial replacement for cement in concrete mixtures. For example, Sear (2001) found that a 30% fly ash replacement for cement resulted in a 17% reduction in CO2 emissions compared to Ordinary Portland Cement (OPC), while maintaining the same 28-day compressive strength **(Sear, 2001). Purnell and Black (2012)** reported even greater reductions, with the use of 40% fly ash resulting in a decrease of up to 35% in eCO_2 emissions.

To promote the utilization of fly ash, the American Concrete Institute **(ACI) Committee 211 (2002)** recommends incorporating 15-25% Class F fly ash and 15-35% Class C fly ash as substitutes for cement. This approach helps minimize carbon emissions and energy consumption while preserving the strength,

durability, and workability of concrete. However, despite the positive environmental benefits and performance advantages, the future use of fly ash in concrete faces uncertainty due to the closure of coal-fired power plants. In the United States, for instance, approximately 40% of power plants are projected to shut down. Similarly, the United Kingdom plans to close all coal-fired power stations by 2025 **(McCarthy et al., 2017)**. These developments indicate that the availability of fly ash, including PFA, is likely to be severely restricted in the coming years.

Given this situation, alternative supplementary cementitious materials, such as ground-granulated blast furnace slag (GGBS), can be employed as a replacement for CEM-1 binder to lower the eCO_2 of concrete.

2.2.4.2 Ground Granulate Blast Furnace Slag(GGBS)

Ground-granulated Blast Furnace Slag (GGBS) is indeed a byproduct of iron-making blast furnaces, which operate at temperatures around 1500-1600 degrees Celsius. The process involves a precisely regulated blend of iron ore, coke, and limestone. During iron production, the iron ore is converted into iron, and the slag, which consists of approximately 30% to 40% silicon dioxide (SiO_2) and 40% calcium oxide (CaO), floats on top of the molten iron **(Mukherjee et al., 2016).** To produce GGBS, the molten slag is tapped off from the blast furnace as a liquid and rapidly quenched with a large volume of water. This quenching process improves the cementitious characteristics of the slag and transforms it into granules that resemble coarse sand. These granules are then dried and pulverized into a fine powder **(Mukherjee et al., 2016)**. The chemical composition of GGBS is similar to that of Portland cement, making it a suitable replacement for cement in concrete production. Utilizing GGBS in concrete not only reduces waste by using a byproduct of the iron-making process but also contributes to a greener environment. The use of GGBS as a partial replacement

for cement can enhance the long-term strength and durability of concrete and lower the CO_2 emissions by 288 kg per tonne of cement **(Park & Kim, 2010)**.

Blast-furnace slag undergoes a hydration process that produces hydration products comparable to cement but through a different mechanism. The initial step in the hydration process of granulated blast-furnace slag involves the collapse and disintegration of the glass structure due to hydroxyl ions (OH^-) formed from liberated portlandite ($Ca(OH)_2$) during cement hydration. Concrete containing 30-50% blast-furnace slag, adequately cured, can strengthen the internal structure of the concrete by making it denser. This, in turn, can increase durability by reducing permeability **(Olivier & Bakker, 2001)**. With its hydraulic properties, blast-furnace slag hydrates similarly to cement and serves as an environmentally suitable alternative material by reusing an industrial byproduct and reducing CO_2 emissions.

Both GGBS and ordinary Portland cement (OPC) can generate calcium silicate hydrates (CSH) through hydration. Although, GGBS particles react pozzolanically with available calcium hydroxide (CH), forming calcium silicate and calcium aluminate hydrates. As a result, the pH of concrete with GGBS (CEM III) is often lower than that of OPC (CEM I). The removal of excess CH refines the pore structure, making it denser and enhancing impermeability.

When GGBS is used at high replacement rates, the resulting concrete has a lighter, brighter off-white color. Different replacement rates can lead to specific characteristic alterations. The International Organization of Scientific Research (IOSR)-Journal of Mechanical and Civil Engineering provides some suggested optimal proportions and their anticipated benefits **(Journals et al., 2015) :**

- 30-45% GGBS: Avoid excessive retardation when used in cold weather.

- 50-70% GGBS: Manage early-age cracking and decrease hydration heat.
- 66-80% GGBS: Enhance resistance to sulfate and chloride penetration.
- 80-95% GGBS: Reduced initial strength gain.

C-S-H formed from the hydration of OPC and GGBS, but GGBS particles additionally react with available CH via a pozzolanic reaction, resulting in the formation of calcium silicate and calcium aluminate hydrates **Figure (2.3)**.

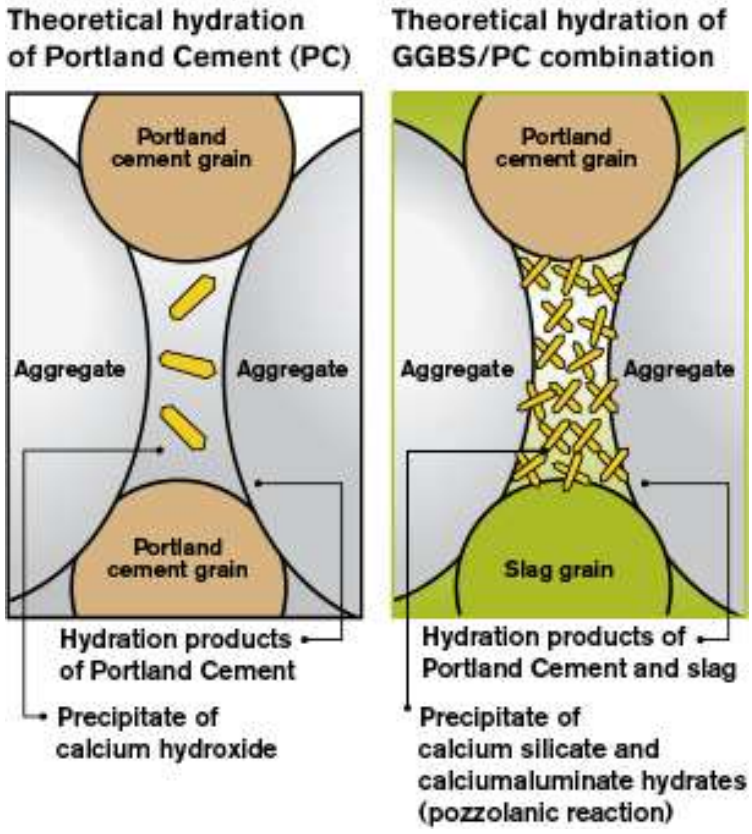

Figure (2.3): - The hydration of OPC and GGBS (Journals et al., 2015)

2.2.5 Chemical Admixtures

Chemical admixtures have five recognized functions: accelerators, retarders, water reduction, air entraining, and plasticizers. Accelerator admixtures quicken the pace of early strength development and they can be used to speed up curing in cold conditions. Retarders are primarily used to delay the rate of concrete setting, which is typical in hot weather. Admixtures that lower water content by 5-10% increase slump without raising the w/c ratio, making concrete more workable. To increase cohesion, compaction, and freeze-thaw resistance, air-entraining admixtures are applied. Plasticizers, also known as superplasticizers, are high-range water reducers that lower water content by 12 to 30%, resulting in highly workable concrete with low w/c ratios.

Corrosion inhibitors are admixtures intended to lower the possibility of reinforcement corrosion. The study conducted by **Luo & De Schutter (2004)** investigated four types of corrosion inhibitors: calcium nitrite-based (amino and ester-based), amino alcohol-based, and migrating corrosion inhibitors **(Luo & De Schutter 2004)**. The calcium nitrite-based inhibitors work by restoring the passive layer on the reinforcement surface. Nitrate ions in the calcium nitrite react with faulty ferrous oxide, helping to rebuild the protective layer. The amino and ester-based inhibitors strengthen the pore structure of the concrete, delaying the entrance of corrosive agents. They are also adsorbed into the reinforcements, creating an additional layer of defense. Amino alcohol inhibitors form a protective coating on the metal surface, providing protection to both the anodic (oxidation) and cathodic (reduction) portions of the corrosion process. Migrating corrosion inhibitors also create a protective coating on the metal surface, shielding both the anodic and cathodic zones from corrosion.

The inclusion of these corrosion inhibitors may have an impact on the compressive strength of the concrete at different stages of curing, potentially

improving or reducing it. However, it is important to note that the effects of these inhibitors on compressive strength may vary **(Luo & De Schutter, 2004)**.

Since additive manufacturers were unable to supply relevant emissions, internal literature sources were consulted for these specific emissions. The principal sources of emissions from additive are gasoline and electricity. Plasticizers are often added at concentrations ranging from 0.25 to 0.8% by weight of cement, therefore the addition has little influence because it is utilized in such small quantities per cubic meter of concrete. Because additives are utilized in such tiny quantities per cubic meter of concrete, the additive manufacturing emission factor was customized for different types of additives from a previous study concrete. The emission factor for admixture manufacture for various admixtures is derived from a prior study **(Flower & Sanjayan, 2007)**.

2.3 Compression and Tension in Concrete

concrete typically exhibits much higher compressive strength compared to tensile strength, with the compressive strength typically being around 10 times greater than the tensile strength **(Nemati, 2015)**. Previous studies have shown a correlation between compressive and tensile strengths, with a coefficient ranging from 0.07 for high strength to 0.11for normal strength. This suggests that as the compressive strengths increases, also the tensile strength tends to increase **(Nemati, 2015)**. Under tension, concrete tends to fracture in a brittle manner, which is why it performs poorly in tension compared to compression. In normal-strength concrete with compressive strengths lower than 60 MPa, the interfacial transition zone (ITZ) becomes the weakest phase under compression. The ITZ is a region, typically 20-50 μm thick, characterized by a higher water-to-cement ratio and porosity between the cement paste and aggregate **(Iacovidou et al., 2017**).

Under high stress, microcracks initiate and expand from the ITZ, resulting in irreversible strain. Eventually, these cracks propagate and join around aggregates, leading to visible and predictable failure. However, in high-strength concrete with compressive strengths higher than 60 MPa, the low water-to-cement ratio reduces the effectiveness of the ITZ. In such cases, cracks tend to migrate through the aggregates, and failure can be more abrupt and brittle. **Figure (2.4)** illustrates a comparison between standard concrete and high-strength concrete, highlighting the differences in their performance and failure mechanisms.

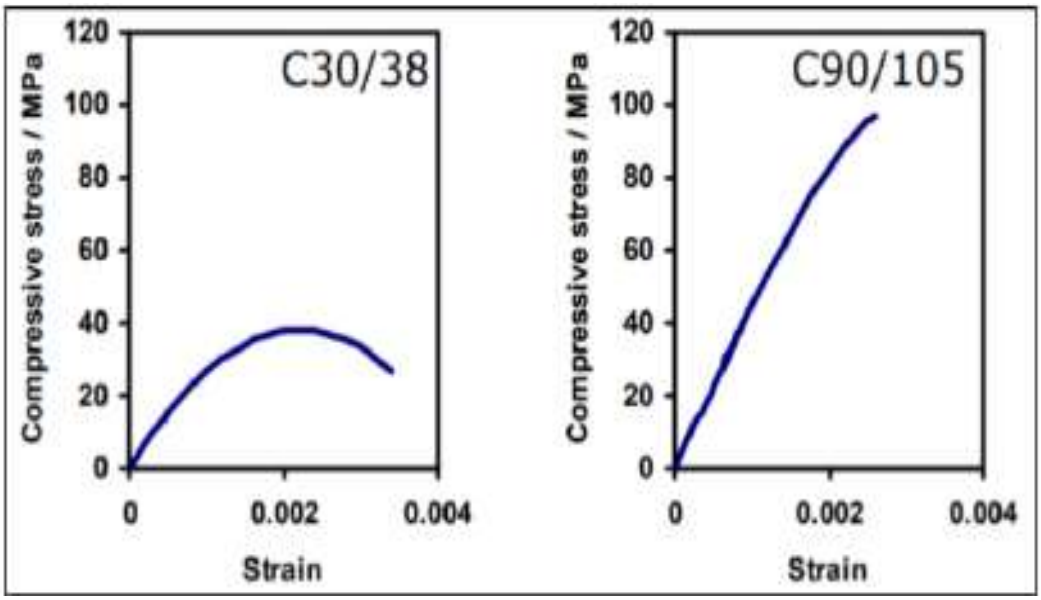

Figure (2.4): - Idealized strain/stress relationship to the Ec2 (Iacovidou et al., 2017)

Reinforcement became important in modern construction due to the brittle nature of concrete and its low tensile strength. Steel reinforcements can improve tensile strength and compressive strength. Multiple reinforcements can be found in structural components, each serving a specific purpose. Main reinforcement bars range in thickness from 6 to 40 mm and are used to resist bending. Additional reinforcements are used to withstand shear in high-load regions, secure

connections, and provide a strong bond with concrete. There are two techniques to offer primary steel reinforcements:

Reinforced Concrete (RC): Before pouring concrete, rebar cages or mesh are inserted in formwork and actively imbedded in the concrete. Applied stresses efficiently transfer between the two materials after hardening under adequate compaction and curing. Experimental samples for this research will be based on this method.

Prestressed concrete is a technique used to develop the performance and load-bearing capacity of concretes structures by introducing compressive stresses into the concrete before it is subjected to any external loads. This is achieved through pre-tensioning or post-tensioning methods. In pre-tensioning, the process involves tensioning (stretching) strands or tendons, which are typically made of high-strength steel, before the concrete is poured. The strands or tendons are anchored at one end, and their other ends are pulled and held in tension using hydraulic jacks. Once the strands or tendons are tensioned to the desired level, the concrete is cast around them. As the concrete cures and gains strength, the steel strands or tendons remain in tension. After the concrete reaches the required strength, the strands or tendons are released from the anchorages, and the excess length is cut off. This transfer of stress from the steel to the concrete creates compression within the concrete, resulting in a precompressed structure.

2.4 Low Carbon Concrete

Concrete is the most popular building material, and each individual consumes around 1 tonne of concrete every year **(Flower & Sanjayan, 2017)**. Because of the massive use of concrete, even little reductions in the quantity of greenhouse gases produced by each ton of manufactured concrete can have a significant global impact. Accurate assessments of the CO_2 emissions of various building materials are becoming increasingly important as customers' environmental consciousness grows.

2.4.1 Embodied Carbon

Building impacts on the environment are frequently classified as embedded and operational **(Ibn-Mohammed et al., 2013)**. Since operational Carbon Dioxide (oCO_2) is the term used to describe emissions linked to the energy required for it services, maintenance, heating, lighting, and air conditioning, among other things, while embodied carbon eCo_2 is all the carbon generated from the full manufacturing process of a material including transportation to the site. However, a sizeable amount of the overall lifecycle emissions comes from (eCO_2) emissions, which are those connected with the building and the lifecycle disposal phases **(Sturgis & Roberts, 2010)**.

Since operational impacts have typically been regarded as more important than embodied effects, regulation has focused on the latter **(Szalay, 2007)**. Because the standards' release, there has been a sharp increase in embodied effects research and industry concern **(Zhang et al., 2020)**. However, due to the complexity of the data, changes in the data, and persistent irregularities in the bounds of space and time, they remain ambiguous **(Moncaster et al., 2018)**.

The required energy to complete the majority of the tasks involved in producing and placing concrete results in CO_2 emissions. Therefore, the consumption of energy for each unit of produced material requires to be audited

in order to estimate the CO_2 emissions related to an activity. Examples of the carbon footprint of concrete and concrete structures are shown in **Figure (2.5)**, accounting all life cycle stages' embodied energy.

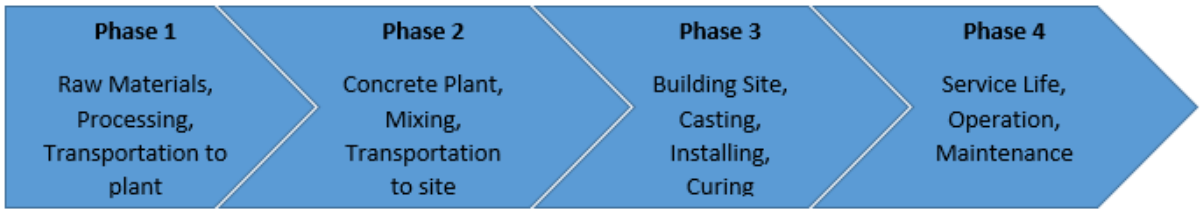

Figure (2.5): - Life cycle stages' embodied energy of concrete structure (Sanal et al., 2016)

Literatures regarding to cement, concrete, and products of concrete have identified many stages of their life cycle that have a significant environmental impacts **(Vold & Ronning, 1995; Nisbet & Van Geem, 1997;Jönsson et al., 1998; Koroneos & Dompros, 2009)**. Although the quality of the final product is generally the same across all cement plants, the production methods, differing performance, and investments in the systems of air pollution control result in a variety of environmental effects. Several estimations of the eCO_2 emissions for each tonne of cement production have been previously developed by earlier studies into the environmental effects of cement manufacture. Fly ash and GGBS, like cement, have been investigated and their emissions were measured. The by-product steel industry is ground granulated blast furnace slag (GGBS), and a coal combustion byproduct (fly ash) are two other cementitious components under consideration. In most cases, these two components are employed to replace partially with cement in a concretes mixture. Because the water and admixtures used in concrete produce insignificant eCO_2 emissions, cement, coarse and fine aggregates, GGBS, and fly ash are the principal material contributors to the environmental concrete repercussions **(Davidovits, 1993; Thormark, 2002; Gartner, 2004; Goggins et al., 2010)** .

One of the most difficult issues in measuring embodied effects from buildings is selected a coefficient of carbon for materials early in the design process. Concrete has nearly endless possible variations, depending on the kind and amounts of cement and aggregates, the admixtures and plasticizers addition, and the unique manufacturer's plants, procedures, and fuels **(Moncaster et al., 2018)**.

2.4.2 Low eCO_2 Concrete Design

A significant amount of the research seeks to lower the eCO_2 of concrete without changing existing design methodologies **(Gartner, 2004; Duxson et al., 2007; Goggins et al., 2010; Cabeza et al., 2013)**. This is accomplished by reducing the amount of cement required by employing cement substitute materials. Concrete additives such as plasticizer, superplasticizer, and air entrainment change the characteristics of the concrete to create more effective and sustainable mixtures **(MPA, 2019)**. Plasticizers improve concrete fluidity, requiring less water to reach the desired workability. This raises the water-to-cement ratio without using any more cement. Air-entrainment, on the other hand, eliminates trapped air pockets in concrete, resulting in a more cohesive mix with greater compressive strength without increase cement content. Because of the large eCO_2 advantages, the inclusion of admixtures has become the standard of concrete mixes in infrastructure design **(Purnell & Black, 2012b)**. However, other eCO_2 optimization strategies should be used concurrently in order to lower the eCO_2 of concrete to an acceptable level **(Gartner, 2004)**.

Increased production of concrete for future usage will result in significant depletion of these natural resources as well as environmental impact. As a result, green concrete will be needed to meet future concrete demand while conserving natural resources. Green concrete is any concrete that has less embodied energy and carbon than standard OPC concrete; it mainly integrates various waste products as either binder or aggregate **(Karthika et al., 2018; Anandaraj et al.,**

2019).Secondary or supplemental cementitious materials (SCMs) are frequently employed as an alternate cement replacement technique in the industry, and the concrete centre now recommends their usage **(The Concrete Centre, 2020)**. They are significantly less costly than cement since they are made from waste materials. Their supply, however, is restricted due to their reliance on other industrial processes. In coal-fired power plants, PFA is a byproduct of coal combustion. The UK's energy is migrating away from coal and toward renewable energy, with just three coal-fired power stations still in operation **(Gov.uk, 2020)**. Therefore, PFA is in particularly short supply. Similarly, the shift to more efficient procedures and fewer byproducts reduces the availability of ground granulated blast furnace slags (GGBS) **(Gartner, 2004)**. As a result, the researchers are looking at several type of SCMs.

Pozzolans, both natural and synthetic, have been proposed as alternative SCMs but are less practical due to the requirement of high-temperature curing and the need for activation with high eCO_2 processes **(Habert, 2013)**. Another potential SCM is calcium sulfates, known as the "Third Cement Series" (TCS), which can be used at room temperature **(Gartner, 2004)**. However, research on this material is limited, hindering its widespread adoption.

Due to the limitations and time-consuming nature of developing SCMs, researchers have shifted their focus from optimizing concrete mix designs to optimizing concrete structural design methodologies to reduce the carbon footprint of concrete **(Yoon et al., 2018)**. SCMs such as silica fume, blast furnace slag, fly ash, rice husk ash, and sugar cane bagasse ash, which are industrial and agricultural waste materials, have been successfully used to produce green binders with low carbon emissions **(Yeo & Gabbai, 2011; Purnell & Black, 2012b; Yoon et al., 2018)**.

Using SCMs not only provides environmental advantages such as reduced CO_2 emissions and energy expenditure but also improves the performance and

durability of concrete **(Thomas, 2018; Rosales et al., 2020)**. The literature emphasizes partial replacements of cement with SCMs, resulting in binary, ternary, or quaternary binders depending on the supplementary materials used. However, further investigation is needed for total replacement (100% SCMs) scenarios **(Shehab et al., 2016)**. It is possible to accomplish this optimum performance in terms of mechanical behavior (compressive strength, bending, etc.) or in relation to criteria that signify durability (porosity, resistance to chloride penetration, resistance to carbonation, accelerated aging, etc.) **(Ramezanianpour & Bahrami Jovein, 2012; Lee et al., 2012; Medina et al., 2019; Khan et al., 2020)**. New combinations of Portland cement and SCMs are created as an understanding of the topic grows, and the proportion of substitution tends to rise. The relevant research highlights partial replacements, which range in coverage from 3 to 80% of SCMs and produce binary, ternary, or quaternary binders depending on the extra materials utilized **(Schöler et al., 2015; Yang et al., 2017; Hemalatha & Santhanam, 2018; Al-Mansour et al., 2019; Juenger et al., 2019; Skibsted & Snellings, 2019)**. However, total replacement (100% SCMs) needs to be further investigated. Overall, the passage highlights the importance of SCMs in developing sustainable and environmentally friendly concrete, and the research and development efforts focused on optimizing their use and expanding their possibilities.

2.4.3 Optimised Low Carbon Concrete

Purnell and Black (2012) conducted extensive research on optimizing concrete mix design to decrease CO_2. This study discovered that optimizing the eCO_2 of concrete buildings might be accomplished by modifying concrete characteristics by adjusting various mix design factors rather than just compressive strength, which is the focus of most investigations. The eCO_2 of 512 samples of cement type 1(CEM1) mix designs was explored utilizing the Building Research Establishment mix design (BRE) approach, a technique developed by

(Teychenne et al., 1997). The parameters were strengths of class; uncrushed or crushed aggregate; high or low slump; and the application of Pulverize Fly Ash (PFA) and superplasticizer, as shown in **Table 2.1** for the 32 mix designs. These 32 mixes design were processed on 512 varied concrete mixes with 16 various target means compressive strengths ranging 17 MPa to 120 MPa. The compressive strength range includes normal strength and high strength concretes, allowing for far more complete research of the compressive strength effects on eCO_2 than earlier work.

Table 2.1: The 32 mix designs used in Purnell and Black (2012) study into the optimum concrete mix design for minimizing CO_2

Mix family	1	2	3	4	5	6	7	8	9	10	11	12	13	14	15	16
CEM I Cement class	52.5 MPa															
PFA content	0%								40% replacement of CEM1							
Superplasticizer	No				Yes				No				Yes			
Aggregate type	Uncrushed		Crushed		Uncrushed		Crushed		Uncrushed		Crushed		Uncrushed		Crushed	
Slump	L	H	L	H	L	H	L	H	L	H	L	H	L	H	L	H

Mix family	17	18	19	20	21	22	23	24	25	26	27	28	29	30	31	32
CEM I Cement class	42.5 MPa															
PFA content	0%								40% replacement of CEM1							
Superplasticizer	No				Yes				No				Yes			
Aggregate type	Uncrushed		Crushed		Uncrushed		Crushed		Uncrushed		Crushed		Uncrushed		Crushed	
Slump	L	H	L	H	L	H	L	H	L	H	L	H	L	H	L	H

Purnell and Black observed that a greater content of cement (and hence greater eCO_2 levels) results in a stronger concrete, which indicates little concrete is needed to offer the same capacity (which decreases eCO_2 for each unit of capacity). As a result, measuring eCO_2 for each unit of function of concrete's was proposed as a more accurate method of computing eCO_2. Because the compressive strength is the most important property for structural engineering. This study used CO_2 per Target Mean Compressive Strength to calculate eCO_2.

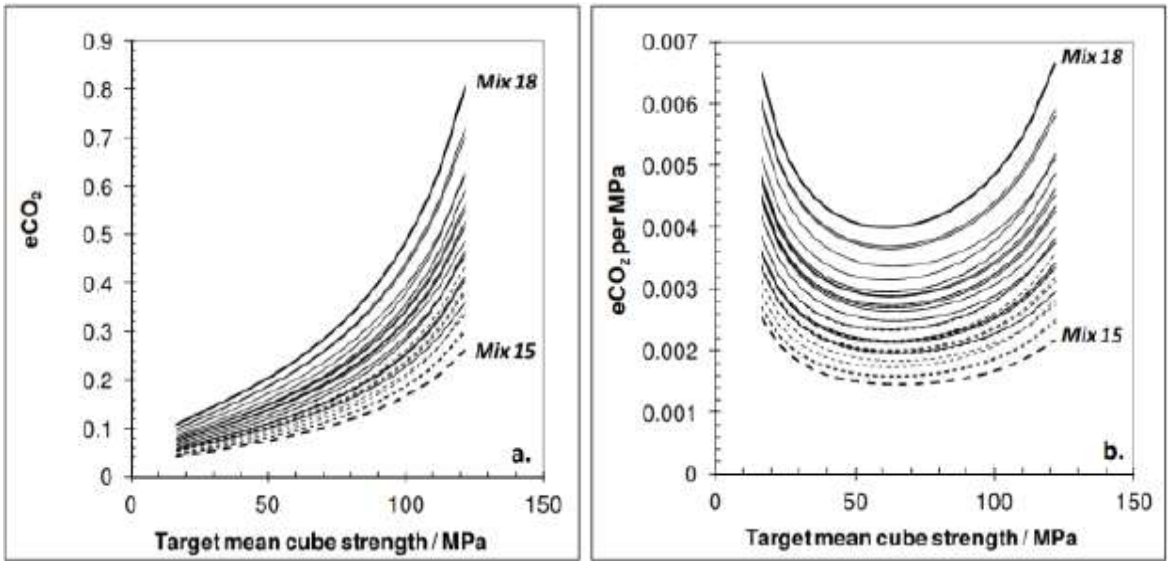

Figure (2.6): - Graph produced by Purnell and Black (2012) showing the performance of 18 concrete mix designs for a CO_2 and eCO_2/MPa

In **Figure (2.6)**, Concrete with a CEM I binder is shown by the solid line, while concrete with a 60% CEM I, 40% PFA binder is represented by the dashed line. The graph's overlapping dashed and solid lines show that altering other mix design components can result in lower eCO_2 values for a given strength of CEM-I. As a result, the commonly held idea that concrete manufactured using mixed cement binder has a smaller carbon footprint than CEM I is incorrect. The cement content dominates eCO_2 levels, which rise linearly as more cement is applied. The nonlinear relate between the w/b ratio and cement content, however, affects the relationship between strength and cement content nonlinearly.

A range of optimized values is thus discovered between 50 and 70 MPa. The lowest eCO_2/MPa is produced by concrete mixes created at specified mean cube strengths in that area. The amount of cement required to create a structural component with a similar level of strength outweighs the lower cement content in weaker concretes. The greater cement content necessary to attain the high strength, however, outweighs the decrease in material consumption that stronger concretes allow due to the rise in strength. Therefore, for every particular mix family, planning for optimum values might result in a decrease of up to 40%. Further research revealed that the reduction in eCO_2 caused by altering the cement strength class from 42.5 to 52.5 MPa or the aggregate type from uncrushed to crushed was only around 9% and 7%, respectively.

The most efficient method for lowering eCO_2 by about 26%, however, was determined to be the use of superplasticizer since it was workable even at a low w/b ratio. This study will look for a link between corrosion resistance and mix designs that are optimized using GGBS rather than PFA.

2.5 Corrosion of Concrete Reinforcement

An electrochemical mechanism causes steel corrosion in concrete. The surface of the corroding steel serves as a mixed electrode, which is a combination of anodes and cathodes electrically connected within the steel's body, on which coupled anodic and cathodic processes take place. Concrete pore water functions as an intricate electrolyte or aqueous media. A reinforcing corrosion cell is then created, as shown in **Figure(2.7) (Ahmad, 2003).**

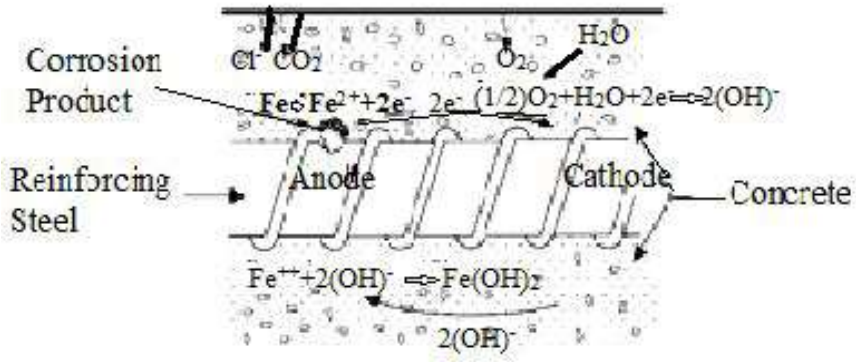

Figure (2.7): - Schematic illustration of the corrosion of steel reinforcement in Concrete (Ahmad, 2003)

Chloride attack and carbonation are the most common and serious causes of corrosion reinforcement in reinforced concretes structures. Chlorides are found in a variety of places. They can be cast in concrete, although they commonly spread through it due to spray of sea salt and direct water of sea wetness. They can also seep inside concrete as a result of the usage of chloride de-icing salts and chloride chemicals storage in tanks of concrete, among other things. Many research have studied examined the processes behind carbonation, chloride attack, and reinforcing corrosion **(Nürnberg, 1984; Živica, 2003)**.

A lot of considerable study have been conducted on durability of concrete, which includes material improvement, corrosion mechanisms, and corrosion control **(Cheng et al., 2005a)**. Corrosion of reinforcing steel in concrete causes cracks and weakens the bond. The fissures may hasten the intrusion of harmful ions, which may worsen concrete degradation and lead to more cracking. Various reports have discussed how fissures affect reinforced concrete members corroding **(Arya & Ofori-Darko, 1996; Ramm & Biscoping, 1998; Mohammed et al., 2001; Ballim & Reid, 2003; Vidal et al., 2004)**.

According to **Bentur**, the time needed to start corrosion in two reinforced concrete samples with different crack widths is shorter for the sample with the

wider crack, but the rate of corrosion is not significantly affected by fracture width **(Bentur et al., 1997)**.

2.5.1 GGBS Effect on Corrosion Behavior

Blended cements, such as Portland blast furnace cement and Portland pozzolan cement, have been found to outperform traditional Portland cement in concrete applications. Ground granulated blast furnace slag (GGBS) is a nonmetallic product that is produced during the manufacture of iron from ore in blast furnaces. The slag is granulated and then crushed to form GGBS. The impermeable covering of amorphous silica and alumina on GGBS particles can delay the reaction between the slag and water. Therefore, an activator such as calcium hydroxide or $NaSiO_3$ is often added to initiate the slag hydration process **(Cheng et al., 2005a)**. The combination of Portland cement and GGBS leads to the formation of a mixture of low CaO/SiO_2 (C/S) ratio, $CaO\text{-}SiO_2\text{-}H_2O$ (C-S-H) and AFm phases, activated by the hydration product of $Ca(OH)_2$. The pozzolanic reaction further increases the C/S ratio in slag-cement blends, resulting in an unstable mixture of low calcium C-S-H and $Ca(OH)_2$. Tests on mortars incorporating GGBS have shown significant reductions in permeability and penetration of chloride ions compared to specimens without GGBS. This is attributed to the altered microstructure of the cementitious paste, which contains more capillary holes filled with low-density C-S-H gel compared to standard Portland cement paste **(Arya & Xu, 1995; Glass et al., 2000; Basheer et al., 2002)**. The use of GGBS can also refine the pore structure of concrete, leading to a decrease in pore diameters and cumulative pore volume, as well as a reduction in the likelihood of reinforcing steel corrosion **(Daube & Bakker, 1986)**.

Cheng demonstrated that using GGBS instead of cement refines the pore structure and minimizes the likelihood of reinforcing steel corrosion. Despite the fact that the pH value for control concrete was 13.2, 12.8 for 40% GGBS replacement concrete, and 12.4 for 60% GGBS replacement concrete, there

appears to be no significant detrimental influence on corrosion behavior due to reduced alkalinity in pore solution **(Cheng et al., 2005b)**.

Despite the reduced alkalinity in the pore solution of GGBS concrete compared to control concrete, studies have found no significant detrimental influence on corrosion behavior. The use of cement replacement materials like fly ash, silica fume, and blast furnace slag has been shown to reduce the likelihood of steel corrosion and improve concrete permeability **(Ramezanianpour & Malhotra, 1995; Osborne, 1999; Irassar et al., 2000)**. Torii study reported that the resistance to chloride penetration in 50% GGBS concrete was comparable to that of 10% silica fume concrete. These findings demonstrate the potential benefits of using GGBS and other cement replacement materials to enhance the performance and durability of concrete structures **(Torii et al., 1995)**.

2.5.2 Corrosion Process of Embedded Reinforcement

The corrosion of reinforcing bars as a common cause of concrete degradation in harsh conditions **(Jones et al., 1997)**. Corrosion can occur due to a decrease in alkalinity caused by carbonation or the breakdown of the passive layer due to chloride ion attack. The time it takes for corrosion to initiate is influenced by factors such as the thickness and quality of the concrete cover and the permeability of the concrete. To mitigate the rapid deterioration of concrete in harsh climates, it is essential to use high-quality and long-lasting concrete. Chloride ions play a significant role in promoting reinforcement corrosion. They can penetrate the protective oxide coating on the steel surface formed in a high pH environment, leading to depassivation of the steel.

Chlorides can also adsorb on the steel surface, enhance metal ion hydration, and accelerate depassivation. Additionally, chlorides can compete with hydroxyl ions for ferrous ions generated during the corrosion process, leading to the formation of ferric chloride, which further deteriorates the passive layer **(Broomfield, 2006; Nilsson, 2019)**.

The use of alternate cementitious materials like GGBS in concrete can help reduce porosity and refine the pore structure, resulting in a decrease in chloride ion mobility. This change in mineralogy of the cement hydrates contributes to the improved resistance to chloride-induced corrosion **(Li & Roy, 1986)**.

Corrosion is an electrochemical process that occurs when different energy levels, an electrolyte (such as the surrounding concrete), and a metallic link (reinforcing bar) interact. The process starts in the anodic zones, where electrons are released from iron atoms, leading to the deposition of ferrous ions at the steel-concrete interface. A half-cell oxidation reaction is used in this technique, i. e. as the anodic reaction and can be expressed as:

$$Fe \rightarrow Fe^{2+} + 2e^{-} \qquad \textbf{(2-2)}$$

Rebar serves as a conduit for the liberated electrons as they go to wet, oxygen-rich cathodic locations. As a result, the cathodic reaction that produces hydroxides is triggered, which is a reduction reaction. The reaction is frequently worded as follows:

$$2e^{-} + H_2O + \frac{1}{2}O_2 \rightarrow 2(OH)^{-} \qquad \textbf{(2-3)}$$

To preserve electrical neutrality, ferrous ions are drawn to cathodic regions where they interact with hydroxides. The outcome of the reaction produces ferrous hydroxides, which are the primary component of rust and may be written as:

$$Fe^{2+} + 2(HO)^{-} \rightarrow Fe(OH)_2 \qquad \textbf{(2-4)}$$

When oxygen and water are present, ferrous hydroxides further oxidize to become ferric hydroxide, often known as rust.

$$4Fe(OH)_2 + 2H_2O + O_2 \rightarrow 4Fe(OH)_3 \qquad \textbf{(2-5)}$$

Ferric hydroxide then dehydrates to produce hydrated ferric oxide (the final form of rust) surrounded by water and can be expressed as:

$$2Fe(OH)_3 \rightarrow 4Fe_2O_3 + 2H_2O \qquad \textbf{(2-6)}$$

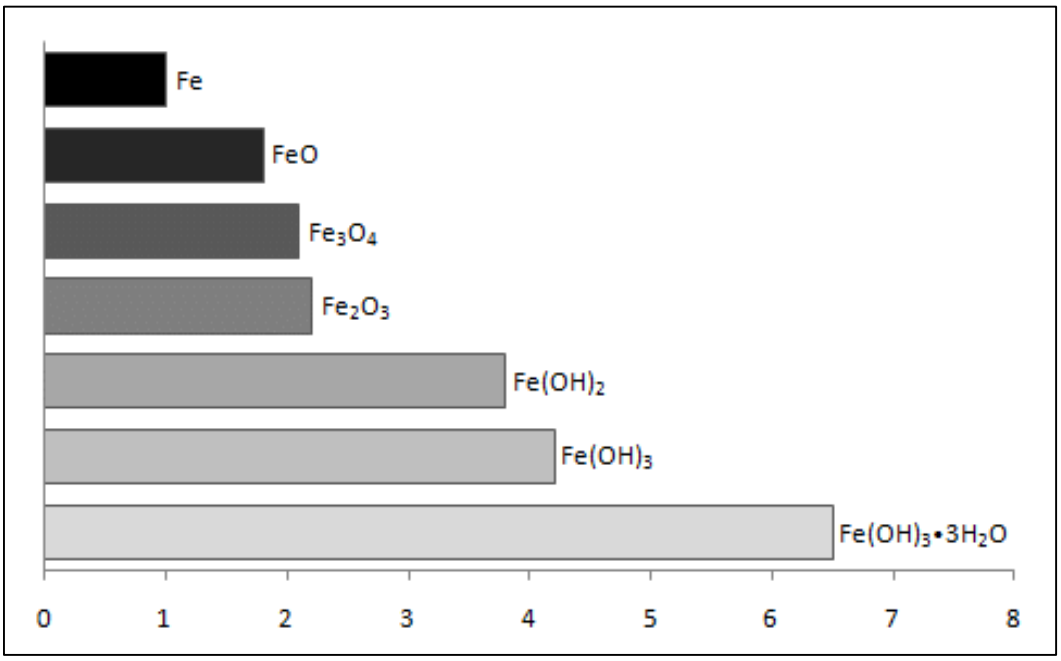

Figure (2.8): - The Relative Volumes of Various Iron Oxides from (Mansfield ,1981)

Rust has a characteristic look due to the reddish-brown colors of ferric hydroxide and ferric oxide. Additionally, the compounds have much higher volumes than pure iron **Figure (2.8),** which causes internal expansions that cause cracks and additional corrosion. Steel rebar completely dissolves if the chemical processes are not regulated.

2.5.3 Chloride Attack

The penetration of chloride ions into concrete is a major cause of deterioration and can lead to the corrosion of reinforcing steel in concrete structures. The presence of chloride ions disrupts the natural passivity of the steel surface and accelerates the corrosion process. So insufficient concrete cover or poor-quality concrete can contribute to the corrosion of steel reinforcement, as they provide less protection against chloride ingress. In harsh environments such

as offshore or coastal regions, where exposure to chloride ions is high, the useful service life of concrete structures is often reduced.

Chloride ions can enter concrete through various sources, including admixtures, contaminated materials, marine environments, brine, and de-icing salts. The behavior of chloride ions is influenced by their concentration levels and the thickness of the passive film on the steel surface. In the case of a multi-layered film, chloride ions can accumulate in localized weak spots, creating ionic defects that facilitate further ion transfer and corrosion. On the other hand, in the case of a monolayer film, chloride ions can compete with hydroxyl ions in areas of high activity on the metal surface, impeding the passivation process. In both cases, localized areas of the steel surface become susceptible to corrosion initiation.

Reactions and mechanisms related to the oxidation of steel due to chloride ions (see **Figure (2.9))**. Initially, negatively charged chloride ions (Cl^-) and positively charged ferrous ions (Fe^{2+}) are attracted to each other and react to form ferrous chloride ($FeCl_2$) **(see Equation (2-7))**. Ferrous chloride ($FeCl_2$) is a soluble complex that can break down in high pH areas of the surrounding solution away from the anodic site. This breakdown results in the formation of insoluble iron hydroxide ($Fe(OH)_2$) and hydrochloric acid (HCl) **(see Equation (2-8))**. The formation of hydrochloric acid (HCl) leads to a decrease in pH, which can break the passive layer of the steel surface. Later, Hydrochloric acid (HCl) can decompose, releasing chloride ions (Cl^-), which can further react with ferrous ions and repeat the reaction described in **Equation (2-7).** This cyclic process of chloride ion release and reaction contributes to the pitting of anodic sites on the steel's surface. The iron hydroxide ($Fe(OH)_2$) formed in **Equation (2-8)** has a tendency to further oxidize when exposed to oxygen. This oxidation process leads to the formation of higher hydroxides with higher volumes. The specific reactions and equations describing this oxidation process are mentioned as **Equations (2-5 & 2-6**) and illustrated in **Figure (2.7).**

$$Fe^{2+} + 2\,Cl^{-} \rightarrow FeCl_2 \qquad \textbf{(2-7)}$$

$$FeCl_2 + 2\,H_2O \rightarrow Fe(OH)_2 + 2\,HCl \qquad \textbf{(2-8)}$$

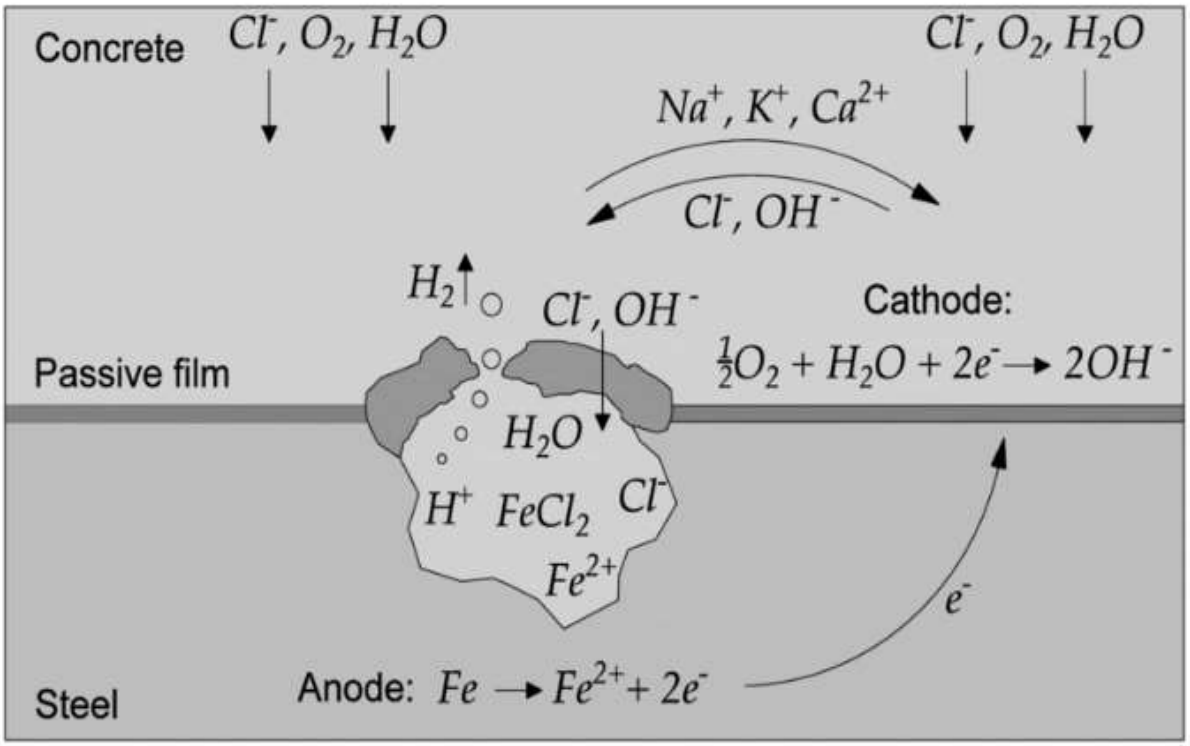

Figure (2.9): - Schematic representation of chloride induced pitting corrosion (Silva,2013)

When supplementary cementitious materials (SCMs) such as pulverized fuel ash (PFA) and ground granulated blast furnace slag (GGBS) are used in concrete, several beneficial effects occur. One of these effects is the reduction of porosity in the concrete. Additionally, the pores that are present become finer in size. These changes in the microstructure of the concrete contribute to a decrease in the mobility of chloride ions within the concrete matrix **(Li & Roy, 1986)**. The initial protection against chloride penetration in concretes containing SCMs may depend on various factors. Firstly, the type of SCM, SCMs have varying chemical compositions and properties, which can influence their effectiveness in reducing chloride penetration and plays a role in determining the level of protection. The

duration of curing is also an important factor. Proper curing of concrete allows for the hydration reactions to occur fully, leading to the development of a strong and dense cementitious matrix. Furthermore, the age of the concrete at the time of exposure to a chloride environment affects its resistance to chloride penetration. Younger concrete generally has a higher permeability and is more susceptible to chloride ingress compared to mature concrete. In the case of PFA and GGBS, their hydration requires the presence of calcium hydroxide, which is released during the hydration of Portland cement **(Mehta, 1983)**. This reaction contributes to the formation of additional hydration products and densification of the cement matrix, thereby aiding in reducing the permeability to chloride ions.

2.5.4 Chlorides Induction during Concrete mixing

Calcium chloride ($CaCl_2$) is a commonly used accelerating admixture in concrete due to its high effectiveness and low cost. Accelerators are employed to expedite the rate of hardening, facilitating early formwork removal, pre-casting, and usage in cold weather conditions. $CaCl_2$ acts as a catalyst, promoting the dissolution of lime and affecting the alite and belite phases, thereby accelerating the hydration process. However, the use of $CaCl_2$ in reinforced concrete is now limited due to its potential damaging effects from chlorides. If chlorides are added during the mixing process, the corrosion rate of reinforcing steel can be accelerated, especially when an undeveloped pore solution with low alkalinity provides abundant water and oxygen. As the concrete hardens and the pH rises, the corrosion rate is expected to decrease, dependent on the concentration of chlorides.

Mixtures with added chlorides have three supplementary effects on corrosion rates.

1- Chloride-induced acceleration at a constant w/c ratio leads to a coarser capillary pore size thus, providing easier ingress of aggressive agents

including additional chlorides, CO_2 boosting carbonation while reducing the concrete resistivity.

2- The ionic concentration in the pore solution and its electrical conductivity are increased; thus, accelerating the corrosion rate.

3- The concrete pore solution pH is altered since sodium chloride (NaCl), and potassium chloride (KCl) increase the pH whereas, calcium chloride ($CaCl_2$) decreases the pH in high concentrations. Furthermore, this affects binding and threshold values as will be discussed in section **(2.5.6)**.

2.5.5 Sources of Chloride Salt's Attack Reinforced Concrete

There are three sources of chloride that attack the reinforced concrete structures **(Ahmed et al ,2022)**. When it contacts the reinforced concrete, the concentration of chloride ions will rise in concrete, result in a decrease in the service life of reinforced concrete structures **(Wang et al., 2016)**.

2.5.5.1 Ground Water

In most zone of the world especially in Iraq, ground water represents a focal problem to the concrete foundations of buildings such as settlements and corrosion of reinforcement ..etc. The ground water in the central and southern Iraq contains a great concentration of salts sulfate and chloride ions in contact with concrete **(Ali, 2017)**, therefore this case is also considered another source chloride ion.

Finnish Transport Infrastructure Agency (FTIA) is monitoring the chloride content of groundwater in cooperation with the finnish environmental administration. The chloride content tendency increases or strongly increases in 49% of the remark points. In the discrete groundwater samples, the chloride concentration various from 0.4 to 700 mg/l as for reference samples. The chloride concentration of typical finnish groundwater is below 25% mg/l (**Lindroos et al.,2005; Finland,2015)**.

2.5.5.2 Marine Environment (Sea Water Attack)

Concrete structures exposed to marine environments face durability challenges primarily due to the ingress of chlorides. The ability of concrete to resist chloride ingress is influenced by various factors related to concrete properties and micro-environmental characteristics **(Costa & Appleton, 1999)**.

In recent times, there has been a significant increase in the construction of concrete structures near, in, or beneath water, such as bridges, high-rise buildings, and oil platforms **(Mark, 2016).** These structures are prone to safety and serviceability issues, particularly corrosion of reinforced concrete, due to the high concentration of chloride ions in seawater **(Shen et al., 2019)**. Although concrete is generally considered a durable material, its properties can be affected over time by environmental factors, weathering, chemical attack, abrasion, and other aggressive processes. As a result, these structures approach the end of their service life due to compromised safety and functionality **(Oh et al., 2002)**. The important factor in physical and chemical processes of deterioration is a penetration of water, chloride, and other aggressive ions into concrete **(Mehta & Monteiro, 2014)**.

2.5.5.3 De-Icing Salts

Reinforced concrete structures (RCS) expose to a splash of de-icing salt on both sides of the road bridges leads to a drop the durability of these structures with the time due to increase the concentration of chloride ions **(Liu et al., 2021).**

Sodium or calcium chloride are the major ingredients in de-icing salts (or mixtures) The quantity and frequency of application are determined by the climate.

The purpose of using de-icing salts, as suggested by **Filanda (2008),** is to ensure safe traffic movement by melting ice and snow during winter seasons. In

Finland, for example, the Finnish Transport Infrastructure Agency typically employs 80,000 to 100,000 tons of sodium chloride (NaCl) per year for de-icing purposes. The amount of de-icing salt applied per road kilometer can vary from 2 tonnes/km up to 20 tonnes/km annually.

2.5.6 Chloride Diffusion from the Environment

When chlorides come into contact with the exterior surfaces of concrete, they can diffuse through the material via capillary pores. Unlike carbonation, the presence of cracks is not necessarily required for chloride transport to reach the embedded steel, but cracks can accelerate the process. The rate of chloride diffusion is influenced by several critical factors:

• w/c ratio: Porosity is decreased by a reduced w/c ratio, which also lowers permeability.

• Cement type: For instance, as compared to CEM I, or OPC, CEM III has a much greater electrical resistivity and reduced chloride permeability **(Yildirim et al., 2011)**.

• Temperature: an association between the temperature gradient and chloride penetration (x) is discovered in a recent research. This association is found to be more pronounced as the concrete's chloride content and temperature differential increased **(Isteita & Xi, 2017; AL-Ameeri et al., 2022)**.

• Concrete's maturity: Age is observed to cause a drop in (x) **(Isteita & Xi, 2017)**.

2.5.7 Chloride Binding and Threshold Values

In some cases, the chloride ions present in the concrete may not contribute to the corrosion process. These chloride ions chemically react with calcium aluminates in the cement paste to form calcium chloroaluminate and are removed from the

pore solution effectively. However, as concrete carbonates, these compounds will break down releasing the chlorides to contribute to corrosion.

Some of the released chlorides are found to be physically trapped in unconnected pores or by being adsorbed **(Andrade, 2006)**. The un-trapped chlorides can then responsible for the process of deuteration of the passive film; however, the rate of effect is dependent on multiple factors. **The ACI 222 (2001)** states that deuteration of the passive film is related to the tricalcium aluminate (C_3A) and tetracalcium aluminoferrite (C_4AF) contents, pH level, w/c ratio and whether the chlorides originated from mixing or later by penetration. Furthermore, it was stated that the threshold value, which is the limit of which no significant corrosion may occur, is also dependent on some of these factors as shown in **Figure (2.10)**.

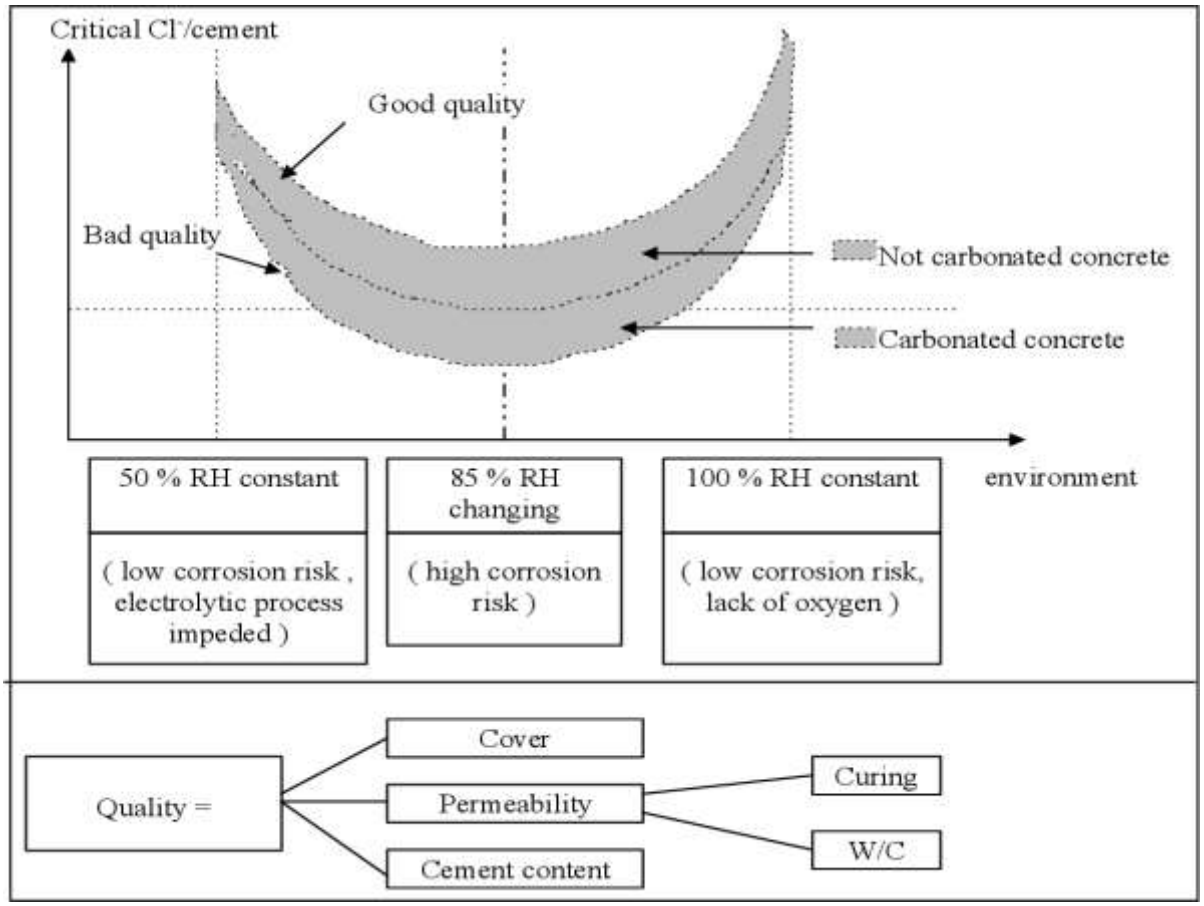

Figure (2.10): - Critical chloride/cement content depending on variables (Liu & Weyers, 1998)

According to the CEB guide to durable concrete structures (1985), the threshold value for chloride content with respect to relative humidity (RH) and quality is 0.4% Cl by cement mass (approximately 1.4 kg/m3 of concrete). Research has shown that the relationship between the chloride/hydroxide ratio and the corrosion rate of embedded steel in concrete is significant **(Thangavel and Rangaswamy, 1998)**. Moreover, it has been observed that concrete with higher w/c ratios is more likely to exhibit a linear relationship between corrosion rate and the [Cl/OH] ratio. Additionally, oxygen diffusion is considered a governing step, and as the pH decreases, the threshold value for chloride content decreases. The **ACI 222 (2001)** specifies, based on other researchers' findings, that the maximum limit for the [Cl/OH] ratio to avoid breakdown of the passive film is 0.29 at pH 12.6 and 0.30 at pH 13.3.

2.5.8 Methods of preventing and Controlling Corrosion

To prevent expensive repairs or problems with health and safety, several preclusions are taken into account throughout the design phase of the construction sector. The designers evaluate the degree of corrosive risk on concrete components based on the environment. Basic maintenance and corrosion prevention techniques include:

2.5.8.1 Mix Design Variables

Optimal concrete mix design plays a vital role in preventing corrosion.

Thick cover: Ensuring sufficient concrete cover over reinforcement bars helps protect them from corrosive substances. The depth of concrete cover should be determined based on the expected environmental conditions and corrosion risk. Increasing the thickness would protect the embedded steel against chlorides and carbonation even more. The Euro-code 2 (EC2) is used as size advice in Europe (25-30) mm **(The European Union, 2011)** .

Low w/c ratio: High strength concretes with low w/c ratios have the potential to be exceedingly dense and impermeable when properly cured and compacted. Accelerator without calcium chloride: As mentioned in **(2.5.4)**, cutting out calcium chloride can further protect reinforcements by not reducing alkalinity.

2.5.8.2 Cathodic protection

Cathodic protection (CP): In some cases, cathodic protection systems can be installed to mitigate corrosion. This method involves applying a direct current to the reinforcement bars, which helps to counteract the electrochemical reactions responsible for corrosion. **Figure (2.11)** displays the two common CP techniques used in industry, namely the impressed current and sacrificial anode methods. These fixes would add years to the structures' useful lives while causing little inconvenience.

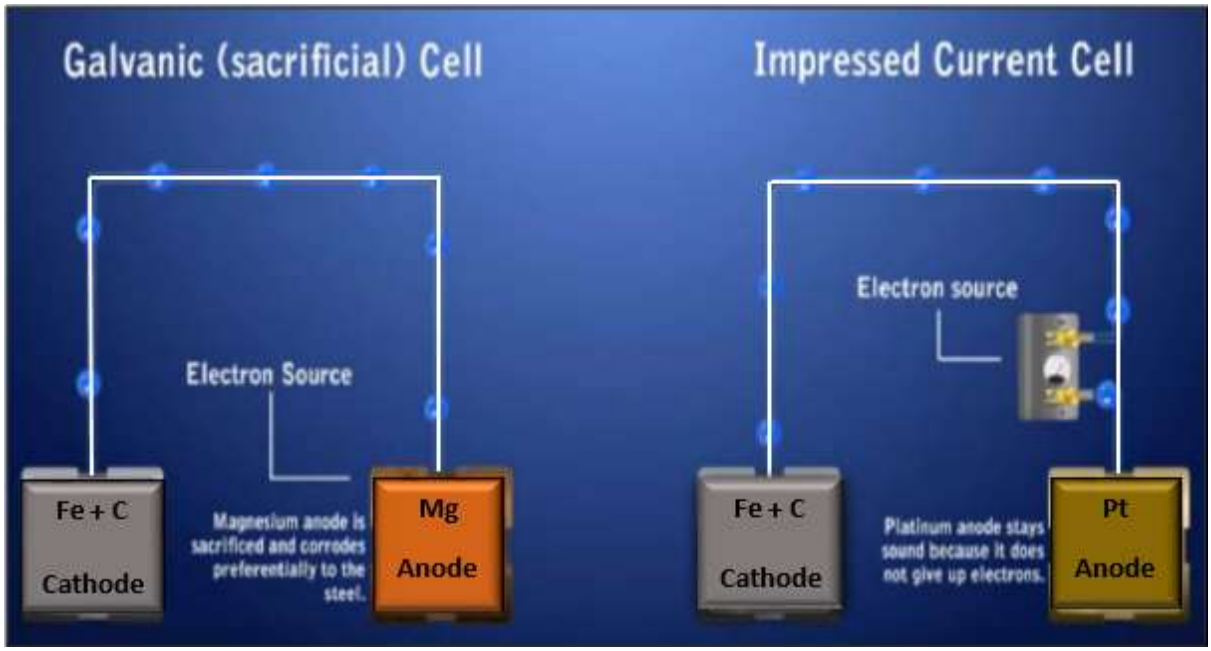

Figure (2.11): - The galvanic cell and impressed current cell scheme (GSG Systems, 2010)

The two methods of corrosion protection described are the sacrificial method and the impressed current method:

- **Sacrificial Method:** This method involves using a sacrificial metal that is more active (i.e., more prone to corrosion) than steel. Metals like magnesium or zinc are commonly used as sacrificial anodes. When these anodes are connected to the steel reinforcement (rebar) in concrete, they supply electrons to the rebar. The more active sacrificial metal corrodes instead of the steel, protecting it from corrosion. This process is known as galvanic protection or cathodic protection **(Masli, 2011)**. The sacrificial metal anode gradually corrodes over time and needs to be periodically replaced.
- **Impressed Current Method:** In situations where the sacrificial method may not provide sufficient protection, the impressed current method is employed. This technique involves using an external power source, typically an electrical current, and an inert anode, such as titanium or platinum-plated niobium. The external power source supplies a controlled electrical current to the steel reinforcement, effectively reversing the electrochemical reactions responsible for corrosion. This process requires monitoring and adjusting the voltage to provide the necessary current to counteract the corrosion. The impressed current method is often used in larger structures, such as bridge beams or girders, where a continuous electrical supply can cover extensive spans of rebar.

Both methods aim to protect the steel reinforcement in concrete from corrosion. The sacrificial method relies on the natural electrochemical potential difference between different metals, while the impressed current method utilizes an external power source to provide the required electrical current. The choice of method depends on factors such as the severity of corrosion, the size and nature of the structure, and the specific requirements of the project.

2.6 Water Absorption in Concrete

The environment has a significant impact on the water absorption capacity and durability of concrete. Concrete's durability is closely related to its permeability, which refers to the ability of fluids to penetrate its microstructure**(Zhang & Zong, 2014)**. High permeability makes concrete susceptible to chemical attack and degradation. To address this concern and reduce environmental impact, the use of additional cementitious materials like ground granulated blast-furnace slag (GGBS) has become a widespread building technique **(Siddique, 2014; Li, 2016; Almeida & Klemm, 2018; Irvine, 2018)**.

GGBS is a byproduct of pig iron production and can replace up to 85% of Portland cement (PC) in concrete composition **(Siddique & Bennacer, 2012; Siddique, 2014)**. The use of GGBS can have both positive and negative effects on concrete durability. On the positive side, it can reduce permeability and increase resistance to harmful processes such as chloride penetration, alkali-silica reaction, and sulfate attack. This is beneficial for enhancing concrete durability and protecting it from chemical assaults **(Loser et al., 2010; Thomas, 2011; Divsholi et al., 2014; Krivenko et al., 2014; Almeida et al., 2015; Klemczak & Batog, 2016; Moretti et al., 2018)**.

However, there are also potential drawbacks associated with higher levels of GGBS in concrete. Increased GGBS content may lead to higher carbonation rates, lower resilience to freezing and thawing, and volumetric instability **(Lura et al., 2001; Lee et al., 2006; Snellings et al., 2012; Bouasker et al., 2014; Divsholi et al., 2014; Valcuende et al., 2015; Ghourchian et al., 2018)**. These factors can negatively impact the long-term durability of concrete. The cementitious capabilities of GGBS are influenced by its chemical composition, fineness, glass content, and the alkali concentration in the reacting system **(Snellings et al., 2012; Siddique, 2014)**.

It is worth noting that GGBS contains fewer alkali compounds compared to PC clinkers, which results in decreased potassium and sodium contents in blended systems over time **(Mehta & Monteiro, 2014)**. Additionally, high GGBS content can lead to lower hydroxide concentrations. These factors need to be considered in concrete mix design and construction practices to ensure the desired performance and durability of GGBS-based concrete**(Vollpracht et al., 2016)**.

Overall, the use of GGBS as a cementitious material offers environmental benefits by reducing the reliance on conventional Portland cement, which contributes to CO_2 emissions. However, careful consideration of the specific application and the potential effects on concrete durability is necessary when incorporating GGBS into concrete mixes.

2.7 Shrinkage in Concrete

Concrete is a widely used construction material that undergoes various physical and chemical changes during its lifespan. One common issue that can occur during the early stages of concrete hardening is shrinkage. Shrinkage refers to the reduction in volume that takes place as the concrete undergoes hydration processes**(Holt, 2005)**.

Several factors can contribute to concrete shrinkage, including the composition of the concrete mixture and the surrounding environmental conditions such as temperature and moisture. The initial hydration of concrete involves a chemical reaction between cement and water, resulting in the formation of a cementitious gel. This gel undergoes a process called self-desiccation, where water is consumed, leading to a decrease in volume and the potential for cracking**(Al-Gburi, 2015; Tazawa, 2020)**.

The presence of Ground Granulated Blast Furnace Slag (GGBS) in concrete can have certain effects on shrinkage. GGBS is a supplementary cementitious material often used as a partial replacement for Portland cement. It has a filler

effect, which means it occupies space in the concrete matrix. This filler effect can result in a higher degree of clinker reaction at early ages but may also contribute to autogenous shrinkage**(Snellings et al., 2012; Scrivener et al., 2015)**.

The refinement of pores by GGBS can enhance the tensile stress induced by water menisci in capillaries**(Tazawa & Miyazawa, 1995; Lura et al., 2001; Valcuende et al., 2015)**. This means that the presence of GGBS can increase the susceptibility of concrete to cracking due to autogenous shrinkage. Autogenous shrinkage occurs as a result of self-desiccation processes in the cementitious material, and GGBS can potentially exacerbate this phenomenon **(Lura et al., 2001; Lee et al., 2006; Snellings et al., 2012; Bouasker et al., 2014; Jiang et al., 2014).**

2.7.1 Influence of Supplementary Cementitious Materials on Shrinkage of Concrete

Ternary cementitious components, such as ground granulated blast furnace slag (GGBS) and pozzolanic materials, are commonly used as partial substitutes for cement in construction. These components not only contribute to the mechanical and durability properties of concrete but also affect its shrinkage behavior.

In alkali-activated slag concrete, which utilizes GGBS as a primary binder, overall shrinkage is typically higher compared to ordinary cement concrete**(Collins & Sanjayan, 2000)**. This is attributed to factors such as high chemical shrinkage, the presence of tiny pores, and the particle shape of blast furnace slag. As the replacement level of GGBS increases at a constant water-to-cement ratio (w/c), the autogenous shrinkage of GGBS concrete also tends to increase compared to plain concrete**(Lee et al., 2006)**.

To mitigate shrinkage in alkali-activated slag concrete, shrinkage-reducing agents can be used under appropriate curing conditions. These agents help reduce

the shrinkage of the concrete during the drying process**(Collins & Sanjayan, 2000)**.

In the case of concrete with a high replacement level of GGBS (e.g., 60%), studies have shown that the use of GGBS as a cement replacement can lead to a significant reduction in shrinkage compared to plain cement mixes. For instance, concrete mixes with 60% GGBS replacement by volume exhibited a 35% reduction in shrinkage at 30 days and a 19% reduction at one year, when cured for 14 days. Additionally, using porous limestone coarse aggregate with water internally cured in combination with GGBS cement showed a more significant decrease in free shrinkage compared to mixes with low absorption coarse aggregate **(Venkatachalapathy, 2016)**.

The addition of silica fume to concrete, on the other hand, can increase both plastic and drying shrinkage strains. Silica fume cement concrete has been found to exhibit a 69% increase in plastic shrinkage compared to conventional concrete. However, short-term shrinkage was higher in silica fume cement concrete, while the long-term shrinkage was somewhat similar to normal concrete **(Ghodousi et al., 2009; Liu & Wang, 2017; Yang et al., 2017)**.

2.8 Summary of literature review

In summary, because the cement concentration in concrete raises the eCO_2, cement plays a major role in the eCO_2 related with the use of concrete in building. While the water/cement ratio is an important factor in determining mix strength, previous research indicates that as the water/cement ratio decreases, compressive strength increases, resulting in a higher cement content in high strength concrete. The type of aggregate used was shown to have an impact on the workability, strength, and durability of concrete. Similarly, the addition of a superplasticizer significantly improves the workability of concrete, allowing for a lower water content for the same cement content, implying that the cement content in the

mixture can be reduced. The use of GGBS as a partial replacement for Portland cement is a well-debated issue that is thought to have a considerable influence on the eCO_2 of the concrete mix without compromising the strength and durability of the concrete. There is some debate regarding whether the mix design approach affects the quantity of eCO_2 released based on the strength of the concrete and the cement concentration. The effect of adjusting the mix design parameters on eCO_2 and concrete durability was studied by investigating the effect of chloride penetration and accelerated corrosion studies of concrete to find the most sustainable mix and the optimum proportion of GGBS added.

CHAPTER THREE

EXPERIMENTAL PROGRAMME

CHAPTER THREE

Experimental Program

3.1 Introduction

This chapter provides a comprehensive overview of the materials used, the mixture proportions employed, the casting and curing procedures, and the testing processes conducted as part of the research work.

The experimental work aims to assess the impact of chloride penetration and corrosion in steel rebar on enhanced low-carbon concrete (LCC) by examining the effect of replacing cement with different ratios of GGBS on concrete's mechanical and fracture behavior, in particular the effect of the replacement ratio of GGBS on CO2 emission and toughness. Following the casting and curing of concrete; test of compressive strengths, test of splitting tensile strengths, test of ultrasonic pulse velocity (UPV) and test of dry shrinkage are carried out to find relevant concrete mechanical properties. Water absorption, corrosion resistance, chloride migration and the depth of penetration of chloride in concrete are also studied to evaluate the durability of concrete.

All testing are conducted to utilizing various approaches in order to produce a relevant database for finding the optimum case or mixture can be used to achieve LCC. The flow chart of this experimental work are depicted in **Figure (3.1)**.

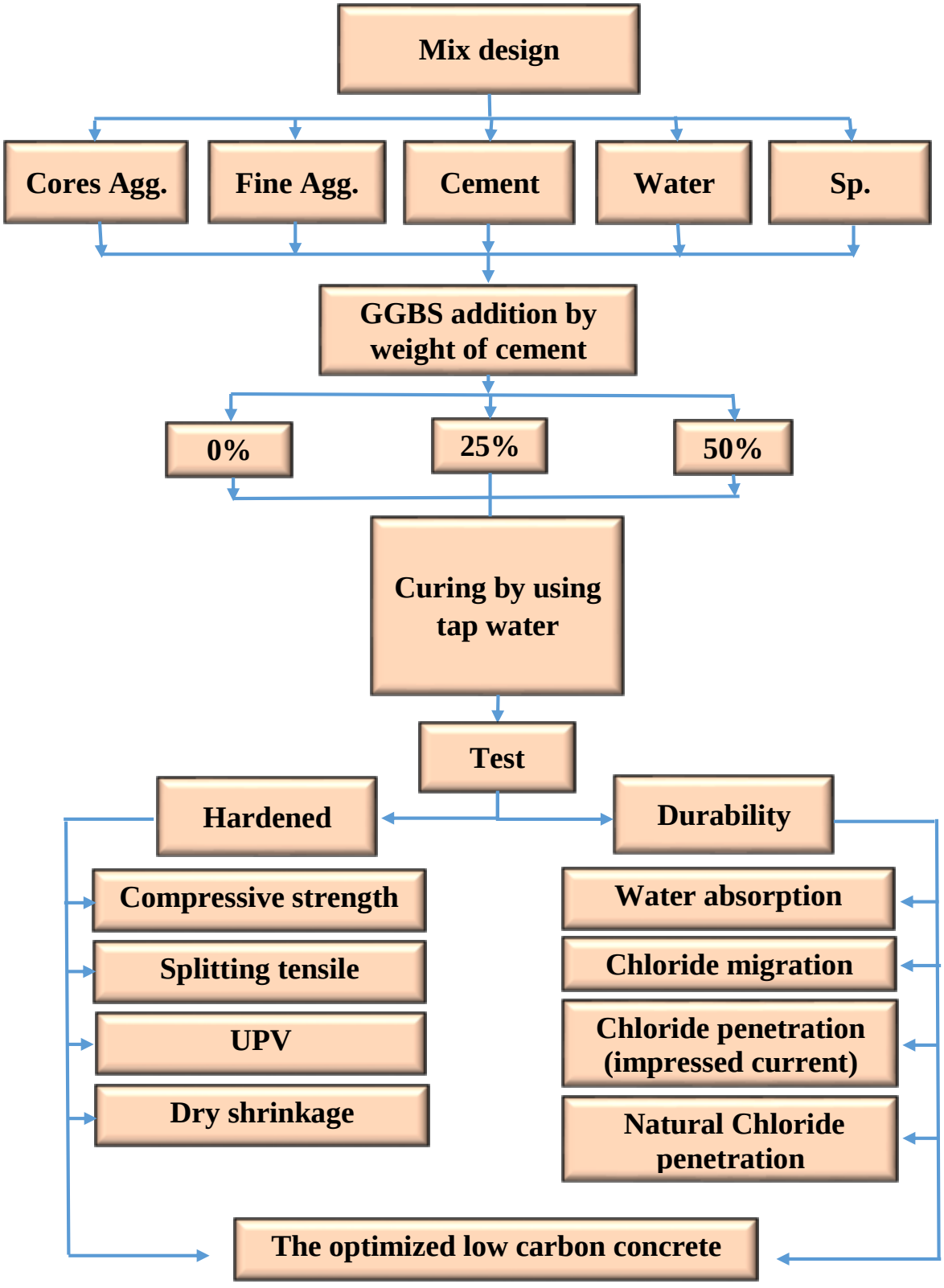

Figure (3.1): - Research Flow Chart.

3.2 Materials

3.2.1 Ordinary Portland Cement (OPC)

The Ordinary Portland Cement OPC that manufactured in Iraq (CEM I-42.5R) under the trade name **"Al MASS"** was used in this study and classified as "Type I" by the American Society and testing materials **(ASTM C 150, 2017)** as shown in **Figure (3.2)**. For cement the physical and chemical qualities are depicted in **Tables 3.1** & **3.2**. The used cement was in accordance with the Specification of Iraqi Standard **(IQS No. 5/2019).**

Figure (3.2): - Ordinary Portland Cement

Table 3.1: Chemical composition and main compounds of the cement*

Compound composition	Percentage by weight	Limit of Iraqi specification No.5/2019	
Lime (CaO)	61.52	-	
Silica(SiO2)	21.67	-	
Alumina(Al2O3)	5.33	-	
Iron oxide (Fe2O3)	3.31	-	
Magnesia (MgO)	2.97	$\leq$ 5.0	
Sulfate(SO3)	2.51	$\leq$ 3.5	
Loss on ignition (L.O.I.)	3.14	$\leq$ 4.0	
Insoluble residue I.R.	0.91	$\leq$1.5	
Lime saturation factor (L.S.F.)	0.86	(0.66 - 1.02)%	
Main compounds (Bogue's Equation)			
Tricalicum Silicate	C_3S	48.08	-
Dicalcium Silicate	C_2S	33.43	-
Tricalicum Aluminate	C_3A	7.53	-
Tetracalcium Aluminoferrite	C_4AF	10.06	-

***Chemical tests were conducted by the environmental laboratory in University of Babylon**

Table 3.2: Physical properties of the cement*

physical properties	Test result	Limit of IQS 5/2019
Fineness using Blains Air Permeability apparatus (cm^2/gm)	3100	>2500
soundness using autoclave method	0.19%	< 0.8%
setting time using vicats instrument **initial (minute)** **final (hours)**	 198 4.5	 > 45 min $\leq$ 10 hrs
compressive strength: **2 days (MPa)** **28 days (MPa)**	 18.4 43.75	 $\geq$10 $\geq$ 42.5

***Physical tests were conducted by the construction materials laboratory at the University of Babylon**

3.2.2 Fine Aggregate

The fine aggregates (sand) was imported from a neighborhood in Karbala region known as **(AL-Akhaidhir)**. The sand sieve analysis, physical and chemical characteristics are presented in **Tables 3.3** and **3.4** respectively. The sand properties meet the Iraqi Standard requirements **IQS No.45/ 1984**.

Table 3.3: Sieve analysis of sand*.

Sieve Size (mm)	Cumulative passing %	Limits of IQS No.45/1984 /zone (2)
10	100	100
4.75	100	90 - 100
2.36	94.85	75 - 100
1.18	86.6	55 - 90
0.6	58.44	35 - 59
0.3	29.75	8- 30
0.15	7.22	0-10

*** The test was carried out in the laboratory of construction materials at the University of Babylon.**

Table 3.4: Physical and chemical properties of sand*.

Physical properties	Test result	Limits of IQS No.45/1984
Specific gravity	2.65	---
Absorption %	0.93	---
Fineness modulus	3.03	---
Sulfate content %	0.16	$\leq 0.5\%$

*** The test was carried out in the laboratory of construction materials at the University of Babylon.**

3.2.3 Coarse Aggregate

Crushed gravel with 2.7 specific gravity has been used as a course aggregate in all mixes. The maximum size was 20 mm and was acquired from local sources in Iraq from a zone known as **(Al-Nibaai)** as indicated in **Figure (3.3)**. The particle distribution and properties of coarse aggregate were consistent with the (**IQS No.45/1984**) as shown in **Table 3.5**.

Table 3.5: Physical and chemical properties of the normal coarse aggregate*.

Sieve Size (mm)	Cumulative Passing %	Limits of IQS No.45/1984
20	100	100
19	78	85 - 100
14	46	---
10	22	---
4.75	1	0 - 25
Chemical properties		
Sulfate content %	0.04%	≤ 0.1%
Specific gravity	2.7	----

*** The test was carried out in the laboratory of construction materials at the University of Babylon.**

Figure (3.3): - Crushed gravel

3.2.4 Ground Granulated Furnace Slug (GGBS)

Ground granulated blast furnace slag (GGBS) was produced by Hanson Cement-UK (see **Figure (3.4)**), GGBS chemical analysis and physical characteristics satisfied **BS EN 15167-1: 2006**, and **Table 3.6** illustrates the properties.

Table 3.6: GGBS chemical composition and significant substances*

Chemical Composition %	result	Limits of BS EN 15167-1: 2006
SiO_2	35.59	---
Al_2O_3	14.32	---
Fe_2O_3	0.35	---
CaO	41.95	---
MgO	7.41	≤ 18%
MnO	0.18	---
Mn_2O_3	0.20	---
TiO_2	0.55	---
St	0.94	---
S^{2-}	0.90	---
SO_3	0.09	≤ 2.5%
L.O.I.	0.66	≤3%
I.R.	0.18	---
C	0.08	---
Cl^-	0.01	≤ 0.1%
Glass content - XRD	2.90	
Relative Density g/cm^2	0.08	---
Fineness using Blains Air Permeability apparatus (m^2/kg)	393	≥ 275

*** Hanson Cement Company carried out these tests**

The GGBS replacement proportion employed in this experiment (0%,25%, 50%) by weight of OPC.

Figure (3.4): - The appearance and color of GGBS

3.2.5 Super-Plasticizer

In all concrete mixture, hyperplast PC200 a high-range water reducer (superplasticizer) was utilized by combining with water (see **Figure (3.5)**). Tap water was utilized for mixing. Furthermore, the total chloride ion concentration of the admixture was 0.1%, **BS EN 934-2:2009+A1:2012** compliant, and was employed at suggested doses of 0.2-0.4% by weight of binder to produce medium workability. The manufacturer recommended using (0.75-2) liters per 100 kg of cementitious material. **Table 3.7** & **Appendix A**1 list the key characteristics of the superplasticizer.

Table 3.7: Properties of the superplasticizer*.

Technical Description	Properties
Appearance	Light Brown liquid
Specific gravity	1.235 at 25± 2 ℃
Chloride content	Nil
Storage life	Up to one year in airtight container.

*** The results were given by the manufacturer.**

Figure (3.5): - Superplasticiser used in study

3.2.6 Steel

160 mm and 360 mm lengths of Ø10 mm steel rebars were used to reinforce the concrete prisms for the corrosion experiment.

3.2.7 Water

This investigation employed drinkable water from the water supply plant, which was free of residual and organic elements that might affect concrete qualities.

3.3 Mixtures Proportion for Concrete

The primary purpose of the study is to investigate the effects of chloride penetration and corrosion in steel rebars on optimum low-carbon concrete LCC. Also, to evaluate the influence of GGBS on the characteristics and durability of low carbon concrete LCC, several GGBS replacement percentage by mass of cement were utilised.

Fifteen mixes were developed with (0%, 25%, and 50%) GGBS substitution, with target mean strengths (25, 30, 35, 40, and 55) MPa. These mixtures were

designed according to Building Research Establishment (BRE) mix design method the ingredients quantity of each mix are listed in **Table 3.8**.

Table 3.8: Design of concrete mixture using the Building Research Establishment approach (1988)

Mix notation	w/cm	Content per concrete unit volume (kg / m^3)					Superplasticizer % *
		Water	Cement	Sand	Gravel	GGBS	
C(25,0%)	0.68	189	278	707	1261	0	0.2
C(25,25%)	0.68	189	208.5	707	1261	69.5	0.2
C(25,50%)	0.68	189	139	707	1261	139	0.2
C(30,0%)	0.55	189	344	640	1263	0	0.2
C(30,25%)	0.55	189	258	640	1263	86	0.2
C(30,50%)	0.55	189	172	640	1263	172	0.2
C(35,0%)	0.47	189	402	594	1251	0	0.2
C(35,25%)	0.47	189	301.5	594	1251	100.5	0.2
C(35,50%)	0.47	189	201	594	1251	201	0.2
C(40,0%)	0.3	189	630	471	1145	0	0.3
C(40,25%)	0.3	189	472.5	471	1145	157.5	0.3
C(40,50%)	0.3	189	315	471	1145	315	0.3
C(55,0%)	0.25	189	756	421	1069	0	0.4
C(55,25%)	0.25	189	567	421	1069	189	0.4
C(55,50%)	0.25	189	378	421	1069	378	0.4

*** Superplasticizer was used as percentage of cementitious mass**

3.4 Mixing, Curing and Preparation of Specimens

The mixing is performed by **BS EN 12390-2:2009** a pan-type laboratory mixing machine with a capacity of (250-300kg). Coarse and fine aggregates are

mixed together in the mixer for 1 minute. This step ensures a uniform distribution of the aggregates before adding other components. After that, 50 % of the required mixing water is combined with the aggregates and mixed for another minute. The purpose of this step is to moisten the aggregates and achieve initial hydration. Once the water and aggregates are mixed, cement and GGBS are added to the mixer. The mixer runs for 1 minute to thoroughly mix the cementitious materials with the moistened aggregates. This step ensures the uniform distribution of cement and GGBS throughout the mixture. Next, the superplasticizer (a chemical admixture used to improve workability) and the remaining water are added to the mixer. The superplasticizer helps in achieving the desired fluidity or workability of the concrete. The mixer operates for 1 minute to ensure proper dispersion of the superplasticizer and uniform mixing of all components.

Tight plastic moulds are used to shape the concrete samples. The interior faces of the moulds are oiled so prevent the concrete from sticking to them after it hardens, **Figures (3.6)** and **(3.7).** The concrete mix is poured into the moulds in three layers, every layer is compacted using a stick to remove any gaps or voids in the mixture. This ensures proper compaction and eliminates air pockets. In this experimental, different types of samples are cast using specific moulds, cubes100 mm are used to study the compressive strength of concrete, cylinders 100x200 mm are used to study the concrete's splitting tensile strength, cylinders (100x50) mm study the chloride penetration into concrete, prisms (100x100x400) mm to study impressed current corrosion, prisms (100x100x200) mm to study natural corrosion, and prisms (75x75x285) mm to study shrinkage for a different GGBS percent concrete mixes. After pouring the concrete into the moulds, the samples are left to cure for 24 hours within the moulds, then removed the concrete from the moulds and putted in a controlled curing room maintains a temperature about 22±2°C (degrees Celsius) and a relative humidity of 95%. The samples are left in

this environment for different durations: 28, 56, and 90 days, respectively, for the cylinders and cubes.

Figure (3.6): - Type of moulds used in the study

Figure (3.7): - Moulding and casting the concrete samples

3.5 Experimental Tests

3.5.1 Embodied Carbon Dioxide

The total quantity of carbon dioxide created during a substance's whole production process is known as embedded carbon dioxide (eCO_2). The values of eCO_2 for the main concrete elements, including reinforcing steel that are utilised to determine the eCO_2 for each mix design are shown in **Table 3.9**. The SCMs are byproducts and require less energy to create, they significantly lower eCO_2/kg

is to be expected. Although a kilogram of steel reinforcement produces CO_2 more than a kilogram of concrete, it does not have the same effect. Furthermore, research indicates that improvements in manufacture efficiency will result a significant reduction in CO_2 emissions from steel production in the coming years **(Association 2013). Table 3.10** demonstrates that using PFA (CEM II) and GGBS in place of Portland cement greatly reduces CO_2 emissions (CEM III).

Table 3.9: eCO_2 of reinforced concrete components from sources in the UK and Europe

Constituents	kg eCO_2/tonne	Reference
Portland Cement CEMI	913	(MPA , 2015)
PFA	4	(MPA , 2015)
GGBS	67	(MPA , 2015)
Silica Fume	14	(MPA , 2015)
Limestone[1]	75	(MPA , 2015)
Aggregate (Uncrushed)	~ 5	(MPA , 2009)
Sand	~ 5	(MPA , 2009)
water	~ 1	(Bull, 2012)
superplasticizer	10	(Flower & sanjayan, 2007)
Reinforcing Steel[2]	1293	(Eurofer, 2013)
1: Information from a single UK provider		

Table 3.10: eCO_2 of common factory-made cement kinds in the UK (MPA, 2015)

Combinations	Secondary-main	kg eCO_2/tonne
CEM I	-	913
CEM II/A-V	6-20 (fly ash)	858-731
CEM II/B-V	21-35 (fly ash)	722-595

Combinations	Secondary-main	kg eCO_2/tonne
CEM II/B-S	21-35 (GGBS)	735-617
CEM III/A	36-65(GGBS)	608-363
CEM III/B	66-80(GGBS)	354-236

3.5.2 Fresh Concrete Tests

3.5.2.1 Slump Test

Test of slump conducted on concrete in fresh form to determine its consistency and workability. The test follows specific procedures outlined in standards such as the American Standard **ASTM C 143/C 143M-05** as shown in **Figure (3.8)**.

The equipment used for the slump test includes a metal slump cone with height of 30 cm, top diameter 10 cm, and 20 cm base diameter. The cone is placed on the base plate during the test and they should be clean and free from any debris or hardened concrete.

The fresh concrete is poured into the slump cone in the form of three equal layers. Each layer should be compacted using a metal tamping rod with of 600 mm length and 16 mm diameter, with one rounded end. Once the three layers are compacted, the slump cone slowly lifted up vertically in a straight motion and placed near the concrete, the height difference is measured using a length measuring tool.

Figure (3.8): - Slump test for concrete mixture

3.5.3 Tests Methods of Hardened Concrete

3.5.3.1 Compressive Strength Test

Test of compressive strengths for concrete is achieved according to **BS EN 12390-3:2009**. Involving this test by using 2000 kN capacity digital machine of testing, as depicted in **Figure (3.9)**. Three cubes measuring 100×100×100mm are prepared for each mix at ages: 28, 56, and 90 days. The purpose of testing the cubes at different ages is to assess the concrete's strength development over time.

Figure (3.9): - The device used for testing concrete cubes under compression

The standard deviation and mean value of three specimens are determined. The compressive strength values are computed as shown in **Equation (3-1)**:

$$\sigma = P/A \qquad \textbf{(3-1)}$$

where:

σ: concrete compressive strength, measured in MPa (N/mm^2)

P: failure maximum load, N

A: specimen cross-sectional area on where the acts of compressive force, mm^2

3.5.3.2 Splitting Tensile Strength

According to the specifications provided in **BS EN 12390-6:2009**, Splitting Strength test of concrete is standardized. This test is carried out to assess the concrete's ability to resist tensile stresses perpendicular to its axis. For every concrete mixture, three cylindrical specimens with dimensions of Ø100 x 200

mm are prepared. These specimens are tested at two different ages: 28 days and 90 days. To perform the test, two plywood bearing strips, each measuring 3 mm thickness, 200 mm length, and 25 mm width, are placed underneath and at the top of the cylindrical specimen. The specimen is then positioned between the bearing blocks of 2000 kN capacity testing machine. This configuration is illustrated in **Figure (3.10)**.

For each concrete mixture, the average splitting tensile strength at age 28 days and 90 days is measured by taking the average of the results obtained from the three cylindrical specimens tested at every age. The splitting strength is determined by using **Equation (3-2)**:

$$f_{SP} = \frac{2F}{\pi d_c L} \qquad \textbf{(3-2)}$$

Where:

f_{sp}: strength of splitting tensile, in (MPa)

F: Maximum load in splitting test applied, in (N).

d_c: diameters Cylinder, in (mm).

L: lengths Cylinder, in (mm).

Figure (3.10): - Splitting tensile test

3.5.3.3 Ultrasonic Pulse Velocity Test (UPV)

In the context of determining the UPV of concrete, the direct transmission method is employed. UPV is a non-destructive test that allows for the evaluation of concrete properties without causing damage to the tested concrete element. The same cube specimens that used for the compressive strength test are utilized. For each mix, triplicate samples of cube (100 x 100 x 100) mm were casted. These samples are examined at 28 days, 56 days, and 90 days after the curing process.

The Portable Ultrasonic Concrete Tester, also known as PUNDIT, is utilized for the UPV measurements. **Figure (3.11)** represents the appearance of the PUNDIT instrument. Before conducting the tests, the PUNDIT device is calibrated to ensure accurate transit time measurements. This calibration involved the use of a reference bar. The tested surface of the concrete specimens is coated by A thin layer of grease. This grease acted as a couplant, facilitating the transmission of ultrasonic energy and preventing dissipation.

In the ultrasonic pulse velocity equipment (UPV) has two piezoelectric transducers, one introduces the pulses into the concrete, and the other transducers acts as a receiver to monitor the velocity of the pulse within the concrete. The nominal frequency of the transducers used to test concrete cubes is 54 kHz, and transmission time was measured in microseconds with an accuracy of 0.1 s. This test was followed **BS EN 12504-Part 4:2012** and The Pulse Velocity is determined by using **Equation (3-3).**

$$V = \frac{L}{t} \qquad \textbf{(3-3)}$$

Where:

V: pulse velocity, in (km/s).

L: space between transducers, (km).

t: time of effective transmit, (s).

Figure (3.11): - Ultrasonic pulse velocity test

3.5.3.4 Dry Shrinkage Test

The length change test method, as per **ASTM C157/C157M, 2004 and ASTM C490, 2004**, enables the assessment of volumetric expansion or shrinkage of concrete that is not caused by applied forces but rather by factors such as changes in moisture content.

For this test, prisms of concrete with dimensions of (75×75×285) mm are used. These prisms have pins that extend 17.5 mm into both specimens ends to facilitate measurements of length change. **Figure (3.12-a)** illustrates the setup with the concrete prism and the pins.

To monitor the change in length, a comparator is employed at designated test times, as depicted in **Figure (3.12-b)**. The comparator allows for precise measurements of length change at specific intervals. Two specimens are prepared for each test condition, ensuring that multiple measurements can be taken to obtain reliable and representative results. The change in length is determined using **Equation (3-4):**

$$\Delta L_X = \frac{(Lx - Li)}{G} \times 100 \qquad \textbf{(3-4)}$$

Where:

ΔLx: lengths Change at age x

L_x: Specimen comparator readings at age x, in (mm)

L_i: Specimen first comparators readings, in (mm)

G: Length of Nominal gages, (250mm)

(a) **(b)**

Figure (3.12): - (a) Pin extend into the both ends of the specimens, (b) Dry shrinkage test

3.6 Durability of Concrete Tests

3.6.1 Water Absorption

The water absorption test is conducted to evaluate certain physical properties of concrete specimens. The properties being measured include absorption of water (WA), porosity of concrete (PR), dry density of concrete (ρ_{dry}), and concrete wet density (ρ_{wet}).

The test procedure follows the guidelines outlined in **ASTM C642: 2013**, which is a standard method for determining the permeable voids in hardened concrete and assessing its resistance to moisture penetration. The test is performed on three 100 mm cubic concrete specimens for each concrete mixture being evaluated. The specimens are tested at various ages of curing: 28, 56, and 90 days and the average values of the physical properties are recorded for each age. After curing period, after removed the specimens from water immersion and are dried in oven for 24 hours at 105 ± 5°C until they reach a consistent mass.

After removing the specimens from the oven, they are left in the air at room temperature until they reach stabilization and the dry mass (M_{dry}) is obtained. After that each specimen is fully flooded in tap water and left for 24 hours to allow water absorption, then the specimens out from water tank and wiped with a piece of cloth to clear away any excess surface water, and the weight of the saturated surface dry (SSD) specimen is obtained. This weight represents the saturated mass (M_{sat}). The hydrostatic balance is used to measure the specimens submerged mass (M_{sub}).

Figure (3.13) likely illustrates the steps involved in the water absorption test, providing a visual representation of the process.

(a)

(b)

(c)

Figure (3.13): - (a)The weight of saturated dry surface specimen, (b) Specimen in oven to get dry weight, (c) The specimen weight that flooded in water

The physical properties calculation is determined by using **Equations (3-5), (3-6), (3-7)**, and **(3-8)**, with water density ρw =1.00 g/cm3:

$$WA(\%) = \frac{M_{sat} - \mathrm{M}_{dry}}{\mathrm{M}_{dry}} \times 100 \qquad \textbf{(3-5)}$$

$$PR(\%) = \frac{M_{sat} - M_{dry}}{M_{sat} - M_{sub}} \times 100 \quad \textbf{(3-6)}$$

$$\rho dry(g/cm^3) = \frac{M_{dry}}{M_{sat} - M_{sub}} \times \rho w \quad \textbf{(3-7)}$$

$$\rho_{wet}(g/cm^3) = \frac{M_{sat}}{M_{sat} - M_{sub}} \times \rho w \quad \textbf{(3-8)}$$

3.6.2 Chloride Ion Penetration Setup

The primary goals of this test are to examine the impact of using GGBS as a cement replacement material on the durability of concrete by measuring the chloride penetration and chloride content in low carbon concrete LCC.

3.6.2.1 Chloride Migration Test

The chlorides ions penetration in concrete is accelerated by this test, the test is conducted according to Nordtest method "chlorides migration coefficient in concrete (**NT Build 492:1999)**. For each mixture, three concrete specimens (Ø100mm×50 mm height) are casted and moist-cured for 28 days as shown in **Figure (3.14).** The samples are placed in vacuum container (see **Figure (3.15)**). Both end surfaces of the sample should be exposed, and absolute pressures in the vacuum vessel must be increased to pressure range of 1–5 kpa with a several minutes, and the vacuum must be remained for 3 hours. The pump of vacuum is then kept running to fill the vessel with saturated solution of CaOH2 (by different pressure between the vacuum container and the other container contain $Ca(OH)_2$) so as to immerse all the specimens to avoid the leaching of $Ca(OH)_2$. Keep the vacuum on for an hour before releasing the air back into the container. After soaking the specimens in lime solution for 18 ± 2 hours and then, the migration of chloride penetration is accelerated by using an electrically circle on solutions of two distinct, NaCl and NaOH, following **NT Build 492:1999**. Each specimen drill in cylinder rubber tube **Figure (3.16)** and fitted by two clamps. The rubber tube filled with 300gm solution of sodium hydroxide (0.3N NaOH) and fixed in

tank containing sodium chloride solution (10% NaCl by mass) **Figure (3.17)**, where electrode in NaOH solution becomes an anode and electrode in NaCl solution acts as a cathode.

Figure (3.14): - Samples of concrete for chloride migration

Figure (3.15): - Vacuum container

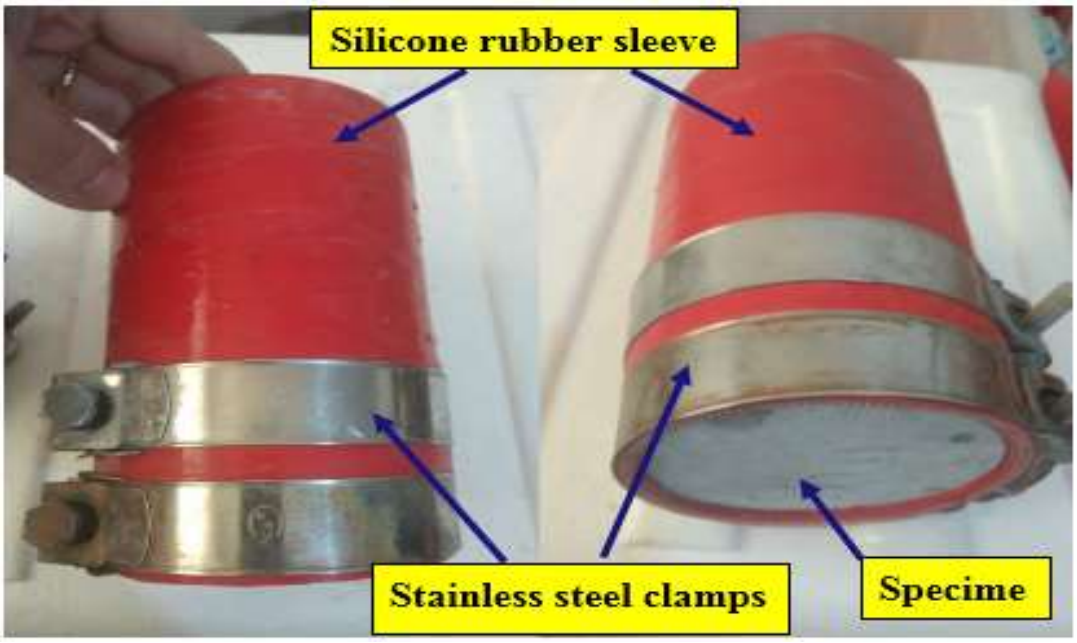

Figure (3.16): - Cylender rubber tube

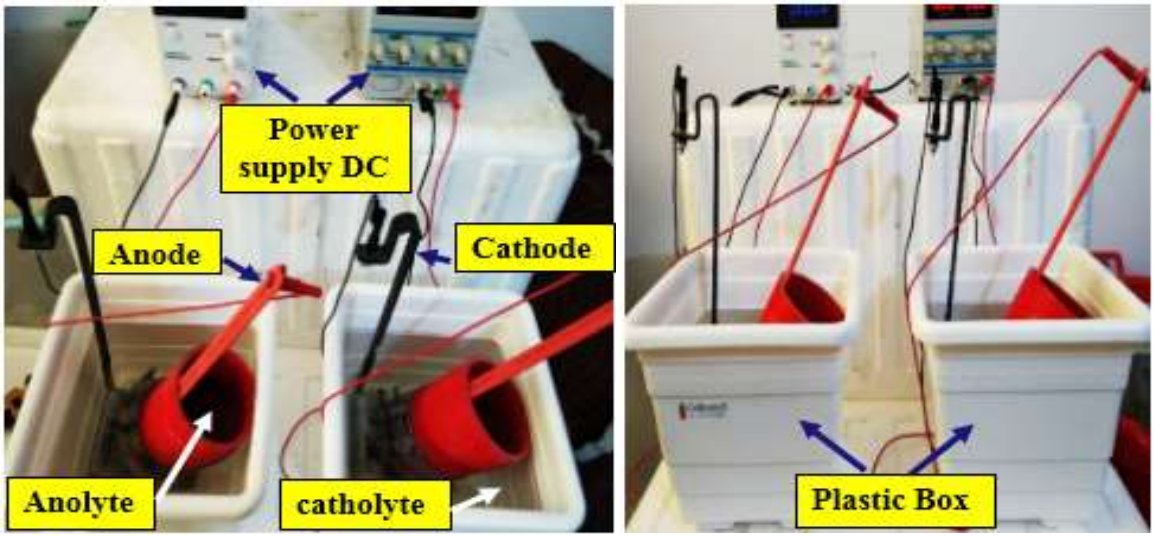

Figure (3.17): - NT Build 492 (1999)

These tests are based on measuring the depth of chloride ion, x_d which is investigated by spraying silver nitrate ($AgNO_3$) solution of a certain concentration of 0.1 N on the split cylinder sample and measured the chloride penetration (x_d) that caused by the reaction between Cl^- and Ag^+ to find chloride penetration depth for concrete prism. The chloride penetration depth in short cylinder can be employed to calculate the diffusion coefficient for non-steady state migration (D_{nssm}) as shown in **Equation (3-9)**:

$$D_{nssm} = \frac{0.0239(273+T)l_t}{(U_v-2)t}\left(x_d - 0.0238\sqrt{\frac{(273+T)l_t\, x_d}{U_v-2}}\right) \quad \textbf{(3-9)}$$

where:

T: final and initial temperature mean in anolyte part (NaOH)

l_t: would be specimen thickness in mm,

x_d : the means of chloride penetration depth(mm),

t: time and

Uv: applied voltage (V).

3.6.2.2 Chloride Penetration

Concrete prism of 100 mm x100 mm x 200 mm reinforced with 160mm steel bar length with Ø10 diametar is used for each mix to determine the depth chloride penetration x_d. Firstly, one face of the sample (the opposite side of the reinforcement) is subjected to specific environmental condition (drying and wetting cycles used), while the other faces are covered by coating of water proofing based (its properties listed in **Appendix A1**) (see **Figure (3.18)**). These specimens of concrete are put into an indoor tank with 5% solution of NaCl as shown in **Figure (3.19)**. A cycles of drying–wetting mechanism with 14 days wetting and 7 days drying in each cycle is done to all specimens to accelerate the corrosion process within a periodical of wetting and drying for 120 days in total.

After nearly 120 days, the specimens of concrete were raised from NaCl solution tank and putted in a shady place (see **Figure (3.20)**). All specimens were broken to obtain the corroded steel bars as shown in **Figure (3.21)**. Then all steel bars are cleaned.

Figure (3.18): - Coating the prism by water proofing based

Figure (3.19): - Pool contain 5% by weight NaCl solution

Figure (3.20): - Out the prism from 5%NaCl solution and put it in a shady place

Figure (3.21): - Measure the chloride penetration

3.6.2.3 Accelerated Corrosion by Impressed Current Test

The steel bars used in the specimens are cut and weighed. This weight measurement serves as a reference to evaluate the mass loss resulting from corrosion. To facilitate the measurement of corrosion, the steel bars are tagged to identify and track them throughout the testing process.

In addition, copper wires are drilled into the prism and inserted the steel bars. These wires serve as electrical connections for monitoring purposes. They are soldered and securely attached, and a changer resistor is included to ensure proper electrical connectivity as shown in **Figure (3.22)**. During the concrete casting process, the steel reinforcement (rebar) is inserted into the wet concrete while the

mixture is being vibrated. This ensures adequate compaction of the concrete around the rebar, providing a strong bond between the concrete and the reinforcement.

It is important to note that, during the hardening process of the concrete, the steel rebar may smoothly settle or tilt. That is considered normal since the rebar is supported only by the fresh concrete. These minor movements do not significantly impact the overall integrity of the specimen.

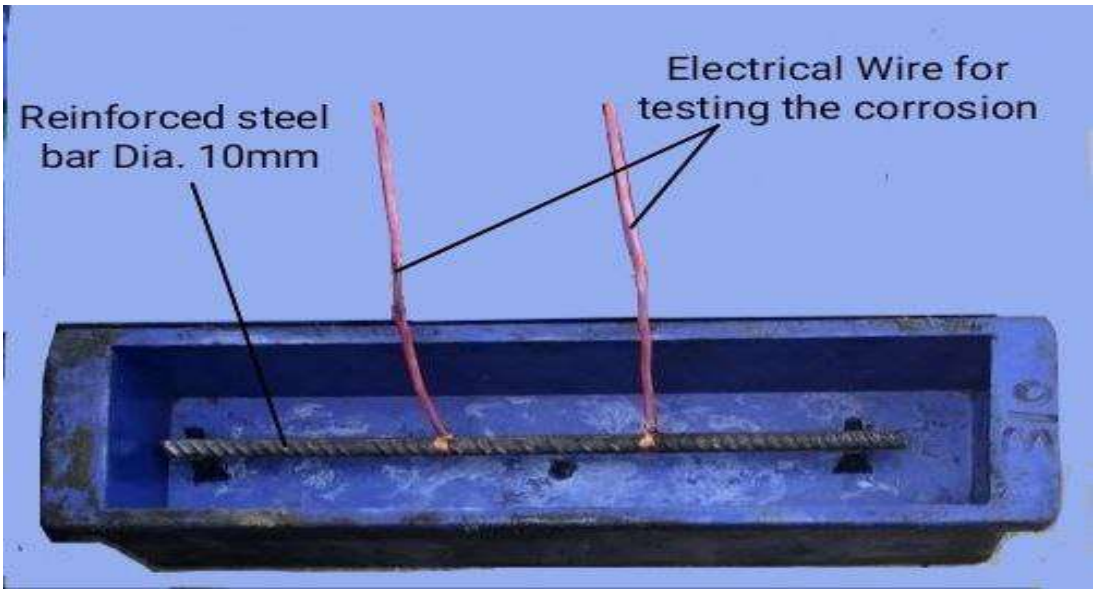

Figure (3.22): - Mould and steel bar to corrosion test

After 24 hours the hardened concrete prisms are removed from moulds and cured for 28 days after completing the curing period the concrete samples are removed from the curing tank and placed together in a plastic tank specifically designed for this purpose.

The plastic tank is filled with a 5% NaCl (sodium chloride) solution, which means that for every 950g of water, 50g of NaCl (salt) is added. This concentration of salt is intended to simulate the corrosive conditions of seawater. The addition of salt to the water lowers its electrical resistance and provides chlorides, which are known to contribute to the corrosion process. In the tank, the solution approximately covers the half bottom of the prisms, while the half top

remains air exposition. It is important noting that the level of the solution in the tank is marked to ensure consistency throughout the testing period. This is important because some evaporation of the solution may occur over time, and maintaining the proper solution level ensures consistent exposure conditions for the specimens.

Figure (3.23) and **Figure (3.24)** likely illustrate the arrangement and setup of the plastic tank with the prisms immersed in the salt solution, providing a visual representation of the experimental setup.

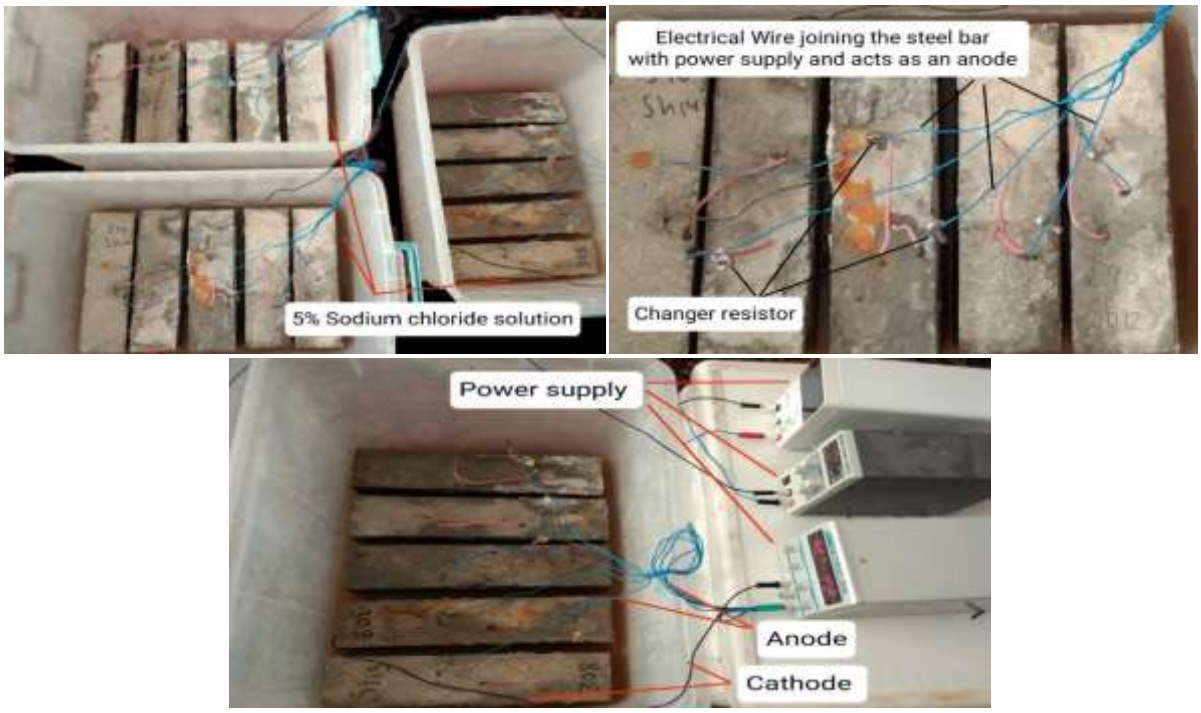

Figure (3.23): - Experimental setup

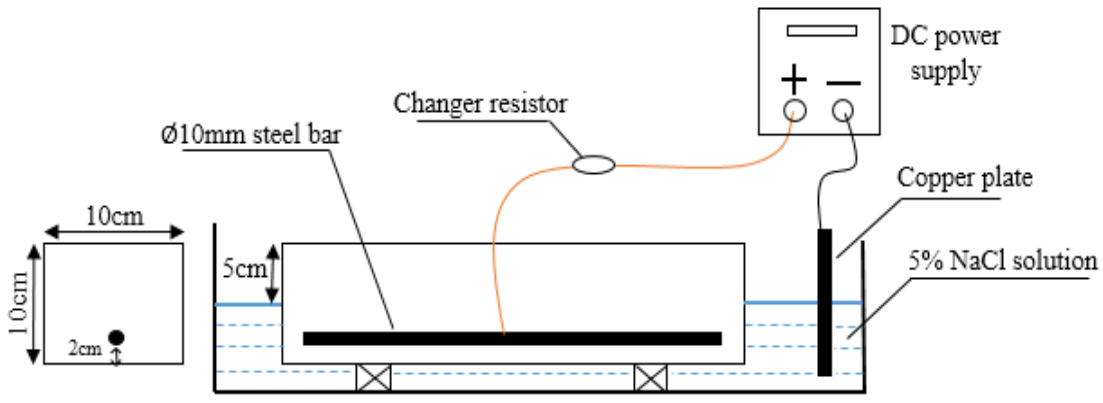

Figure (3.24): - Schematic of experiment setup

Then the wires are connected in parallel to a constant ampere DC power supply. The specimens are introduced to accelerate corrosion process in the same tank by connecting the fitted wires in parallel circuits to a constant current (33.93 μA) till the end of test duration.

The impressed current and required time to create 10% degree of corrosion in steel rebar are determined according to Faraday's Low as in **Equation (3-10):**

$$t = (m \times z \times F)/(M \times I) \qquad \textbf{(3-10)}$$

Where:

$t = time\ (second)$

$m = mass\ loss\ due\ to\ corrosion(gm)$

$z = valance\ (2)$

$F = faradays\ constant\ (96480\ A.sec.)$

$M = metal\ atomic\ weight\ (55.85)$

$I = imposed\ current\ (A)$

$Total\ steel\ rebar\ length\ = 36\ cm$

$Steel\ rebar\ density\ = 7.85 gm/cm^3$

$Mass\ of\ steel\ rebar\ = 7.85 \times \pi \times (0.5)^2 \times 36\ = 221.95\ gm$

$10\%\ corrosion\ degree\ = 0.1 \times 221.95\ = 22.195\ gm$

$Apply\ corrosion\ current\ density\ (icorr) = 0.3 mA/cm^3$

$I\ = 0.3x2x0.5x\ \pi x36\ = 33.93\ mA$

$t = (22.195x2x96480)/(55.85x33.93)\ = 26\ days$

The current is induced using a constant ampere (33.93 A) power source DC joined with ammeter to monitor the current. The current direction is changed, such that the steel bar served as an anode and a stainless steel plate put in the tank in solution of sodium chloride acted as a cathode.

The steel reinforcing bars are exited after 26 days, cleaned of rust using a shot blast and a stiff brush of metal, and weighed to ascertain the actual mass loss of the steel reinforcing bars (see **Figure (3.25)**)

Figure (3.25): - The blast shooting machine used to clean the corroded bars

3.6.2.3.1 Cracks Width Measurement

Due to the corrosion of steel bar, cracks appeared on the surface of concrete specimen parallel to the steel bar, the cracks width is measured by using micro-crack as shown in **Figure (3.26).**

Figure (3.26): - Measuring the crack width

3.6.3 Chloride Concentration (Profile of Chloride)

The Volhard Titration is used to discover the chloride content in concrete according to **NT BUILD 208 -3:1996**. This test technique is used to determine the total content of chloride of concrete that has been hardened by soaking the concrete powder in a nitric acid solution and then performing Volhard Titration.

Theory of this test as follows:

- a liquid containing chloride ions and an excess of silver nitrate. Silver chloride precipitates from the chlorides.

$$Ag^{+} + Cl^{-} \rightarrow AgCl\ (s) \qquad \textbf{(3-13)}$$

- The surplus silver ions are titrated using a thiocyanate solution.

$$Ag^{+} + SCN^{-} \rightarrow AgSCN\ (s) \qquad \textbf{(3-14)}$$

- The development of a red iron(lll)complex indicates an excess of thiocyanate ions.

$$Fe^{+3} + SCN^{-} \rightarrow FeSCN^{+2} \qquad \textbf{(3-15)}$$

Preparation of test sample is based by Core drilling machine with a diameter of at least 16 mm used to take sample in depth (10,20,30, 40 and 50) mm from

the specimens (prism (100×100×200) mm) that used for natural chloride penetration test and taken the sample from corrosion region that occurred at the impressed current test specimens (prism (100×100×400) mm) shown in **Figure (3.27).**

Figure (3.27): - Core drilling to take the powder samples

Selected samples should be smashed with a Hammer or similar instrument to ensure that no material is wasted and processed in a mill (see **Figure (3.28)**) until a particle size of less than 0.1mm is produced as shown in **Figure (3.29)**.

Figure (3.28): - Convert the concrete to powder in grinding machine

Figure (3.29): - Concrete powder samples

The Procedure of the chloride concentration test can be carried out by:

- 1 gm from the sample is placed in 250 ml glass bottle, then distilled water about 20 ml is added and shacked the bottle to ensure the particles separate. The shake the bottle is done by magnetic stirrer.
- Add about 10ml concentrated nitric acid, shake the bottle by magnetic stirrer.
- Hot distilled water is boiled and shacked again.
- Cooled the mixture approximately 1 hour until room temperature is reached.
- The solution should Filtered and rinse the Filter 1% Nitric Acid twice and more.
- Add distilled water until the sample has same volume.
- two burettes are used, everyone with a volume 25 ml. The first one used for the solution of silver nitrate (0.1N) and the other for the solution of ammonium thiocyanate (0.1N).
- Add silver nitrate ($AgNO_3$, 0.1N) solution in excess from burettle, about 10 ml.

- (2-3) ml benzyl alcohol ($C7H_8O$) is added and (1) ml ammonium thiocyanate (NH_4SCN). (0.1N) solution insert the stopper into glass bottle and by magnetic stirrer, the bottle is shaked.
- The reaming amount of silver nitrate is titrated with saturated ammonium ferri-sulphate ($NH_4\ Fe(So)_2 \times 12H_2O$ about 400 g/l) solution. Shake the glass bottle by magnetic stirrer and maintain the process of titration at a slower speed while continuously intensively stirring until the solution is permanently faintly red.

Figure (3.30) and **Figure (3.31)** show the material used and the procedure of this test.

Figure (3.30): - Material used in this test

Figure (3.31): Steps of the test to find chloride content

The chlorides content (Cl^-% by mass of concrete powder) is then determined according to **Equation (3-11):**

$$Cl^- \% = 3.545 \frac{V_1 * N_1 - V_2 N_2}{m} \qquad \textbf{(3-11)}$$

V_1: silver nitrate solution amount was added (ml)

N_1: silver nitrate solution normality

V_2: ammonium thiocyanate solution added amount of during the titration (ml)

N_2: ammonium thiocyanate solution normality

M: powder sample weight (g).

3.6.4 Cementitious Mixture Apparent Chloride Diffusion

This test technique includes the measurement of the apparent coefficient of chloride diffusion in hardened mixtures of cementitious in the laboratory.

Depending on **BS EN 12390-11:2015** or **ASTM C 1556-11a: 2016**, the total chloride concentration profile was used to calculate (Da) the diffusions coefficient of apparent, and concentrations of surface(Cs).

The Da and Cs may be computed by minimizing the square differences between the experimental profiles of chlorides concentrations results and Second Law of Fick of the non-linear best fitting of **Equation (3-12)**, as shown in **Figure (3.32)**.

$$C(x,t) = C_i + (C_S - C_i)\left[1 - erf\left(\frac{x}{2\sqrt{D_a \cdot t}}\right)\right] \qquad \textbf{(3-12)}$$

where:

C (x, t) : concentration of Chlorides at depths (*x*) with time t; C_i : initial concentrations of chloride (% concrete mass); C_s: chlorides concentration at surface as % concrete mass; D_a : Coefficient OF diffusion of chloride (m^2/sec); *erf* : function of errors for partial eq. solution.

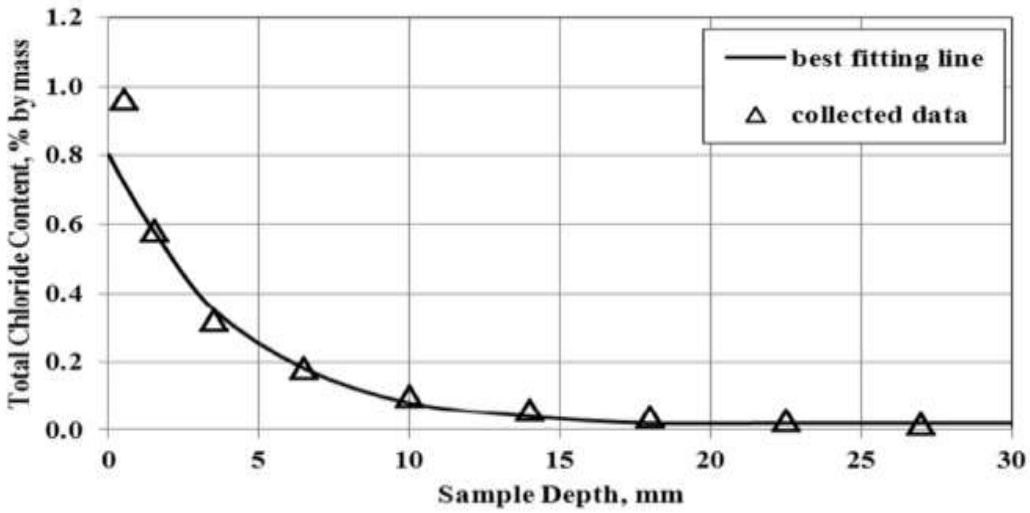

Figure (*3*.32): - BS EN 12390-11:2015 or ASTM C 1556-11a: 2016 chloride profile with fitted curves for surface chloride concentration

CHAPTER FOUR
RESULTS & DISCUSSION

CHAPTER FOUR

Results and Discussion

4.1 Introduction

In this chapter, the results of the experiments related to this study will be presented and discussed in detail. The effect of the cement replacement with (0%, 25% and 50%) GGBS on carbon dioxide emission will be investigated and computed. The results and their discussion will be presented, in terms the results of fresh concrete, mechanical, and durable properties concrete. slump test is for fresh concrete properties. Compressive strength, splitting, UPV, drying shrinkage are for hardened concrete test, and water absorption, chloride migration, chloride penetration, corrosion and chloride concentration are for durability tests.

4.2 Embodied Carbon Dioxide Calculation

Table 4.1: Embodied Carbon Factors

Concrete element constituent	CO_2/kg	References
water	0.001	**(Scottish Water 2008)**
cement	0.912	**(BCA, 2008; Hammond, 2008)**
GGBS	0.01	**Hammond, 2008**
FA	0.005	**Hammond, 2008**
CA	0.005	**Hammond, 2008**
SP	0.01	**(Flower & Sanjayan, 2007)**

The results listed in **Table 4.2** are based on the data in **Table 3.10** and **Table 4.1**, the CO_2/kg for each mix = [water content x 0.001+cement content x 0.912 + GGBS content x 0.01+ FA content x 0.005+ CA content x 0.005+ SP. Content x 0.01] / density of mix, and these results show an increase in eCO_2 values with the increase of strength concretes. This is to be anticipated when the cement content

rises and the w/c ratio falls. Otherwise, when eCO_2 values are compared to the intended mean strength, they exhibit a nonlinear behavior for mixtures because the nonlinear connection between strength and cement content is modified by the w/c ratios.

Table 4.2: Embodied carbon dioxide (eCO_2) calculation for mixes

Mixes	f_{cr}	CO_2/kg	CO_2/MPa
C(25,0%)	28.73	0.11	0.003766718
C(25,25%)	27.78	0.08	0.002969146
C(25,50%)	25.15	0.06	0.002256261
C(30,0%)	32.78	0.13	0.003709813
C(30,25%)	32.74	0.10	0.002904677
C(30,50%)	30.03	0.07	0.001971893
C(35,0%)	36.95	0.15	0.003782337
C(35,25%)	39.97	0.12	0.002931117
C(35,50%)	41.87	0.08	0.001908988
C(40,0%)	47.48	0.24	0.005037425
C(40,25%)	47.13	0.18	0.003838583
C(40,50%)	46.93	0.12	0.00261294
C(55,0%)	54.82	0.29	0.005216074
C(55,25%)	50.34	0.22	0.0042925
C(55,50%)	47.7	0.15	0.003064577

As a result, this modifies the popular misconception that larger cement percentage always has a greater environmental impact. Therefore, to achieve an

accurate depiction, it is preferable to compute eCO_2 based on the structural performances instead of total emissions.

Also, the results illustrate that the C(35, 25%) and C(35, 50%) mixes have the minimum eCO_2/MPa values compared to the other strengths that containing the same percentage of GGBS. The eCO_2/MPa decreases with the increase addition of GGBS, it appears that mixes with 50% GGBS have the most significant drop compared to the optimum strength of 35 MPa its 0.001935 CO_2/MPa. The data is also displayed graphically in **Figure (4.1)**.

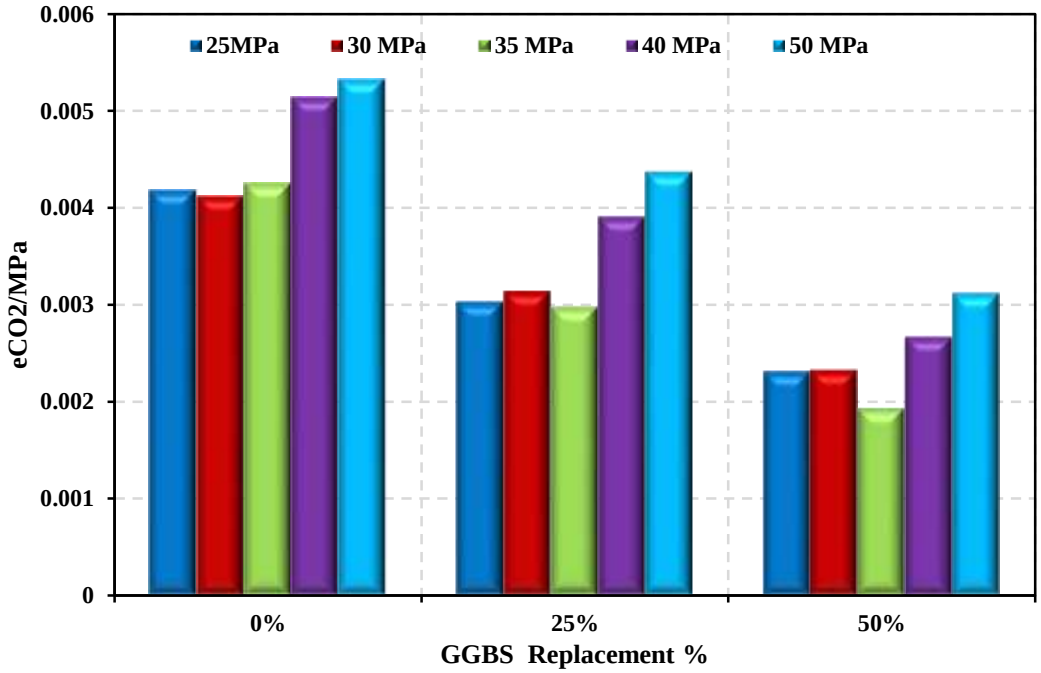

Figure (4.1): -The eCO_2/MPa for mixes with different percentage of GGBS replacement

4.3 The Fresh properties of Concrete

4.3.1 Slump test

It can be seen from **Table 4.3,** the slump values of concrete without GGBS were more than concrete containing GGBS and it decreases with the increase of GGBS replacement. The explanation of such behavior could be related to the differences in the fineness of GGBS and cement, as well as to the differences in

the amount of water absorption according to the fineness and surface area of GGBS, the larger surface area of GGBS needs more mortar to cover it, leading to less paste being accessible for lubrication, which ultimately decreases the workability of concrete. However, other research reported different physical properties of GBBS. The different properties of GGBS may be due to the various location sources of GGBS **(Ahmad et al., 2022)**. Moreover, the rough surface roughness and increased water absorption capacity of GGBS contribute significantly to the detrimental influence on the workability of concrete mixtures **(Patra & Mukharjee, 2017)**.

Table 4.3: The slump test result of LCC

Mix samples	Slump (mm)	Mix samples	Slump (mm)	Mix samples	Slump (mm)
C(25,0%)	55	C(25,25%)	48	C(25,50%)	40
C(30,0%)	58	C(30,25%)	50	C(30,50%)	42
C(35,0%)	60	C(35,25%)	52	C(35,50%)	43
C(40,0%)	58	C(40,25%)	49	C(40,50%)	32
C(55,0%)	45	C(55,25%)	38	C(55,50%)	28

4.4 Mechanical Properties

4.4.1 Compressive Strength Results

One of the most crucial characteristics of concrete is compressive strength. The test for all mixtures are experimentally carried out according to **BS EN 12390- 3:2000** by using 135 cube specimens (100x100x100) mm at age of 28, 56 and 90 days. Results for all mixtures are presented in **Table 4.4**.

Table 4.4: Mean compressive strength gains of concrete with different addition percentage of GGBS

Mixes	Compressive strength at age		
	28 days	56 days	90 days
C(25,0%)	28.73	29.75	36.22
C(25,25%)	27.78	31.31	42.26
C(25,50%)	25.15	40.37	41.47
C(30,0%)	32.78	40.2	42.90
C(30,25%)	32.74	42.20	42.69
C(30,50%)	30.03	37.44	41.28
C(35,0%)	36.95	41.55	44.76
C(35,25%)	39.97	43.06	43.73
C(35,50%)	41.87	49.24	49.84
C(40,0%)	47.48	47.55	49.56
C(40,25%)	47.13	50.82	50.99
C(40,50%)	46.93	48.79	51.44
C(55,0%)	54.82	56.67	57.77
C(55,25%)	50.34	52.38	54.73
C(55,50%)	47.7	49.71	57.92

Key observations from the compressive strength results are:

4.4.1.1 Effect of Age on compressive strength

There is a significant increase in the compressive strength with increasing the curing age at 56 and 90 days compared to 28days as shown in **Figure (4.2) &(4.3)**.

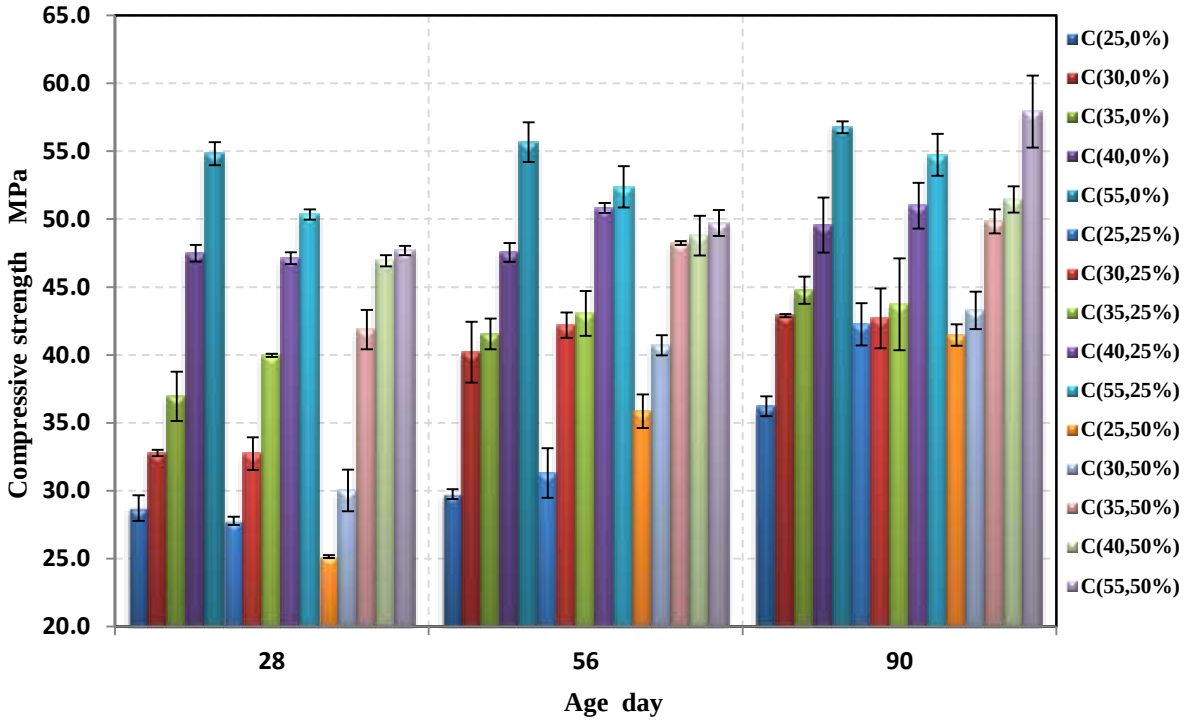

Figure (4.2): - Effect of age on compressive strength for concrete with difference percentage of GGBS replacements

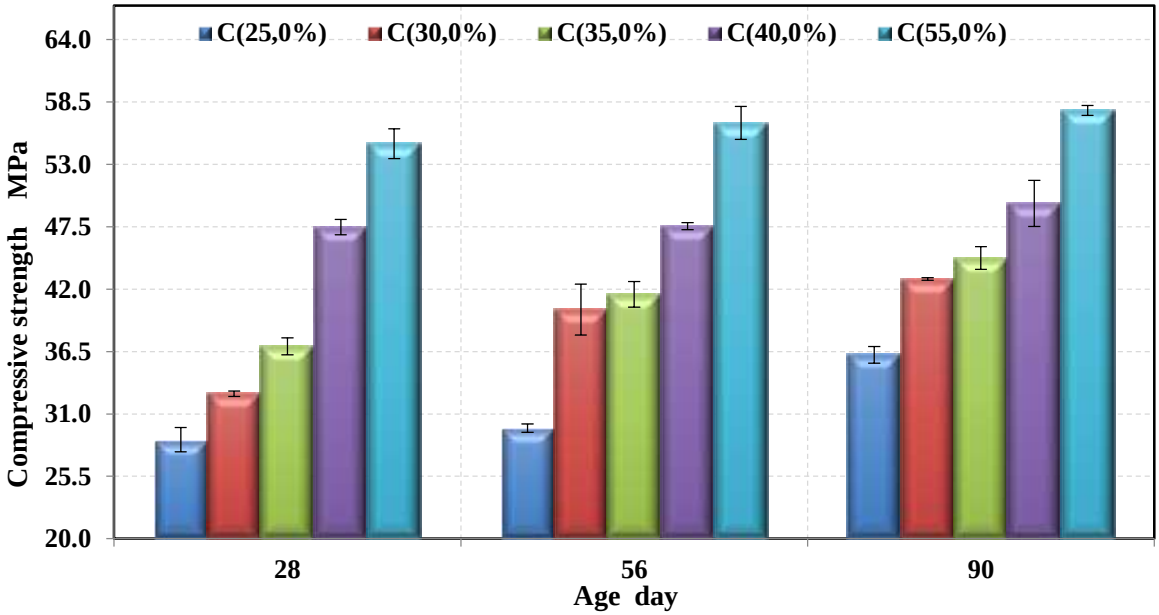

Figure (4.3): - The development of compressive strength with curing age for concrete mixtures with 0%GGBS

In **Figure (4.3),** it's clear that the compressive strength for mixes increased with progress of curing age. The increase in compressive strength with age is to

produce more C-S-H $_2$ due to cement hydration and improve the microstructure of concrete **(Neville, 2011).**

The increase percentages in compressive strength gain with curing period for (0, 25 and 50) % GGBS at age 56 and 90 comparing with 28days are presented in **Table 4.5**.

Table 4.5: The compressive strength increase percentages of mixes with different GGBS% with age

Concrete mixture	Increase in compressive strength% at age	
	56days	90days
C(25,0%)	3.55	26.07
C(25,25%)	12.71	52.11
C(25,50%)	42.54	64.89
C(30,0%)	22.64	30.86
C(30,25%)	28.88	30.39
C(30,50%)	35.56	44.12
C(35,0%)	12.44	21.14
C(35,25%)	7.72	9.39
C(35,50%)	15.21	19.02
C(40,0%)	0.15	4.38
C(40,25%)	7.83	8.18
C(40,50%)	3.95	9.61
C(55,0%)	1.54	3.55
C(55,25%)	4.05	8.72
C(55,50%)	4.20	21.42

The data show that C(40,0%) and C(55,0%) have a minimum development in compressive strength about 0.15% and 1.54% at age 56 days and 4.38% and 3.55% at age 90 days respectively because that with the curing age, the hydration rate of cement in concrete decreases, which resulting in a reduction of the growth

rate of concrete strength. While, the maximum increase percentages were 42.54% and 64.89% at age 56 days and 90 days respectively for mix C(25,50%). According to **(Li & Zhang, 2019)** the increase of strength is mainly related to the content of cement hydration and the degree of hydration. Hence, with the increase of GGBS content, the compressive strength of concrete specimens decreases at initial stage due to the reduction of hydration product of cement. When the curing age is more than 28 days, the pozzolanic effect of GGBS is taken gradually, and the active ingredient in GGBS reacts with the hydration products of cement to form a new cementing material C-S-H, which could improve the bond property of interface transition zone and the strength of cement stone.

4.4.1.2 Effect of Percentage Replacement of GGBS on compressive strength

The compressive strength for concrete with higher percentage of GGBS decreases at age 28 days of curing, but it increases with increasing the curing days. At early age, the reduction of compressive strength due to replacement the cement by GGBS may be associated to the efficiency factor and design of supplementary cementitious materials (SCMs) in concrete when it replaces by cement, that leads to the strength is reduced **(Papadakis & Tsimas, 2002)**. In the other hand, the pozzolanic reaction is slow and depends on the calcium hydroxide availability, the strength gain takes longer time for the GGBS concrete **(Lothenbach et al., 2012)**. The chemical reaction of the Portland cement is expressed as follows:

Cement compounds

$$(C3S, C2S) + H_2O\ (H) \rightarrow C\text{-}S\text{-}H + Ca(OH)_2\ (CH) \qquad \textbf{(4-1)}$$

The pozzolanic reaction is shown in **Equation (4-2) (Mehta, 1983; Memon et al., 2002)**;

$$Ca(OH)_2\ (CH) + SiO_2\ (S) + H_2O\ (H) \rightarrow C\text{-}S\text{-}H\text{–}gel \qquad \textbf{(4-2)}$$

The dissolved aqueous $Ca(OH)_{2(aq)}$ concentration in the solution of concrete depends on the degree of hydration, cement content and cement compounds, C_3S and C_2S **(Park, 2008)**. The total amount of Ca $(OH)_2$ in the solid phase of cementation composite is calculated from the chemical composition of the hydration of cement compounds, C_3S, and C_2S as shown in **Equations (4-3)** & **(4-4) (Neville, 2011; Ishida *et al*., 2014):**

$$2C_3S + 6H \rightarrow C_3S_2H_3 + 3CH \qquad \textbf{(4-3)}$$

$$2C_2S + 4H \rightarrow C_3S_2H_3 + CH \qquad \textbf{(4-4)}$$

where:

C_3S is Tricalcium silicate and its molar weight (228 g/mole), C_2S is Dicalcium silicate and its molar weight (172 g/mol) and *CH* is calcium hydroxide and its molar weight (74 g/mole).

Then;

$$C_{CH} = \frac{M_{CH}}{2*M_{C_2S}} * C_{C_2S} + \frac{3M_{CH}}{2*M_{C_3S}} * C_{C_3S} \qquad \textbf{(4-5)}$$

where:

C_{CH} is $Ca(OH)_2$ content, M_{CH}, M_{C_2S} and M_{C_3S} are molecular weight of $Ca(OH)_2$, C_2S and C_3S respectively, $C_{C_2S}$and C_{C_3S} are C_2S and C_3S percentage by weight of cement respectively.

So, the concentration of $Ca(OH)_2$ can be determined by cement content and degree of cement hydration by:

$$[Ca(OH)_2] = \frac{C_{CH}*C*\propto}{M_{CH}} \qquad \textbf{(4-6)}$$

where:

$[Ca(OH)_2]$ is $Ca(OH)_2$ concentration in mole/m^3 , M_{CH} is molecular weight of $Ca(OH)_2$ (74 g/mole), C is the weight of cement in m^3 and $\propto$ is hydration degree.

In the cement used in this study, the C_2S and C_3S percentages are 33.34% and 48.08% by weight of cement respectively and assuming the hydration of cement was (80,85 and 90)%, then [$Ca(OH)_2$] by :

$$[Ca(OH)_2] = 3.721\ C \ \ldots\text{for 90\% hydration degree} \quad \textbf{(4-7)}$$

$$[Ca(OH)_2] = 3.515\ C \ \ldots\text{for 85\% hydration degree} \quad \textbf{(4-8)}$$

$$[Ca(OH)_2] = 3.308\ C \ \ldots\text{for 80\% hydration degree} \quad \textbf{(4-9)}$$

Table 4.6 shows the amount of [$Ca(OH)_2$] that is calculated for different mixes.

Table 4.6: Calculation of $Ca(OH)_2$ content in solid phase

Mixes of concrete	Cement content(kg/m^3)	$Ca(OH)_2$ content according to degree of hydration(mole/m3)		
		80%	85%	90%
C(25,0%)	278	919.62	977.09	1034.57
C(25,25%)	208.5	689.71	732.82	775.93
C(25,50%)	139	459.81	488.55	517.28
C(30,0%)	344	1137.94	1209.06	1280.18
C(30,25%)	258	853.46	906.80	960.14
C(30,50%)	172	568.97	604.53	640.09
C(35,0%)	402	1329.80	1412.92	1496.03
C(35,25%)	301.5	997.35	1059.69	1122.02
C(35,50%)	201	664.90	706.46	748.01
C(40,0%)	630	2084.02	2214.27	2344.52
C(40,25%)	472.5	1563.01	1660.70	1758.39
C(40,50%)	315	1042.01	1107.14	1172.26
C(55,0%)	756	2500.82	2657.13	2813.43
C(55,25%)	567	1875.62	1992.84	2110.07
C(55,50%)	378	1250.41	1328.56	1406.71

As it can be seen from the above reactions, calcium hydroxide is produced by the hydration of Portland cement compounds and consumed by the pozzolanic reaction. The pozzolanic reaction can only take place after the Portland cement hydration starts **(Neville, 2011)**.

The percentage of replacement in the concrete mixtures has a significant influence on the compressive strength of the concrete samples. It can be seen that the mixture with the highest GGBS replacement percentage presents the highest increase in the compressive strength. This shows that as the GGBS content increases, the strength-gain increases in time. The compressive strength gains of the GGBS concrete mixtures are presented in **Figure (4.4)**.

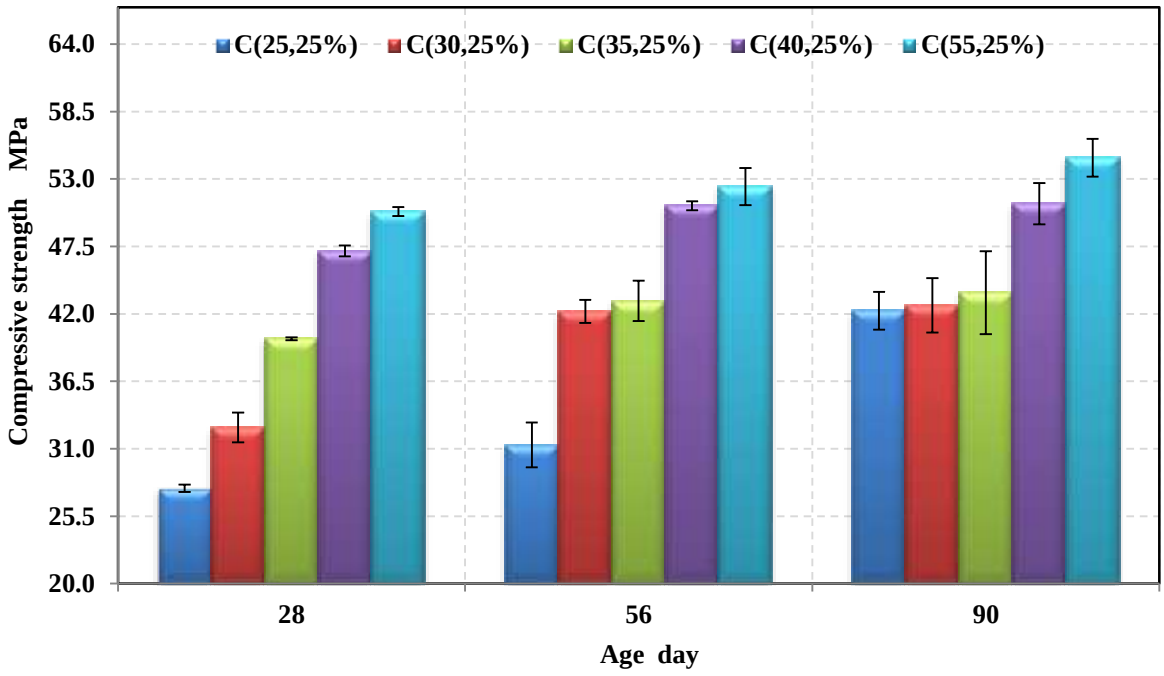

Figure (4.4): - Developing the compressive strength of concrete mixes 25%GGBS with progress in age

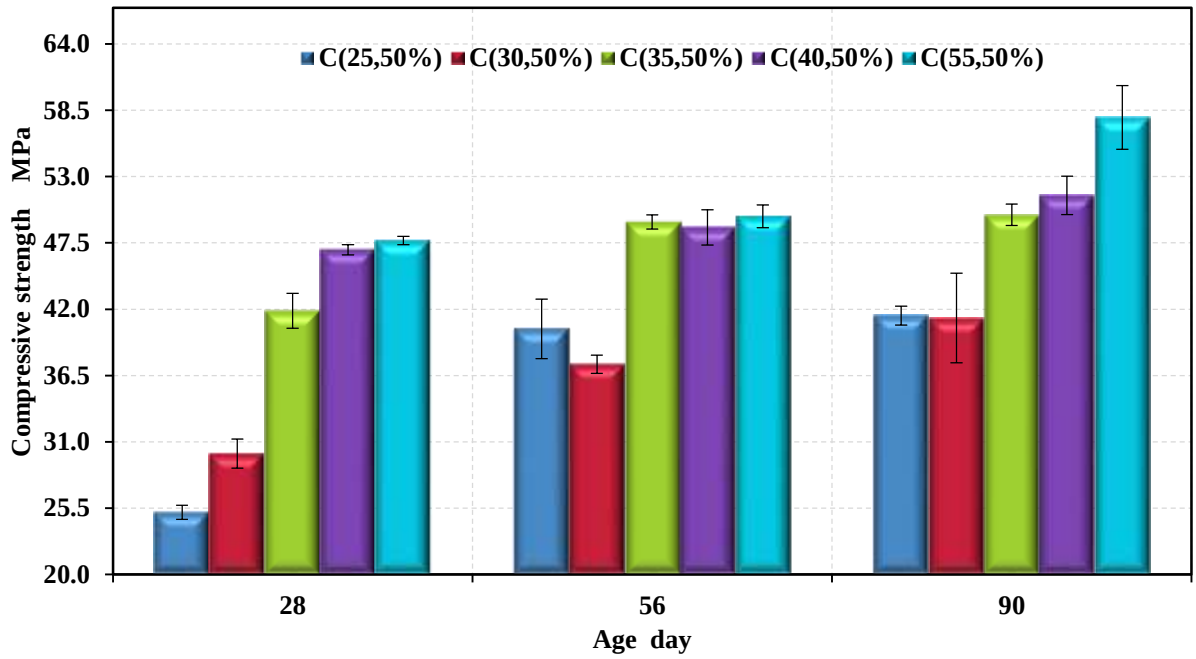

Figure (4.5): - Developing the compressive strength of concrete mixes 50% GGBS with progress in age

As shown in **Figure (4.4)** and **(4.5),** the compressive strength gains increases with curing age, but this increase depends on the GGBS% replacement.

4.4.2 Splitting Tensile Strength

The splitting strength is a method to find tensile strength of concrete indirectly and this test is considered one of the important properties of hardened concrete. The results for all concrete mixture are presented in **Table 4.7**, which illustrates the changes in splitting strength at various curing age and percentage replacement of GGBS.

Table 4.7: The splitting strength result of concrete mixtures with different GGBS percentage

Mixes	Splitting strength at age	
	28 days	90 days
C(25,0%)	3.12	3.36
C(25,25%)	2.51	3.48
C(25,50%)	2.65	2.97
C(30,0%)	3.2	3.58
C(30,25%)	2.9	3.86
C(30,50%)	2.85	3.06
C(35,0%)	3.08	3.67
C(35,25%)	2.63	3.52
C(35,50%)	3.06	3.82
C(40,0%)	2.78	3.28
C(40,25%)	2.67	3.78
C(40,50%)	2.58	2.76
C(55,0%)	3.22	3.6
C(55,25%)	2.95	3.69
C(55,50%)	2.4	3.11

The results will be presented according to the main factors affecting splitting strength as follows:

4.4.2.1 Effect of Age for Normal Curing

The increase in splitting strength with ages for concrete with 0%GGBS is illustrated in **Figure (4.6)**. The increase is 11.53%, 12.22%, 19.15%, 17.98% and 11.8% for C(25,0%),C(30,0%),C(35,0%), C(40,0%), and C(55,0%) respectively at 90 days compared to 28 days.

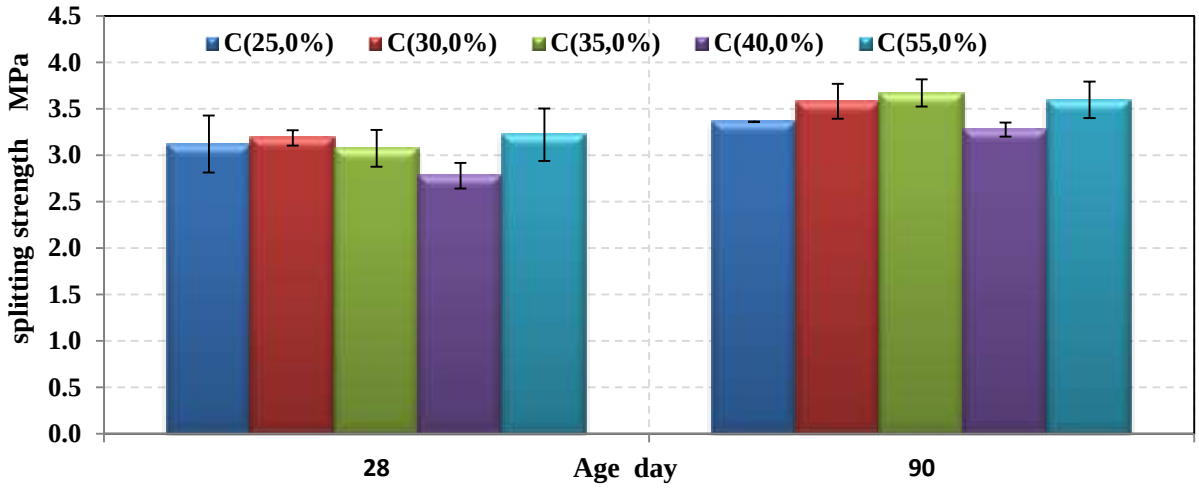

Figure (4.6): - The splitting strength of reference concrete

From **Figure (4.7),** it's clear that the splitting tensile strength increase for all mixes at age 90 days. Generally, the period of curing is acted to precipitate of C-S-H due to the cement hydration, increases the interfacial transition zones and improves that lead to improve splitting tensile strength with curing age and these results agree with other researches **(Chen and Kwan, 2012; Li and Kwan, 2015)**.

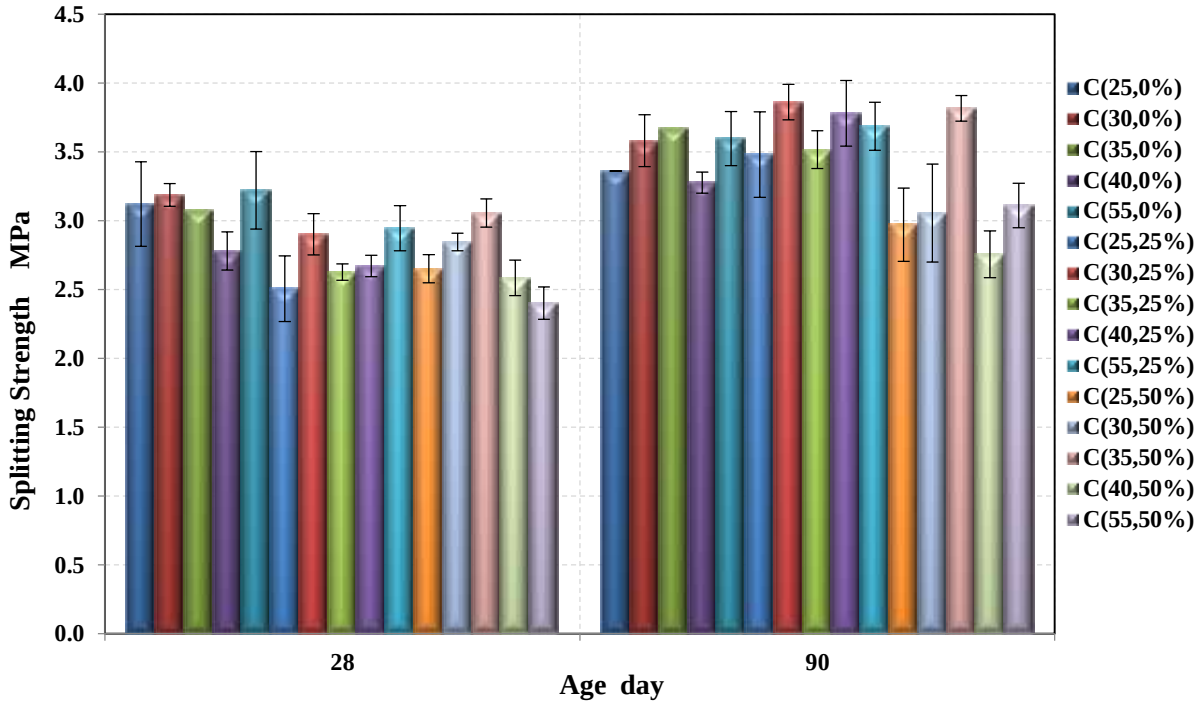

Figure (4.7): -The development of splitting strength with progress in age

4.4.2.2 Effect of Percentage Replacement of GGBS on splitting strength

The splitting tensile strength decreases in concrete contained GGBS% replacement when compared with mixes without GGBS at age 28. These reductions are 19.55%, 9.09%, 14.61%, 3.9% and 8.38% for mix C(25,25%), C(30,25%), C(35,25%),C(40,25%) and C(55,25%) respectively , 15.06%, 10.65%, 0.65%, 7.19%, and 25.46% for mix C(25,50%), C(30,50%), C35,50%), C(40,50%) and C(55,50%), but at age 90 days there are different behavior. There were an increase in the splitting tensile strength by 3.57%, 7.82%, 4.08%, 15.24% and 2.50 % for mixes C(25,25%), C(30,25%), C(35,25%), C(40,25%) and C(55,25%) respectively as shown in **Figure (4.8)**.While for mixes with 50% GGBS, the reductions in the splitting tensile strength are 11.6%, 14.52%, 4.08%, 15.85% and 13.61% for C(25,50%), C(30,50%), C(40,50%)and C(55,50%), but for mix C(35,50%) there is an increase about 4.08% as comparing with the same mixture without GGBS replacement, as illustrated in **Figure (4.9).**

This reduction in splitting tensile strength of mixtures at 28 days related to the slow hydration and slow development in the strength, however at age of 90 days, there is a significant increase in tensile strength gain for mixtures with 25% GGBS replacement related to the pozzolanic reaction **(Zhou et al., 2012)**.

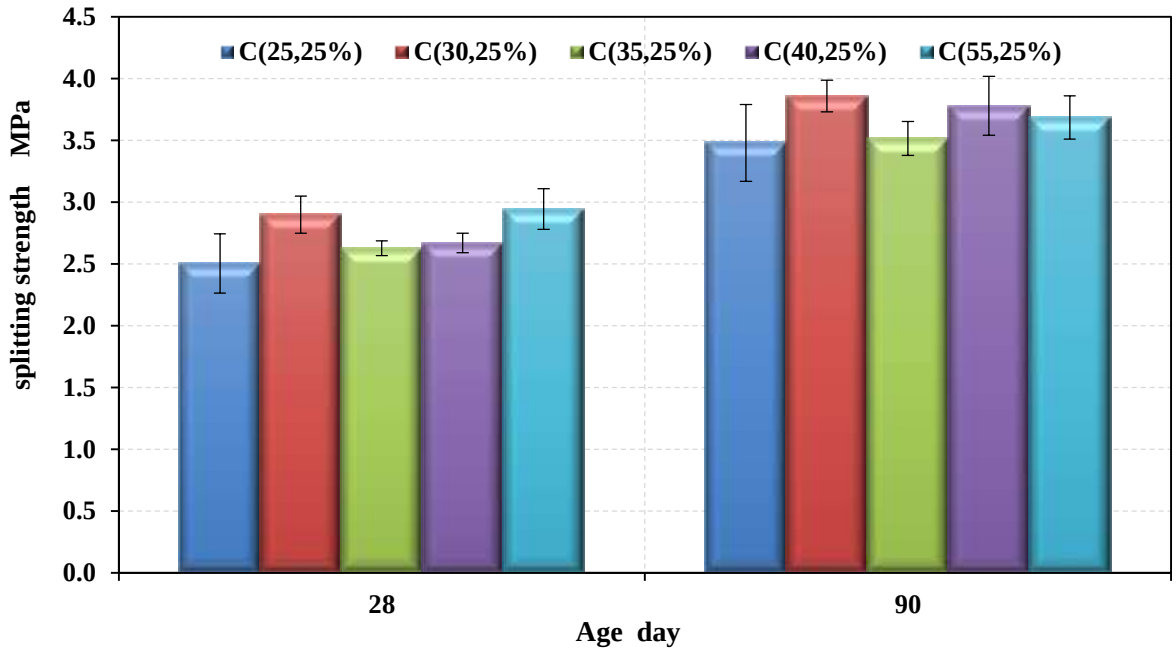

Figure (4.8): - The splitting strength of concrete with 25%GGBS

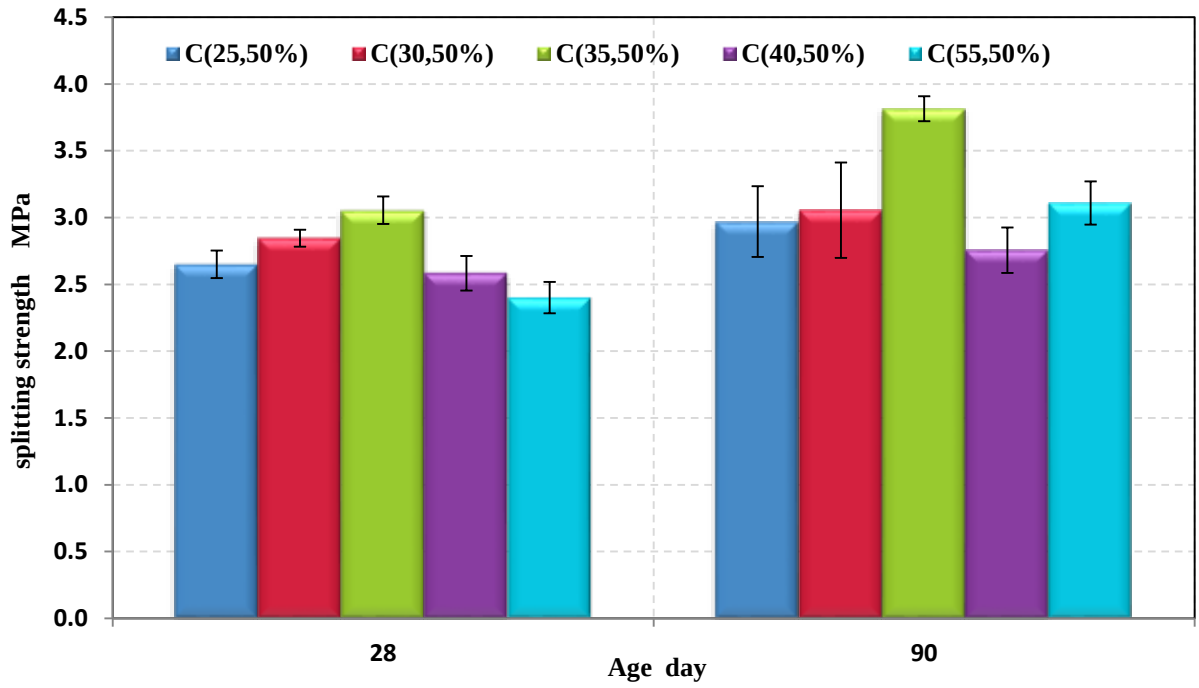

Figure (4.9): - The splitting strength of concrete with 50%GGBS

4.4.3 Ultrasonic Pulse Velocity Test

The ultrasonic pulse velocity test is conducted for hardened concrete and carried out at 28 ,56 and 90 days. The results values of ultrasonic pulse velocity test at various curing ages are presented in **Table 4.8**.

Table 4.8: The result of UPV test for concrete

Mixes	The average of UPV km/sec at age of		
	28 days	56 days	90 days
C(25,0%)	4.612	4.657	4.703
C(25,25%)	4.657	4.657	4.774
C(25,50%)	4.545	4.657	4.750
C(30,0%)	4.612	4.703	4.750
C(30,25%)	4.657	4.726	4.847
C(30,50%)	4.657	4.798	4.897
C(35,0%)	4.657	4.703	4.847
C(35,25%)	4.657	4.774	4.847
C(35,50%)	4.612	4.798	4.897
C(40,0%)	4.703	4.726	4.847
C(40,25%)	4.657	4.750	4.847
C(40,50%)	4.657	4.774	4.897
C(55,0%)	4.750	4.798	4.897
C(55,25%)	4.657	4.798	4.897
C(55,50%)	4.612	4.847	4.948

The main observations from the ultrasonic pulse velocity test results are:

4.4.3.1 Effect of Progress Age for Normal Curing

There is a clear increase in the ultrasonic pulse velocity with increase the curing age and with the increase in compressive strength as presented in **Figure (4.10).** The figure shows that mix C(55) record highest increase at age 90 days when compare with other mixes, while mixes C(35) and C(40) are equaled at age 90 days. As shown in **Figure (4.11)**, the increase in velocity of ultrasonic pulse with age due to increase the density of concrete because of cement and GGBS

reaction led to produce more C-S-H and Ca(OH)2 and improve the microstructure of concrete **(Véronique et al., 2005).**

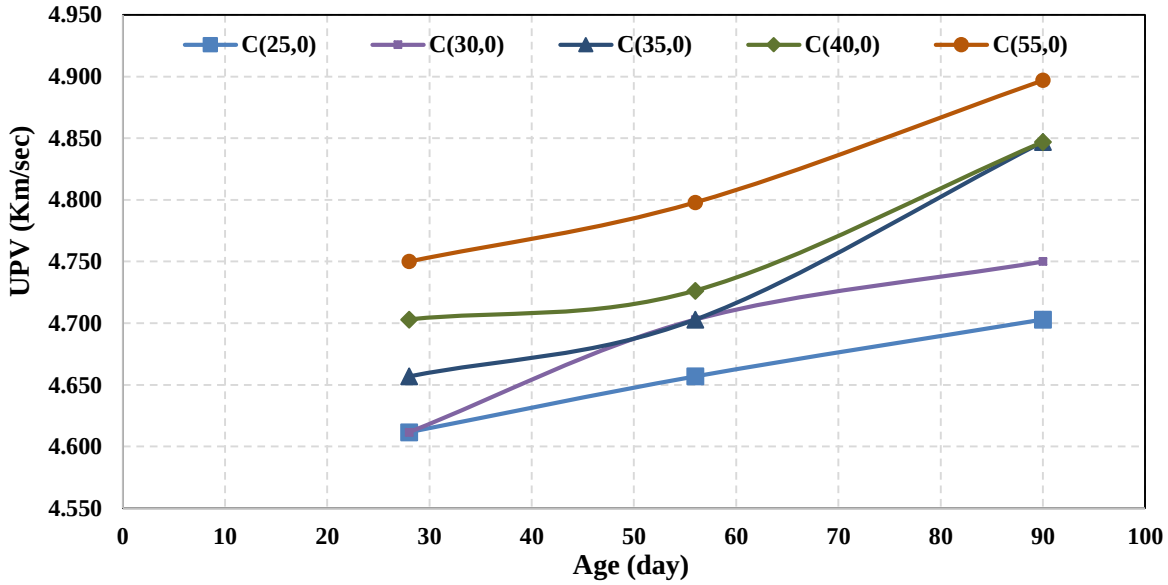

Figure (4.10): - Relationship between the age of curing and UPV for concrete mixtures with 0% GGBS

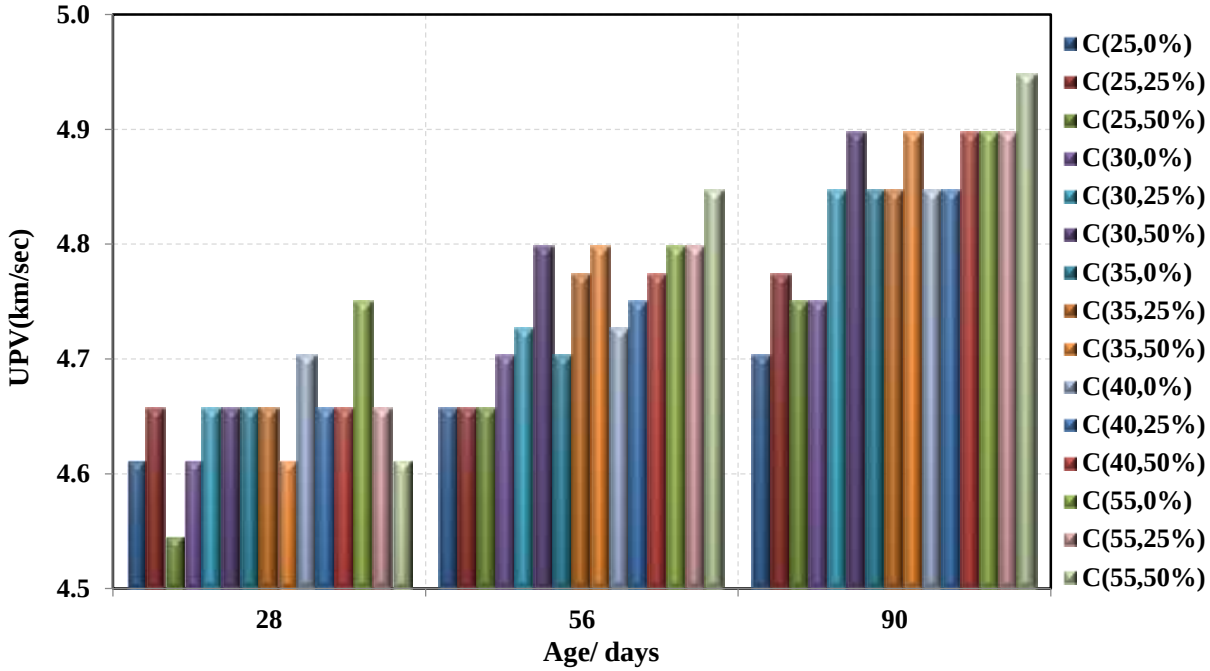

Figure (4.11): - Effect of age on velocity of ultrasonic test for mixture with different percentage of GGBS replacement

4.4.3.2 Effect of Percentage Replacement of GGBS on UPV

As determine in **Figure (4.11)**, **(4.12)** and **(4.13)**, the velocity of ultra-sonic pulse increase with the increase of curing time also with the increase of replacement percentage of GGBS.

The speed of the ultrasonic pulse increases with the increase in the percentage of GGBS utilization in the mixtures due to the increase in the interactions of the cement and GGBS and make a greater proportion of the CSH (calcium silicate hydrate) gel and much less lime (calcium hydroxide) in the concrete, when GGBS is used. The CSH gel is the binder that holds together the aggregates and gives concrete its strength, whereas the lime contributes little to concrete strength and this leads to fill voids in the concrete and increase its hardness **(Mukherjee et al., 2016)**.

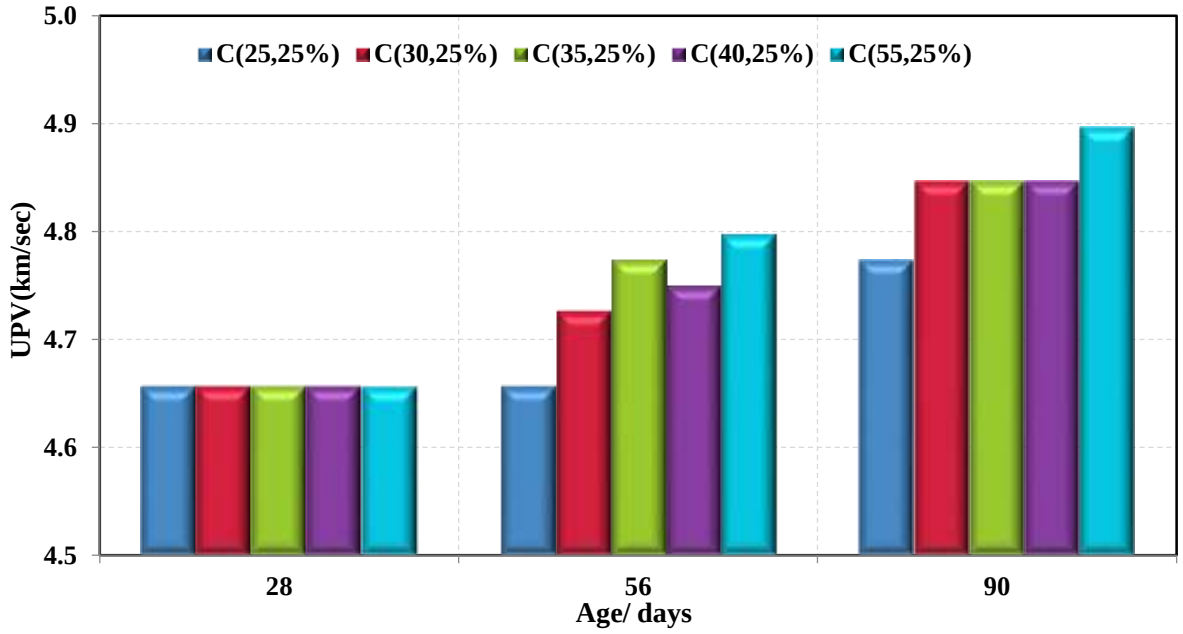

Figure (4.12): - Effect of age on velocity of ultrasonic test for mixture with 25% of GGBS replacement

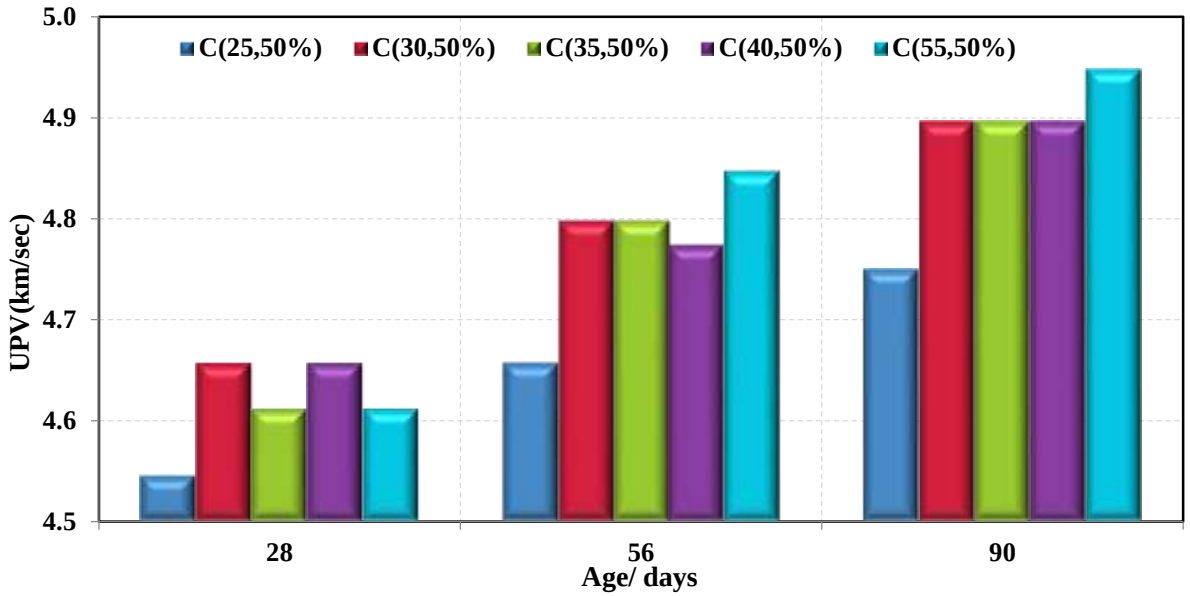

Figure (4.13): - Effect of age on velocity of ultrasonic test for mixture with 50% of GGBS replacement

4.4.4 Drying Shrinkage (Length changes)

After casting and demolding samples, these samples are cured in water and the length change is measured at 1 week, 2 week and 4 weeks representing the wetting stage. After 28 days of curing, the samples were out from water curing and exposed to lab atmospheric in order to measure the length change every two weeks for 16 weeks. The expansion in concrete sample is computed due to wetting and drying shrinkage is also calculated at drying period and these results for various concrete samples containing different percentage of GGBS are shown in **Table 4.9**.

4.4.4.1 Effect of Cement Content on Drying Shrinkage (Length changes)

The effect of curing and drying period for mixes without GGBS addition is plotted in **Figure (4.14)**, there is an increase in wetting expansion and drying shrinkage strain with the increase in compressive strength due to the higher volume of paste and denser matrix **(Pittman & Ragan, 1998; Yuan et al., 2015)**. The drying shrinkage continues in increasing until 16 week, the highest drying shrinkage is for higher compressive strength C(55) at 8 weeks. That is to say, the

less cementitious material the concrete has, the stronger its dry shrinkage resistance will be. Part of the small increase in drying shrinkage is due to reduce aggregate content of the higher compressive strength **(Li & Zhang, 2019)**.

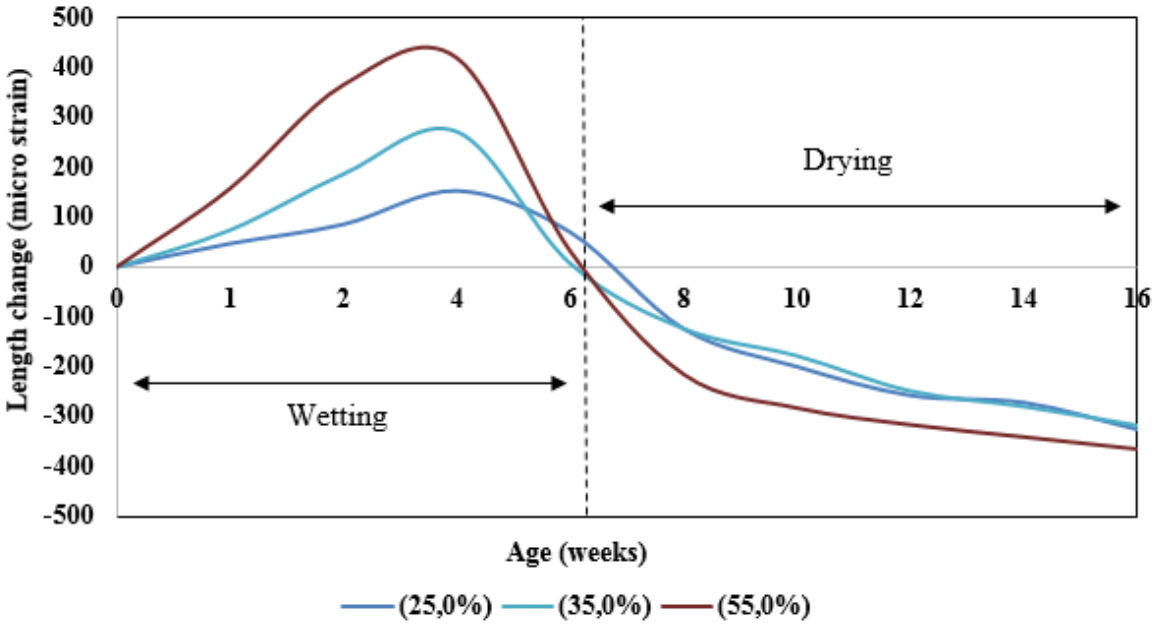

Figure (4.14): - The strain due to wetting and drying cycle of concrete mixture with 0% GGBS

Table 4.9: Result of wetting & drying of concrete mixtures

Mixes	The average of strain (micro strain) *								
	Wetting period at age of			Drying period at age of					
	1 week	2 weeks	4 weeks	6 weeks	8 weeks	10 weeks	12 weeks	14 weeks	16 weeks
C(25,0%)	+46.40	+84.93	+152.09	+69.25	-124.10	-199.69	-257.17	-271.37	-325.01
C(25,25%)	+182.97	+235.51	+278.99	+67.03	-81.52	-186.59	-248.19	-268.12	-324.28
C(25,50%)	+75.54	+196.04	+410.07	+115.11	-77.34	-127.70	-154.68	-206.83	-250.00
C(35,0%)	+74.28	+186.59	+271.74	+7.25	-123.19	-177.54	-248.19	-278.99	-317.03
C(35,25%)	+148.55	+336.96	+442.03	+230.07	-76.09	-153.99	-188.41	-199.28	-215.58
C(35,50%)	+174.46	+273.38	+291.37	+149.28	-59.35	-178.06	-208.63	-208.63	-237.41
C(55,0%)	+157.01	+364.49	+418.69	+31.78	-214.95	-282.24	-315.89	-340.19	-364.49
C(55,25%)	+95.14	+247.74	+377.41	-68.67	-172.70	-248.16	-330.02	-368.91	-439.06
C(55,50%)	+23.80	+138.56	+153.38	+34.87	-115.25	-244.09	-328.54	-383.52	-447.97

*Positive signal (+) refers to expansion strain and negative signal (-) refers to drying shrinkage strain.

4.4.4.2 Effect of GGBS content on Drying Shrinkage

The effect of the slag content on drying shrinkage is examined and the results are presented in **Figure (4.15)**. As can be seen that for all mixes the drying shrinkage increase with time. Hence, for mixtures C(25) with (25,50)% GGBS, the change of shrinkage strain is reduced with increasing the addition of GGBS. Drying shrinkage of specimens is resulted from the evaporation of internal water through pore structure, in virtue of the low external ambient humidity of specimens **(Toledo Filho et al., 2005)**. The concrete with admixtures has a low pore radius, which reduces the evaporation path of water, due to the filling effect of GGBS. Simultaneously, the C-S-H formed by the chemical reaction of GGBS and hydration products would fill the void of cement stone, reducing the evaporation of free water in samples.

When the content of GGBS is more than 25%, the shrinkage strain of specimens increases extensively with time for mixture C(35) & C(55), this corresponds to **(Toledo Filho et al., 2005)**, When the content of additives in the concrete is too much, the shrinkage will enhance its value to some extent. It can be explained in terms of porosity. Additives remain after optimizing the distribution of cement particles. After that, the porosity of cement paste will be slightly increased due to smaller admixture particles compared to cement particles. Hence, drying shrinkage increases with the addition of additives.

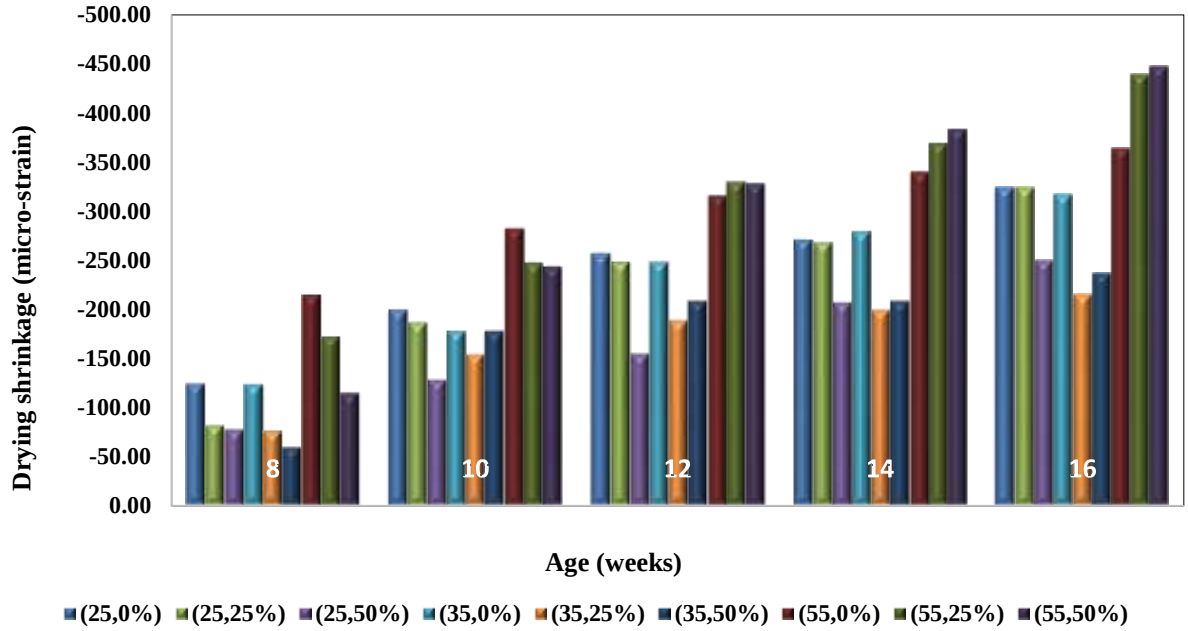

Figure (4.15): - The drying shrinkage of concrete with different percentage of GGBS

4.5 Durability

The durability of concrete is considered one of the most important relevant issues. For examining the durability of concrete containing GGBS as partial replacing cement different tests are conducted. Water absorption (conducted at 28, 56 and 90 days), chloride migration coefficient, chloride penetration, corrosion (impress current), and chloride concentration are carried out to assess and investigate the durability of concrete mixtures.

4.5.1 Water Absorption

The total water absorption percentage of concrete with different percentage of GGBS is illustrated in **Table 4.10** and **Figure (4.16).**

Table 4.10: Water absorption of concrete result

Mixture of concrete	Water Absorption at age of: %		
	28 days	56 days	90 days
C(25,0%)	3.85	3.39	3.31
C(30,0%)	3.78	3.18	3.10
C(35,0%)	3.31	3.00	2.86
C(40,0%)	3.02	2.72	2.68
C(55,0%)	2.78	2.51	2.40
C(25,25%)	4.18	2.97	2.94
C(30,25%)	3.95	2.69	2.52
C(35,25%)	3.70	2.58	2.38
C(40,25%)	3.23	2.61	2.45
C(55,25%)	2.83	2.50	2.35
C(25,50%)	4.26	2.82	2.72
C(30,50%)	3.99	2.68	2.55
C(35,50%)	3.61	2.45	2.33
C(40,50%)	3.23	2.48	2.33
C(55,50%)	3.01	2.41	2.31

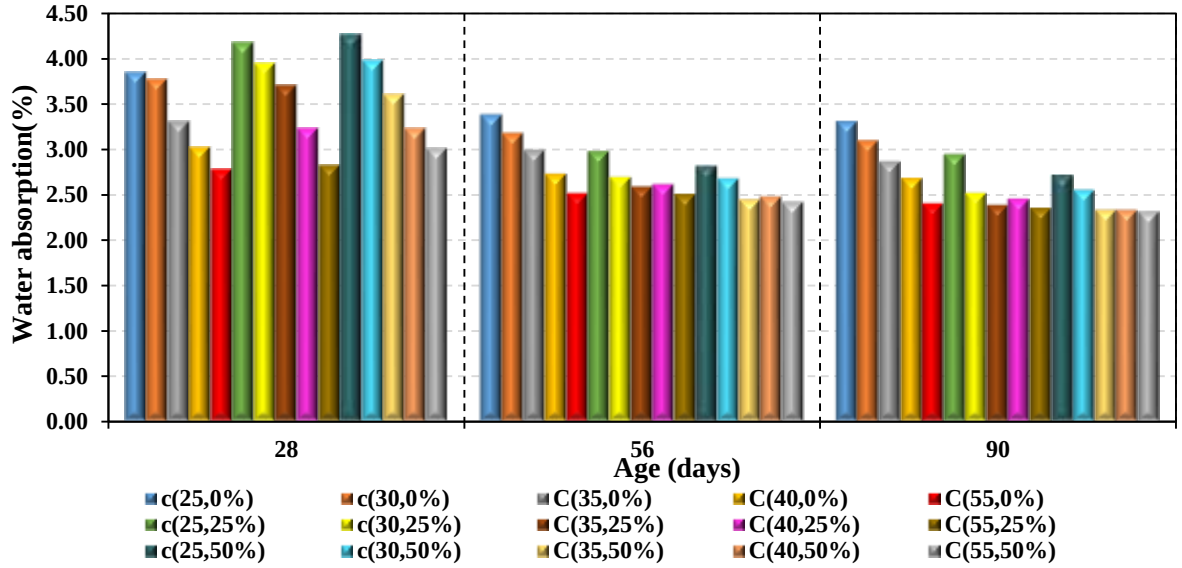

Figure (4.16): - Water absorption of concrete mixture with different content of GGBS

As illustrated in **Figure (4.16),** the mixes at age 28 days shown increase in water absorption with increase of GGBS content. As reported by **Lothenbach et al. (2011)**, the overall porosity of concrete with GGBS is higher due to the lower total volume of C-S-H formed by GGBS when compared to pure PC systems.

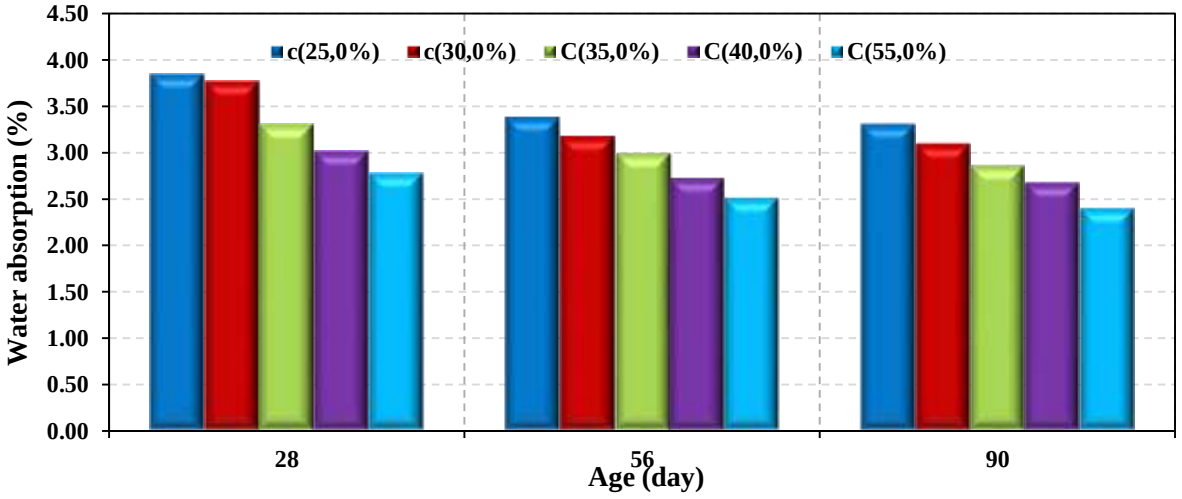

Figure (4.17): - Water absorption of references concrete mixture

With age progress, the water absorption reduced with increasing in curing time (see **Figure (4.17)**) and GGBS content. The reduction in water absorption of concrete refers to improve the microstructure of concrete with time. The cement and GGBS hydration can product (C-S-H and $Ca(OH)_2$) led to fill the

voids and lower the porosity and permeability of concrete **(Chen and Kwan, 2012;Scrivener et al., 2015; Li and Kwan, 2015)**.

The water absorption lowering with increasing curing and GGBS content. The lowering water absorption is at age 90 days for mix C(35) and C(55) with 25% and 50% GGBS as determine in **Figures (4.18)** and **(4.19).**

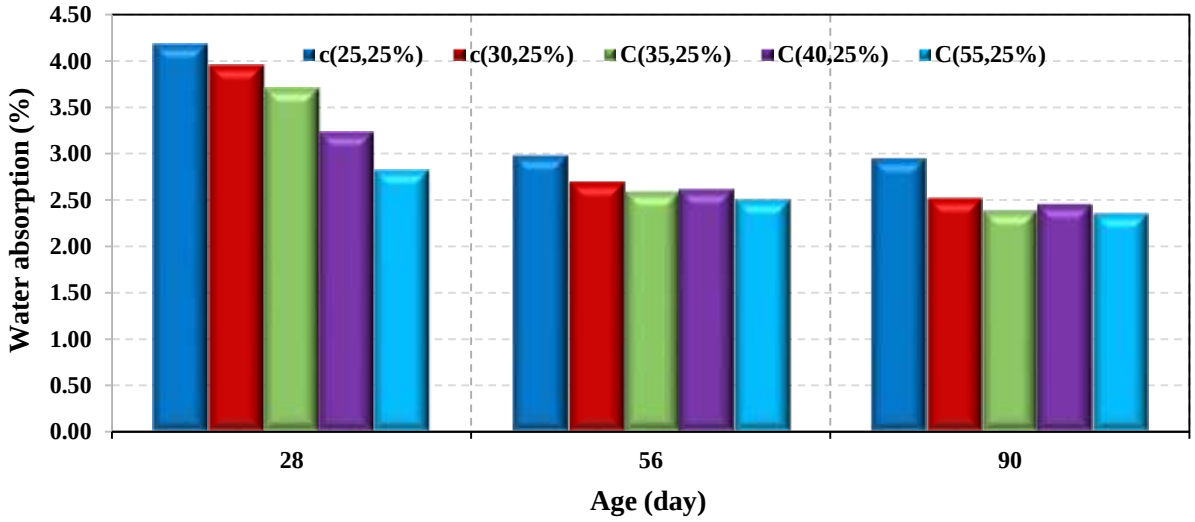

Figure (4.18): - Water absorption of concrete mixture with 25%GGBS

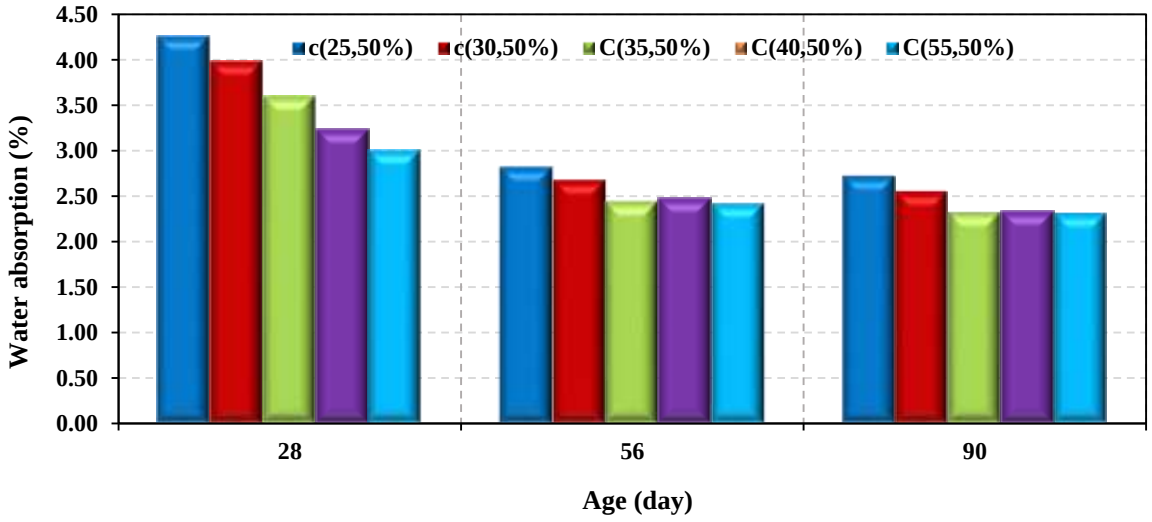

Figure (4.19): - Water absorption of concrete mixture with 50%GGBS

4.5.2 Porosity

The porosity test results of concrete with different percentage of GGBS are listed in **Table 4.11** and **Figure (4.20)**. For mixtures without GGBS, the porosity percentage decreases with an increase in compressive strength and age due to the increase in cement content that lead to increase the C-S-H products by hydrating and filling the voids and that improves the microstructure of concrete as shown in **Figure (4.21).**

Table 4.11: Porosity % of concrete mixture

Mixture of concrete	Porosity of concrete % at age of:		
	28 days	56 days	90 days
C(25,0%)	8.60	7.75	7.61
C(30,0%)	8.52	7.30	7.19
C(35,0%)	7.51	6.91	6.72
C(40,0%)	6.91	6.30	6.28
C(55,0%)	6.55	5.92	5.74
C(25,25%)	9.28	6.81	6.81
C(30,25%)	8.95	6.33	5.92
C(35,25%)	8.40	6.01	5.61
C(40,25%)	7.44	6.10	5.79
C(55,25%)	6.63	5.91	5.60
C(25,50%)	9.53	6.43	6.31
C(30,50%)	9.00	6.21	6.04
C(35,50%)	8.22	5.52	5.50
C(40,50%)	7.43	5.81	5.51
C(55,50%)	6.99	5.67	5.50

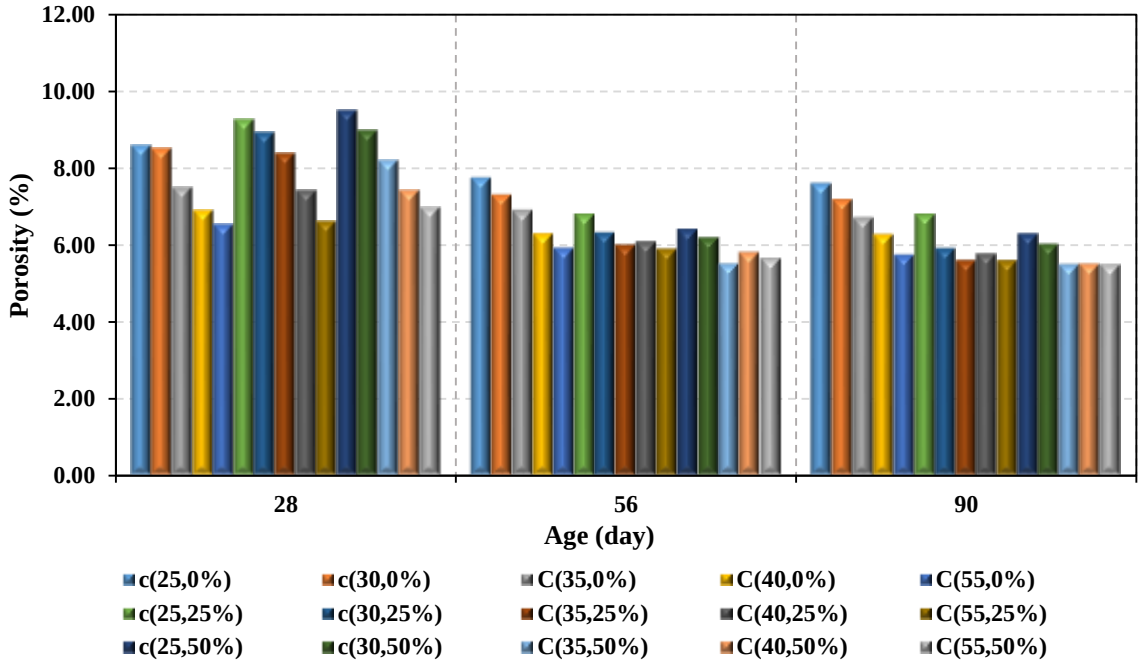

Figure (4.20): - Porosity of concrete mixture with different %GGBS

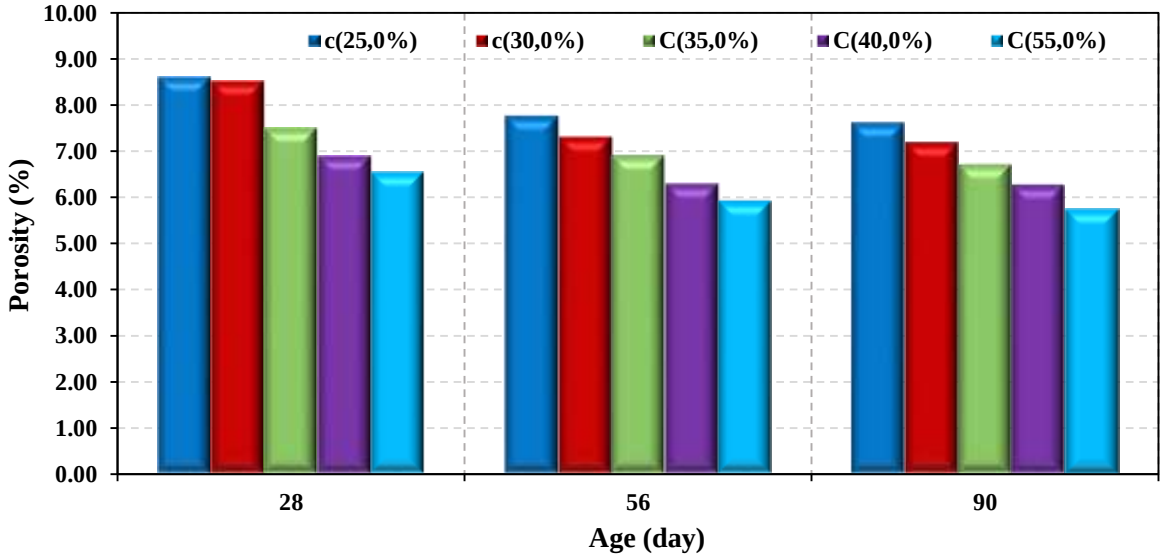

Figure (4.21): - Porosity percentage of concrete with 0% GGBS

The porosity of concrete increased with increasing the GGBS% replacement at age 28 days (**see Figure (4.20)**) due to the lower volume of C-S-H formed by GGBS when compared with cement, this situation would be changed at age 56 and 90 days. Mixture C(25) with both 25% and 50% GGBS recorded the highest porosity as compared with other mixes, mix C(35,25%) and C(35,50%) has approximately the same porosity to mix C(55,25%) and C(55,50%) respectively.

C(35) could be considered for durability requirements instead of C(55). However, more researches should be carried out.

4.5.3 Chloride Ion Penetration

4.5.3.1 Chloride Migration in Concrete

As mentioned previously, the non-steady-state chloride migration coefficient of the concrete specimen can be computed based on **NT BUILD 492**. The migration of chloride test is performed with short concrete cylinders at the age of 28 days. The concrete can be classified according to the concrete resistance against chloride penetration. The criteria of the classification are listed in **Table 4.12**. The computed chloride migration coefficients of the specimens from different mixtures are presented in **Table 4.13**. These samples of concrete are exposed to two solutions and electrical circle with (DC) of 30Voltage for 24 hrs. This test is based on depth of chloride penetration ion, which is tested by splitting cylinder sample and spraying silver nitrate ($AgNO_3$) solution of a specific concentration of 0.1 N. The chloride penetration depth in splitting short cylinder can be employed to find D_{nssm} **Figure (4.22).**

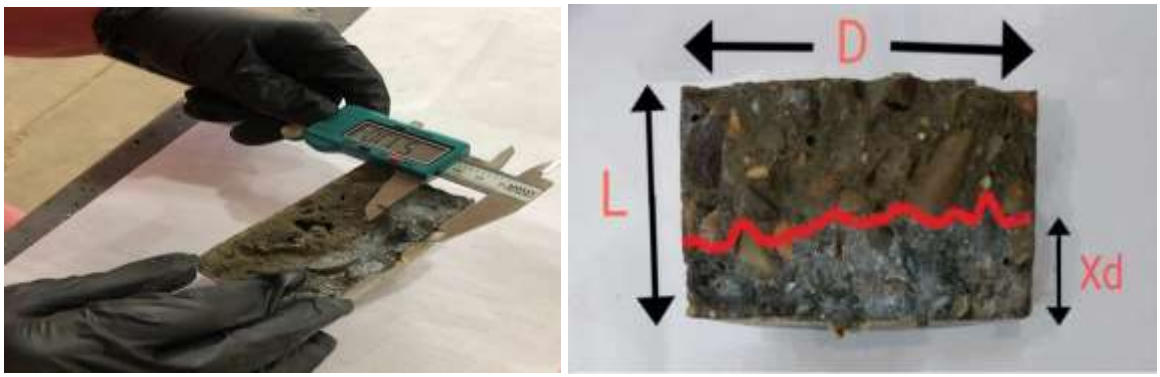

Figure (4.22): - The measuring of chloride penetration depth to calculate chloride migration coefficient

Table 4.12: Resistance to chloride penetration of various types of concrete based on the 28-day chloride diffusivity (Nilsson L et al., 1998)

Chloride diffusivity, at 28 days (× 10^{-12} m^2/s)	Classification of resistance to chloride penetration
>15	Low
10–15	Moderate
5–10	High
2.5–5	Very high
<2.5	Extremely high

Table 4.13: Chloride migration coefficient results of the concrete with different %GGBS for resistance to chloride penetration.

Mixes	Chloride migration coefficient D_{nssm} 10^{-12}(m^3/sec) with GGBS %		
	0%	25%	50%
C25	15.20	8.16	4.09
C30	13.99	6.76	3.89
C35	13.13	6.14	2.76
C40	12.10	5.46	3.01
C55	8.06	4.89	2.80

Table 4.13 and **Figure (4.24)** show the D_{nssm} coefficient at age of 28 days decreases with an increase in the compressive strength. Also, the mixtures with the addition of GGBS achieved higher chloride resistance and the resistance increases with the increase of the replacement percentage of GGBS.

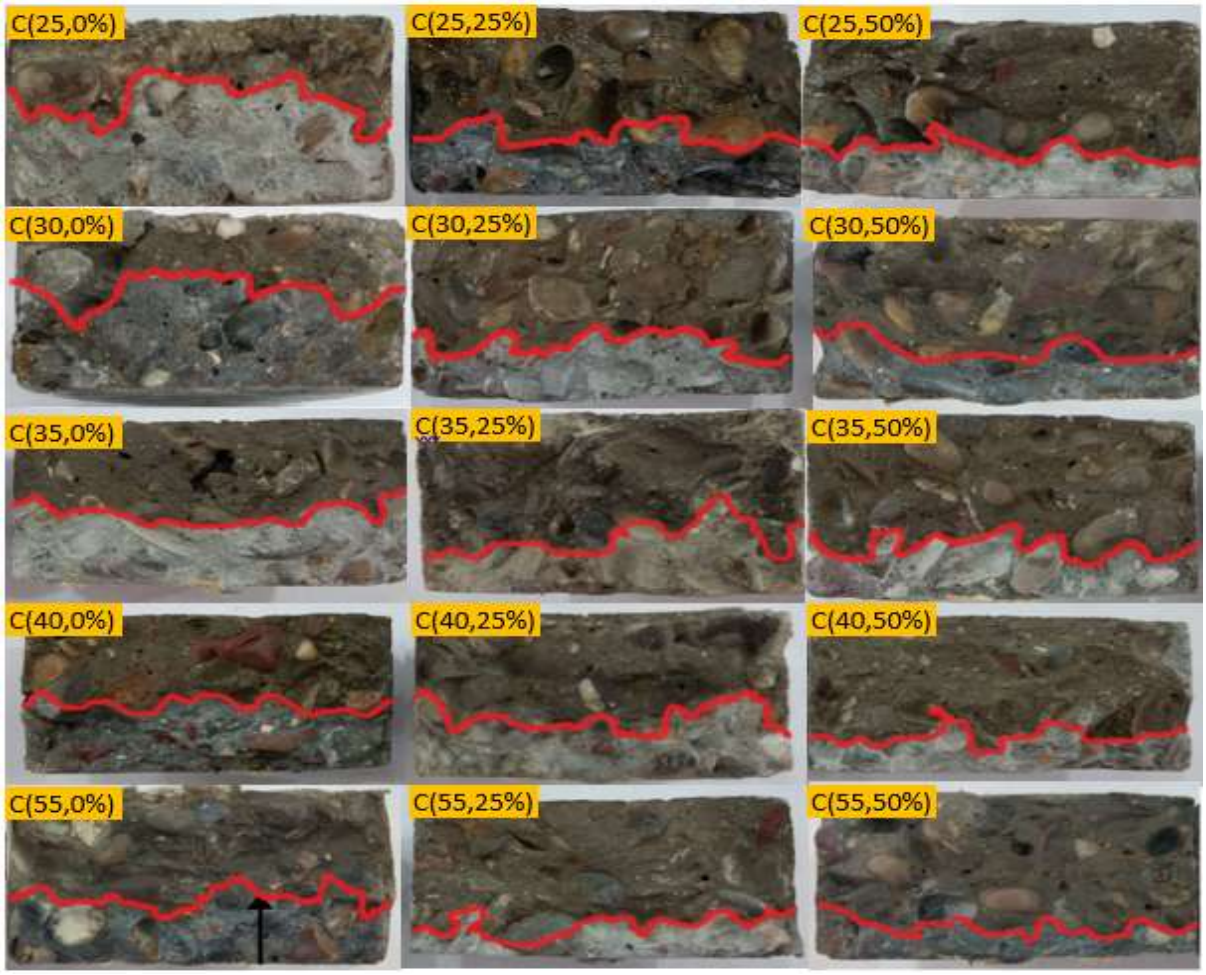

Figure (4.23): - Effect of chloride migration coefficient on concrete mixture with different percentage of GGBS

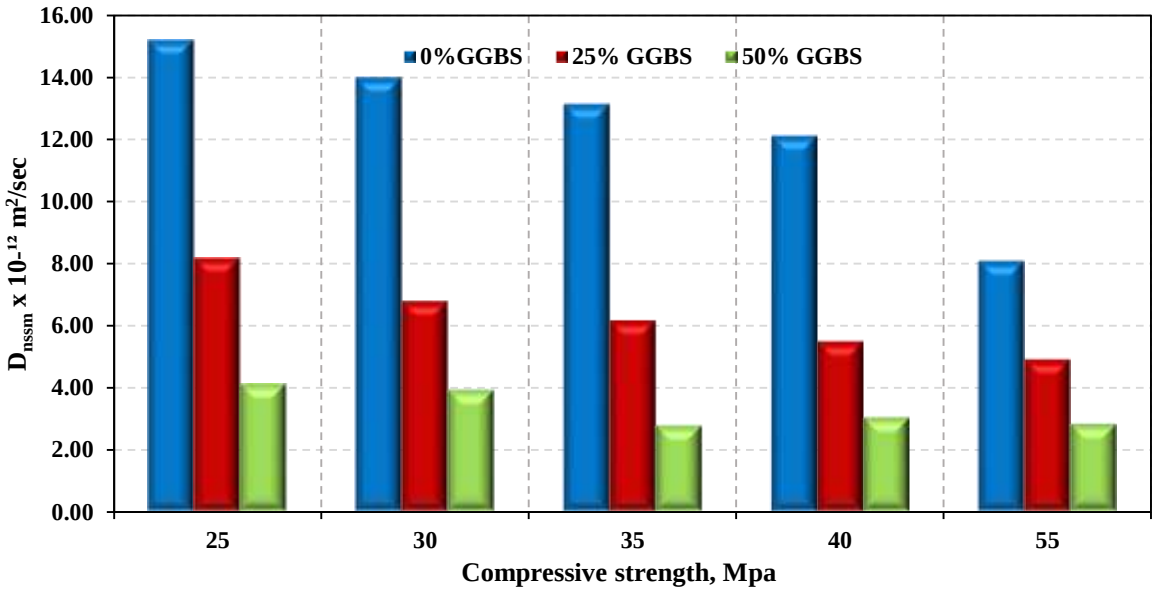

Figure (4.24): - The relation between compressive strength and D_{nssm} of concrete mixtures

The chloride migration coefficient for mixtures C25(25%, %50) is achieved an improvement of 46% and 73% compared to mixture C(25,0%), for mixes C30(25%,50%) the improvement in chloride resistant is 25% and 72% when compared to C(30,0%), for mixes C35(25%,50%). The improvement is 53% and 79% to mix C(35,0%), for mixes C40(25%,50%) the reduction in D_{nssm} coefficient is 55% and 75% when compared to C(40,0%) and for mixes C 55(25%,50%) the reduction in D_{nssm} is 39% and 65% to mix C(55,0%) as shown in **Figure (4.25)**. Mix 55 MPa with addition (0, 25 and 50)% GGBS achieve greater resistance to chloride penetration when compared to other mixes with the same addition percent, while mix C(35,50%) has a minimum chloride migration coefficient compared to all mixes. This phenomenon is consistent with the low water absorption and porosity as mentioned previously **(Onuaguluchi and Panesar, 2014).**

The classification of the concrete resistance against chloride penetration for Mixes with 0% of GGBS are moderate except mix C25 is low and mix C55 is high, but when the percentage of GGBS replacement be 25% the classification is

high for all mixes except mix C55 is very high, also for mixes with 50% GGBS replacement the classification is very high, this relates to the low porosity of mixes with GGBS.

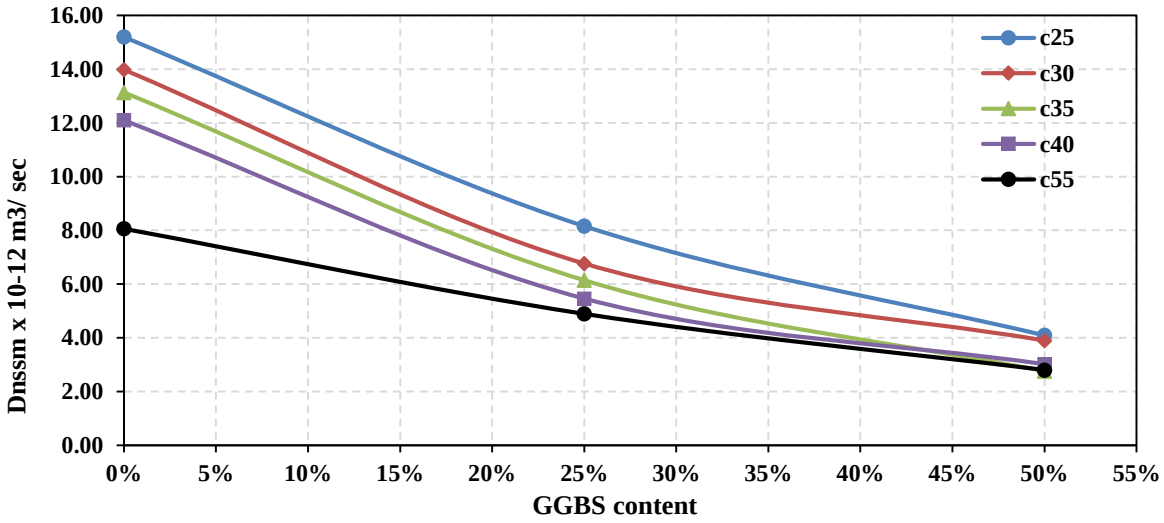

Figure (4.25): - The effect of GGBS content on D_{nssm} of concrete mixtures

4.5.3.2 Chloride Penetration

The surface of sample that near to the steel bar is subjected to accelerated environmental conditions, drying and wetting cycles used, while the other faces were coated with a waterproofing layer. These samples were exposed to 5% chloride solution ions during the wetting and drying cycle for 120 days in total. The test is based on establishment of the penetration depth of chloride ion, xd which is measured by spraying a solution of silver nitrate ($AgNO_3$) with a specified concentration of 0.1 N onto the detached short prism and measuring the penetration of chloride (xd) as a result of the change in color due to reaction of each of Cl^- with Ag^+ to find the penetration depth of chloride for the purpose as shown in **Figure (4.26)**.

Figure (4.26): - The chloride penetration depth in concrete mixture

The penetration depth of chloride (xd) for concrete with different percentage of GGBS are shown in **Table 4.14** and **Figure (4.27)**. The penetration of chloride decreases with increasing compressive strength and increasing the addition of GGBS as percentage replacement of cement due to the improvement in microstructure of concrete by the more hydration of cement and GGBS and refined the pores in concrete structure **(Divsholi et al., 2014)**. In the case of mixture C(25,0%), the greatest penetration depth of around 44 mm after 120 days was achieved, whereas mixture C(55,0%) achieves the greatest penetration depth of about 23 mm. The results also show that the penetration depth lowered with increasing addition of GGBS. For 25% percentage of replacement GGBS, the lower penetration depth at mix C(35), it was about 15 mm also at 50% GGBS, the mixes C(35) and C(55) illustrated the minimum depth of chloride penetration it was 16.63 and 11mm repressively.

The effects of absorption are not just confined to the surface layer as suggested by **(Hong & Hooton, 1999)** but it can lead to quite high values of penetration depth after a few cyclic exposures. Cyclic exposure increases the surface chloride content of concrete, which can have a major influence on the

depth of chloride penetration **(Arya et al., 2014)**. Unfortunately, it is not possible to determine the depth of the colored zone from the chloride profiles or even confirm its existence.

Table 4.14: Chloride penetration depth result for concrete with different percentage of GGBS

Mixes	Depth of Chloride penetration(mm) at point:						
	Point 1	Point 2	Point 3	Point 4	Point 5	Point 6	Average
C(25,0%)	44.5	41.77	45.14	37.32	43.83	53.78	44.39
C(25,25%)	11.85	19.89	25.46	27.56	17.13	12.36	19.04
C(25,50%)	20.38	17.48	12.17	17.36	21.88	27.04	19.39
C(30,0%)	37.45	28.51	25.83	26.98	26.28	36.78	30.31
C(30,25%)	34.79	30.8	21.31	32.83	32.4	18.65	28.46
C(30,50%)	36.24	27.83	22.96	14.19	13.93	20.68	22.64
C(35,0%)	38.13	25.34	35.9	22	37.42	22.74	30.26
C(35,25%)	21.85	15.06	3.31	15.74	21.87	17.33	15.86
C(35,50%)	9.85	36.74	24.5	11.38	8.15	9.14	16.63
C(40,0%)	18.8	25.24	24.21	23.95	25.86	27.57	24.27
C(40,25%)	21.86	16.58	20.18	30.02	33.8	13.9	22.72
C(40,50%)	16.61	17	14.06	18.71	14.98	20.35	16.95
C(55,0%)	31.28	23.57	25.9	20.24	24.23	14.91	23.36
C(55,25%)	29.11	21.06	21.19	9.89	12.17	11.74	17.53
C(55,50%)	9.23	8.32	9.44	4.84	20.98	13.16	11.00

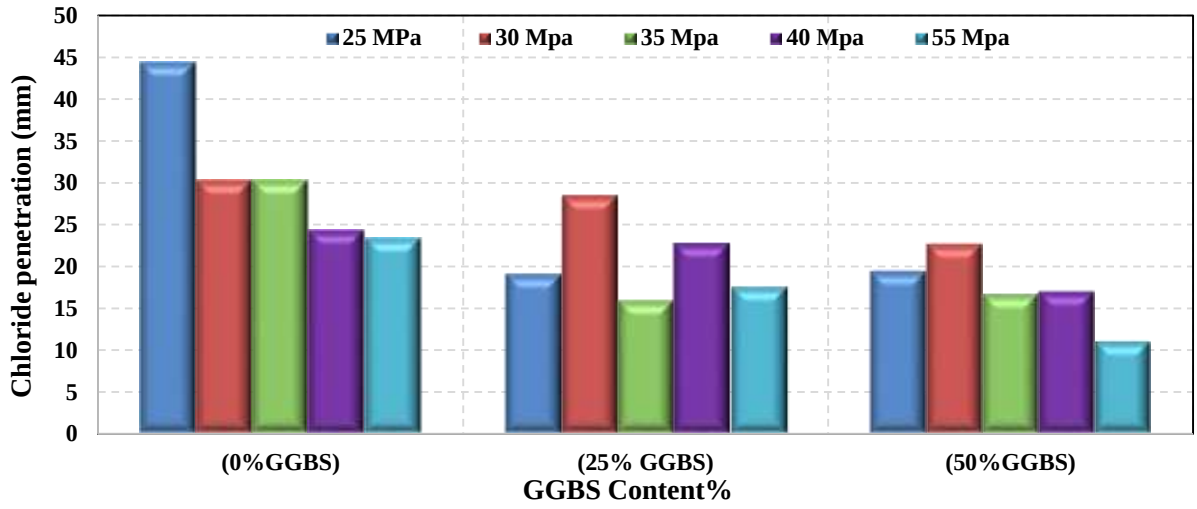

Figure (4.27): - Chloride penetration depth of concrete mixtures

4.5.3.3 Corrosion Calculation (Impressed Current)

After 26 days of subjecting to chloride solution and impress current, the concrete prisms are carefully broken to get out the rebar that embedded in the concrete without damage, then the rebars are cleaned by using sand blast machine and stiff metal brush to get out the rust.

The weights of the rebars are measured and recorded before casting and after sand blast shooting; the loss of mass that occurred due to the corrosion is calculated and listed in **Table 4.16** and **Figure (4.28) & (4.29)**.

The corrosion rate of each rebar can be calculated as follows:

$$\text{Corrosion Penetration Rate (CPR)} = (K \times W)/(A \times T \times D) \quad \textbf{(4.10)}$$

where: K = constant for unit required, W = Mass Loss (g), A = Exposed Surface Area (cm^2), T = Exposure Time (hours) and D = Alloy Density (g/cm^2)

Table 4.15: The K- factor depending on corrosion rate unit (Metal Samples Company, N.D)

Desired Rate of Corrosion Unite (CR)	Area Unit (A)	K-Factor
mils/year(mpy)	in^2	5.34×10^5
mils/year	cm^2	3.45×10^6
millimeters/year (mmy)	cm^2	8.75×10^4

Constants specific to this experiment:

• The exposed surface area of embedded steel rebar = 113.04 cm

•Exposure time = 624 hours

Steel rebar density = 7.85 g/cm^3

Table 4.16: The mass loss of rebars and corrosion penetration rates

Sample rebar	Original mass (g)	Mass after sand blast (g)	Mass loss (%)	Corrosion rate (mm/yr)
C(25,0%)	313	291	7.03	3.48
C(25,25%)	308	284	7.79	3.79
C(25,50%)	306	286	6.54	3.16
C(30,0%)	308	281	8.77	4.27
C(30,25%)	306	280	8.50	4.11
C(30,50%)	309	285	7.77	3.79
C(35,0%)	307	276	10.10	4.90
C(35,25%)	301	282	6.31	3.00
C(35,50%)	293	271	7.51	3.48
C(40,0%)	294	270	8.16	3.79
C(40,25%)	312	288	7.69	3.79
C(40,50%)	302	280	7.28	3.48
C(55,0%)	309	292	5.50	2.69
C(55,25%)	304	283	6.91	3.32
C(55,50%)	296	283	4.39	2.05

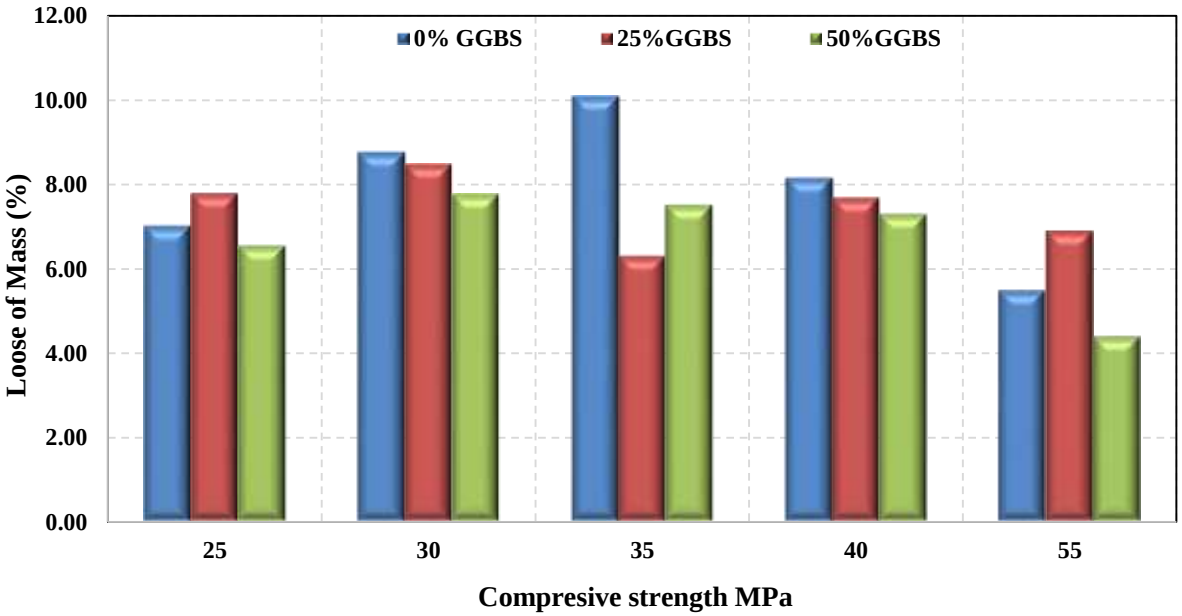

Figure (4.28): - Effect of compressive strength concrete on mass loss of rebars due to corrosion for different GGBS content in concrete mixtures

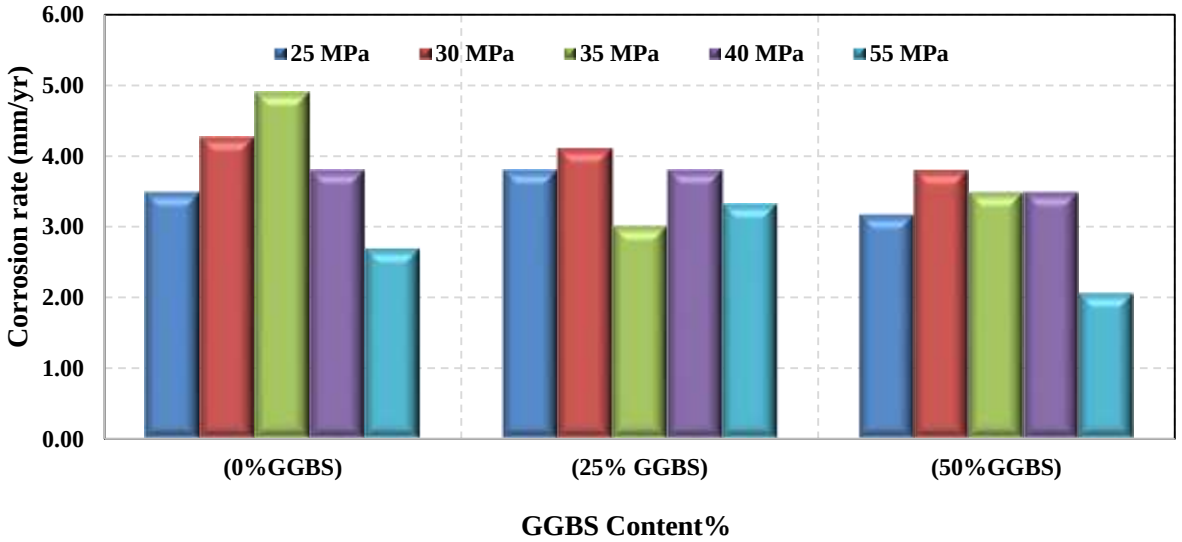

Figure (4.29): - The effect of GGBS content on the corrosion rate of concrete samples

The mixture C(35)MPa with 0% GGBS achieved highest corrosion rate when compared to other mixes as shown in **Figure (4.29)**,but when the addition replacement of GGBS was 25%, the mix C35 corroded is the least.

According to the results, samples with higher strengths and GGBS content rusted is the least. However, the wear of C (35, 25%) rebar is less than that of C (55,25%) rebar, indicating that high strength concrete does not necessarily lead to lower wear rates and prove that designing for optimum strength of 35 MPa and

adding an optimal 25% replacement of GGBS can result in significant eCO_2 savings and enhancing the resistance of corrosion without any need for over-designing.

4.5.3.3.1 Measurement of Crack Caused by Corrosion

Cracked width of samples illustrated in **Figure (4.30)** tends to decrease steadily with increasing GGBS percentage. Mixture C(25,0) has the lowest crack width among other mixes with the same percentage of GGBS is due to the build-up of corrosion products filling and blocking cracks. Hence, the chloride ingress is reduced, and the resistance is increased or stabilised until new cracks are formed or previous cracks are expanded **(W. Zhang et al., 2017).** With 25% replacement of GGBS, mixture C(35) shows the minimum width of crack and equal to mix C(55,25%), and mix C(55,50%) reaches the highest reduction in crack width.

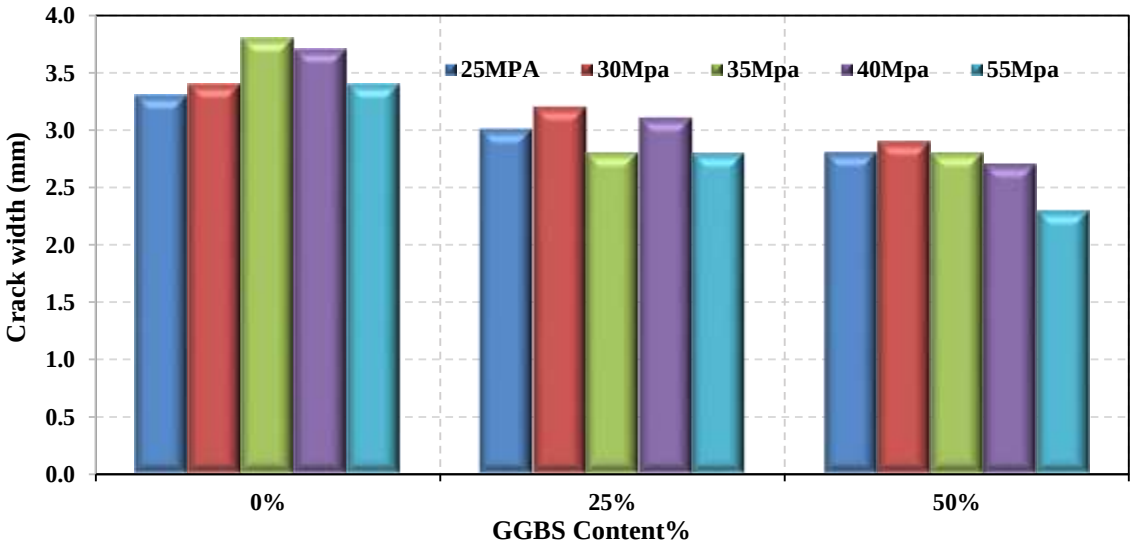

Figure (4.30): - The effect of GGBS content on crack width cause by corrosion

4.5.4 Chloride Concentration (Profile of Chloride)

The chloride concentration test is conducted by measuring Cl^- concertation with depth for concrete containing different percentage of GGBS.

4.5.4.1 Chloride concentration for Impress Current symbols

The chloride concentration in concrete at the region of corroded rebars are presented in **Table 4.17** and **Figure (4.31)**. The results showed the chloride concentrations decrease with increasing the compressive strength and addition of GGBS. For mixtures without GGBS the lowest content of chloride is at mix C(55) due to increase of cement and the amount of hydration and that lead to minimize the voids and porosity. The result presented at 25%GGBS addition the lower chloride concentration is in mixture C(35) and C(55) also at 50% GGBS replacement, the mix C(35) and C(55) has the minimum chloride content compared to other mixtures. For this concept the mix C(35,25%) and C(35,50%) can be used instead of high compressive strength C(55).

Table 4.17: Chloride concentration test result for concrete mixture

Chloride concentration(Cl^-) by mass of concrete (%) for mixture at depth 20mm					
Mix	**Cl^- % by concrete mass**	**Mix**	**Cl^- % by concrete mass**	**Mix**	**Cl^- % by concrete mass**
C(25,0%)	1.028	C(25,25%)	1.241	C(25,50%)	1.240
C(30,0%)	1.311	C(30,25%)	1.241	C(30,50%)	1.311
C(35,0%)	1.347	C(35,25%)	0.992	C(35,50%)	1.063
C(40,0%)	1.240	C(40,25%)	1.205	C(40,50%)	1.134
C(55,0%)	0.780	C(55,25%)	0.992	C(55,50%)	0.638

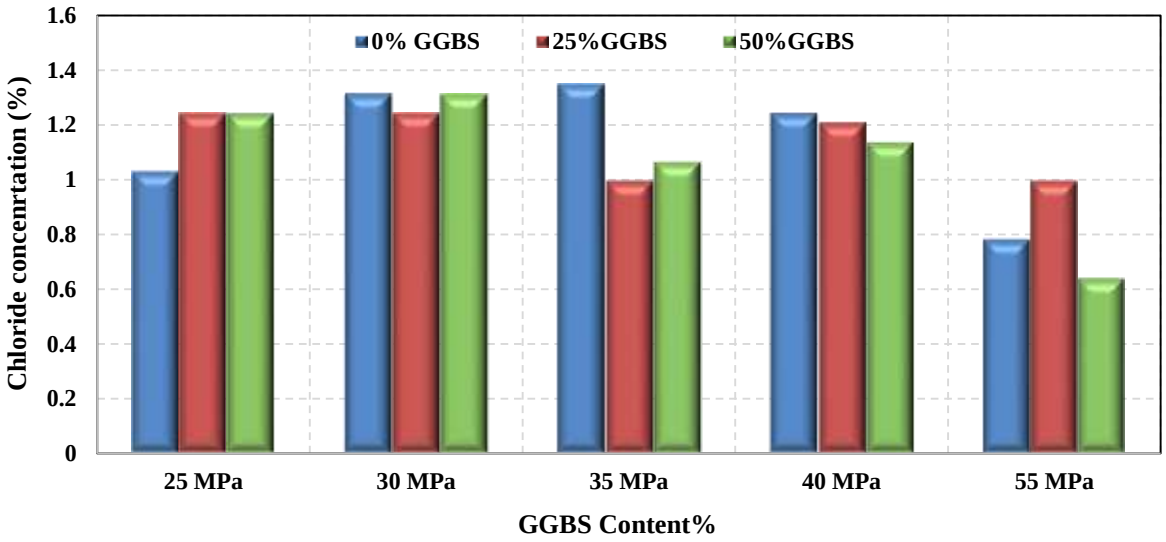

Figure (4.31): - Chloride concentration in Reinforced concrete samples with different %GGBS

4.5.4.2. Chloride concentration with chloride penetration depth

Table 4.18 and **Figure (4.32)** present the result of Cl- concentration values at the end of exposure to 5% NaCl solution (120 days). The results illustrate the chloride concentrations decrease with increasing depth and they vary according to the strength of concrete and the amount of GGBS addition. The result presented the reduction in chloride concentration with increasing depth (10, 20, 30, 40 and 50) mm and increasing GGBS content in concrete mixtures. The reduction of chloride concentration at 10mm depth is 7.89%, 15.79%, 2.86%, 8.57%, 5.88%, 11.76%, 18.42%, 26.32%, 6.90% and 13.79% for C(25,25%), C(25,50%), C(30,25%), C(30,50%), C(35,25%), C(35,50%), C(40,25%), C(40,50%), C(55,25%) and C(55,50%) respectively as comparing with concrete mixture without GGBS .This behavior can be attributed the consistent with the low water absorption and porosity as mentioned previously.

Repeated exposure to wet–dry cycles appear to increase surface chloride levels, which is probably directly responsible for the increase in corrosion depth. Thus it would seem that the most significant effect on long-term chloride penetration of absorption is its effect on surface chloride content **(Arya et al.,**

2014). Also the corrosion depth, defined as the depth at which the chloride concentration equals the threshold for corrosion **(Life-365, 2008),** increases with increasing number of exposure cycles.

Table 4.18: the concentration of chloride by weight of concrete% for mixes with different percentage of GGBS at different depth

Mixes	Chloride concentration(Cl-) by mass of concrete (%) for mixture at depth				
	0-10mm	10-20mm	20-30mm	30-40mm	40-50mm
C(25,0%)	1.347	1.064	0.957	0.532	0.177
C(25,25%)	1.241	0.993	0.674	0.355	0.177
C(25,50%)	1.134	1.064	0.709	0.355	0.177
C(30,0%)	1.241	0.993	0.674	0.390	0.177
C(30,25%)	1.205	0.780	0.674	0.284	0.177
C(30,50%)	1.134	0.993	0.390	0.319	0.177
C(35,0%)	1.205	1.028	0.780	0.355	0.177
C(35,25%)	1.134	0.886	0.390	0.319	0.177
C(35,50%)	1.064	0.780	0.355	0.319	0.177
C(40,0%)	1.347	1.064	0.425	0.355	0.177
C(40,25%)	1.099	0.957	0.532	0.355	0.177
C(40,50%)	0.993	0.886	0.248	0.284	0.177
C(55,0%)	1.028	0.922	0.284	0.355	0.177
C(55,25%)	0.957	0.851	0.355	0.284	0.177
C(55,50%)	0.886	0.744	0.284	0.248	0.177

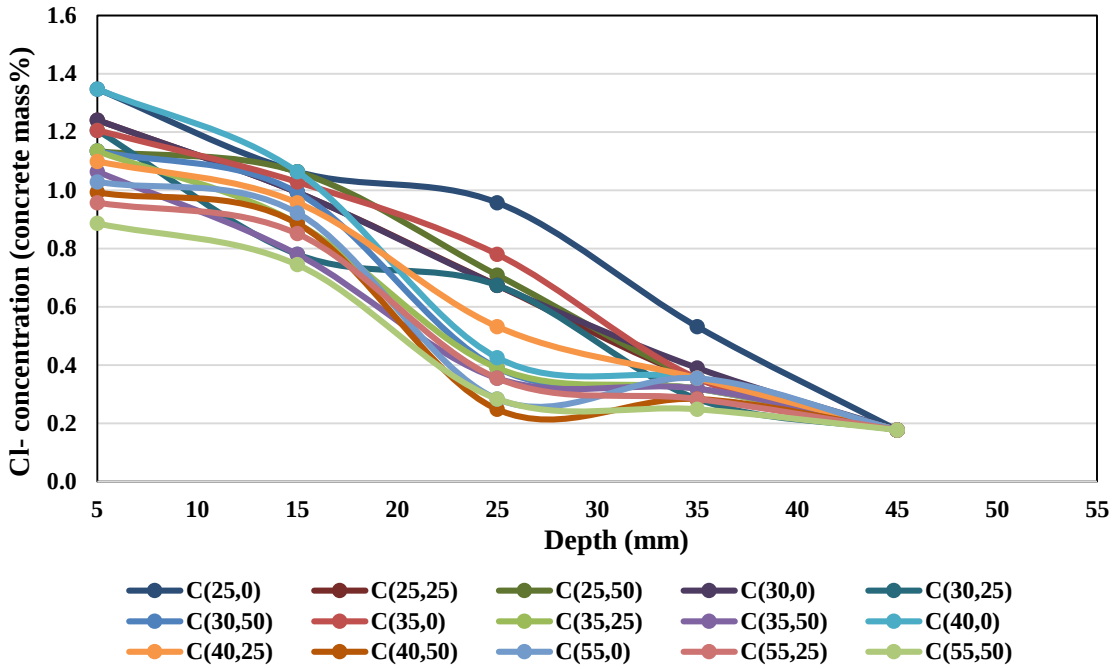

Figure (4.32): - Total chloride concentration profile of mixtures at 120 days

Chloride represents chlorides and the extent of chlorides gathering on the concrete surface. The result diffusion chloride coefficient (Da) and surface chloride concentration (Cs) values at 120 days are presented in **Table 4.19** and **Figure (3.33) (**the calculations of Da and Cs are illustrated in **Appendix –A2)**. The test scale for the values of Cs (the accumulation of chlorides on the concrete surface) and Da (rate of diffusion of chloride into concrete) are computed as mentioned in chapter three in paragraph **(3.6.4).**

Table 4.19: The result of factors (Da, Cs)

Mixtures	Da (*10^{-11}) (m^2/s)	Cs (by mass of concrete%)	Ci (by mass of concrete %)
C(25,0%)	2.9	1.75	0.177
C(25,25%)	2.8	1.7	0.177
C(25,50%)	2.7	1.52	0.177
C(30,0%)	2.9	1.55	0.177
C(30,25%)	26	1.44	0.177
C(30,50%)	2.2	1.48	0.177
C(35,0%)	2.8	1.58	0.177
C(35,25%)	2.4	1.39	0.177
C(35,50%)	1.8	1.36	0.177
C(40,0%)	2.5	1.63	0.177
C(40,25%)	2.4	1.48	0.177
C(40,50%)	1.7	1.48	0.177
C(55,0%)	2.3	1.3	0.177
C(55,25%)	1.8	1.28	0.177
C(55,50%)	1.8	1.16	0.177

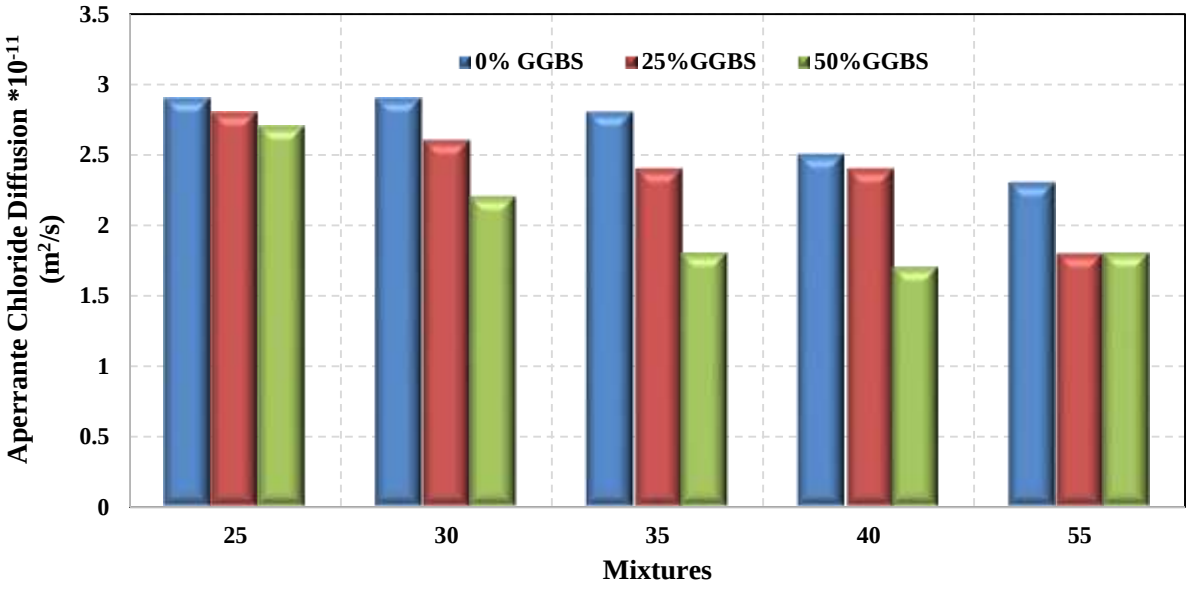

Figure (4.33): - Apparent chloride diffusion of concrete mixture with different % GGBS

Both factors, D_a, C_s reflect to the penetration and concentration of chloride in concrete that exposed to chloride environmental conditions. The results showed that Da decreases with increasing the compressive strength and with the depth of specimen **Figure (4.33).** Therefore, when the percentage of GGBS replacement increases, the D_a also decreases. The lower D_a is at mix C(50) with 0% and 50% GGBS replacement when compared with mixes contain the same addition, but D_a is equal to mix C(35) and higher than C(40) when the replacement of GGBS is 25%. This depends on the permeability of concrete. The profiles are mainly influenced by two transport mechanisms: diffusion and capillary suction of chloride solution in concrete **(Bernal et al., 2016).**

The values of Da and surface concentration of all mixtures are computed according to **Equation (3-12)**, are presented in **Appendix A**2.

5. Summary

The goal of the study is to see if the optimal low carbon GGBS concrete would have better mechanical and durable properties than concrete of comparable or greater strength. This entailed the construction of fifteen concrete mixtures, which are cast and cured then compressive strength, splitting strength, water

absorption, drying shrinkage, migration of chlorides, corrosion, chloride penetration and chloride content tests are placed after 28 days curing. After computing the embedded carbon per MPa for the mix design, it is discovered that the optimum is between 30-40 MPa and mix(C35) had the lowest eCO_2 levels. Furthermore, the C35,50 percentage giving the highest reduction in eCO_2. There is a significant increase in compressive strength for all with the curing age increases and with increase of GGBS content. According to the result, Mix C55 MPa with addition (0, 25, 50) % GGBS achieved greater chloride penetration resistance when compared to other mixes with the same addition percent, while mix C(35,50%) has a minimum chloride migration coefficient compared to all mixes. The concrete combinations with 50% GGBS shows the strongest resilience over time, according to the findings of the accelerated wear. That is predicted due to the high GGBS addition's poor permeability. Last but not least, it is discovered that the C(35,25%) rebar has corroded less than the C(55,25%) rebar after being extracted and shot blasted, demonstrating that engineering for optimal strength of 35 MPa does not always result in reduced wear rates. Instead of utilizing a stronger concrete with the same amount of GGBS, the optimal strength of concrete C35 with 25% and 50% GGBS replacement can be fairly dependent, which tends to save carbon emissions and costs while improving corrosion protection

CHAPTER FIVE

CONCLUSIONS & RECOMMENDATIONS

CHAPTER FIVE

Conclusions and Recommendations for further students

5.1 Conclusions

The goal of the study is to see if the optimal low carbon GGBS concrete would have better mechanical and durable properties than concrete of comparable or greater strength. This entailed the construction of fifteen concrete mixtures, which were cast and cured then compressive strength, splitting strength, water absorption, drying shrinkage, migration of chlorides, corrosion, chloride penetration and chloride content tests were placed after 28 days curing. The main points can be concluded from the experimental results as follows:

1- **Embodied Carbon Dioxide Calculation**

- After computing the embedded carbon per MPa for the mix design, it is discovered that the (C35) concrete has the lowest eCO_2 levels. Furthermore, compared to the other two strengths that have the identical GGBS percentage replacement, the C(35,50) percentage giving the highest drop in eCO_2.

2- **Fresh properties**

- ***Slump test:*** When the cement partially replaced by (25%, 50%) GGBS, the slump of all mixes ((25, 30, 35, 40 and 55) MPa) reduce with the increasing of GGBS percentage.

3- Mechanical properties

- ***Compressive strength:***
  - There is a significant increase in compressive strength for all with the curing age increases. The data shows that C(40,0%) and C(55,0%) have a minimum development in compressive strength about 0.15% and 1.54% at age 56 days and 4.38% and 3.55% at age 90 days respectively, while, mix C(25,50%) achieved maximum increase by 42.54% and 64.89% at age 56 days and 90 days respectively .
  - The rate of GGBS replacement and the age of the concrete influence the development of compressive strength. The result show, at the early stage of curing, the concrete specimen's compressive strength decreases with the GGBS content increasing. Within the same scope of this investigation, higher replacement percentages of GGBS led to better ultimate strengths with time.
- ***Splitting tensile strength:***
  - With more curing age, all mixtures' splitting strength increases.
  - There is a reduction in splitting strength at early age for concrete containing GGBS. In addition, when the GGBS percentage increase to 50%, the splitting strength decrease. C(35) mixture with 25,50% of GGBS showed about 14.58% and 3.95% increase in tensile strength for mix C(35,25%) and C(35,50%) in comparison with the same mixture without GGBS.

- ***UPV TEST:***
  - There is a clear increase in the ultrasonic pulse velocity with increasing the curing age and with the increasing in compressive strength. The results show that mix C(55) records highest increase at age 90 days when compared with other mixes, while mixes C(35) and C(40) are equal at age 90 days.
  - The velocity of ultra-sonic pulse UPV increases as curing time lengthens also with the excess of the percentage of GGBS.
- ***Drying shrinkage:***
  - With an increase in compressive strength, drying shrinkage strain increased. According to these results, the highest drying shrinkage is for higher compressive strength C(55) at 8 weeks due to reduce aggregate content and increase cement content.
  - With time and GGBS concentration, specimen shrinkage strain rises noticeably. The result illustrate that mixes C(35) & C(55) have maximum shrinkage when the content of GGBS is more than 25% for mixture.

4- <u>Durability:</u>

- ***Water absorption:*** Based on the result, at early age of curing, there is an increase in water absorption with increasing GGBS content. With age progress, there is a clear reduction in concrete water absorption.
- ***Chloride Migration:*** The chloride migration coefficient at age of 28 days decrease with compressive strength increasing. In addition, the mixtures with the replacement of GGBS recorded higher chloride

resistance and this resistance increase with increasing the replacement percentage of GGBS. According to the result, Mix 55 MPa with addition (0, 25, 50) % GGBS achieved greater chloride penetration resistance when compared to other mixes with the same addition percent, while mix C(35,50%) has a minimum chloride migration coefficient compared to all mixes. As a result, the commonly held idea that higher-strength concrete provides superior resistance to chloride ion penetration is not always correct.

- ***Chloride Penetration depth:*** The chloride ions penetration results show that the penetration depth lowered with increasing the replacement of GGBS. For 25% percentage of GGBS replacement, the lowest penetration depth is at mix C(35), it is about 15 mm also at 50% GGBS the mixes C(35) and C(55) illustrate the minimum depth of chloride penetration, it was 16.63 and 11mm repressively.
- ***Corrosion (Impressed Current):***
  - The concrete combinations with 50% GGBS show the strongest resilience over time, according to the findings of the accelerated wear. Last but not least, it is discovered that the C(35,25%) rebar has corroded less than the C(55,25%) rebar after being extracted and shot blasted, demonstrating that engineering for optimal strength of 35 MPa does not always result in reduced wear rates.
  - Cracks with different width in the samples are formed by corrosion and tend to decrease steadily with increasing the GGBS percentage in the mix. From the result, the mixture C(35,25%) shows the minimum width of crack and equal to mixture

C(55,25%), and mixture C(55,50%) reached the highest reduction in crack width value.

- Instead of utilizing a stronger concrete with the same amount of GGBS, the optimal strength of concrete C35 with 25% and 50% GGBS replacement can be fairly dependent, which tends to save carbon emissions and costs while improving corrosion protection. The additional time dedicated to this experiment may result in a better knowledge of the behaviours of cracked and uncracked samples over the long run. In order to guarantee that trail mixes are meet the proper quality, they should be cast and tested before experimenting.

- ***The chloride concentration***
  - The chloride concentrations at the rebar region (after corrosion by impressed current method) decreases with increasing the compressive strength and increasing GGBS. At (5,50 % of GGBS, mix C(35) and C(55) have the minimum chloride content compared to other mixtures. For this concept the mix C(35,25%) and C(35,50%) can be used instead of high compressive strength C(55).
  - The result presented the reduction in chloride concentration with increasing depth (10, 20, 30, 40 and 50) mm and increasing GGBS content in concrete mixtures.

5.2 Recommendations for further students

- Studying the effect of other SCMs materials (silica fume, metakaolin, rice husk ash, and etc.) on embodied carbon dioxide (eCO_2) in concrete and its effect on concrete infrastructure tests.
- The tests can be conducted specifically focusing on carbonation. Carbonation refers to the reaction between carbon dioxide in the atmosphere and the calcium hydroxide in concrete, resulting in the formation of calcium carbonate. To choose the optimum mixture that achieve the lower carbon dioxide emission and higher resistance to carbonation.

REFERENCES

REFERENCES

Aginam, C. H., Chidolue, C. A., & Nwakire, C. (2013). Investigating the Effects of Coarse Aggregate Types on The Compressive Strength of Concrete. International Journal of Engineering Research and Applications (IJERA), 3(4), 1140–1144. https://pdfs.semanticscholar.org/ebef/84c9fbd5ebe30e6d022eb074063bd704fbca.pdf

Ahmad, J., Kontoleon, K. J., Majdi, A., Naqash, M. T., Deifalla, A. F., Ben Kahla, N., Isleem, H. F., & Qaidi, S. M. A. (2022). A comprehensive review on the ground granulated blast furnace slag (GGBS) in concrete production. Sustainability, 14(14), 8783.

Ahmad, S. (2003). Reinforcement corrosion in concrete structures, its monitoring and service life prediction - A review. Cement and Concrete Composites, 25(4-5 SPEC), 459–471. https://doi.org/10.1016/S0958-9465(02)00086-0

AL-Ameeri, A. S., Rafiq, M. I., Tsioulou, O., & Rybdylova, O. (2022). Modelling chloride ingress into in-service cracked reinforced concrete structures exposed to de-icing salt environment and climate change: Part 1. Structural Control and Health Monitoring, 29(10), e3032.

Al-Gburi, M. (2015). Restraint effects in early age concrete structures. Luleå tekniska universitet.

Ali, T. S. (2017). Effect of ground water sodium chloride attack on reinforced concrete footings. J Geotech Eng, 4(1), 1–7.

Al-Mansour, A., Chow, C. L., Feo, L., Penna, R., & Lau, D. (2019). Green concrete: By-products utilization and advanced approaches. Sustainability (Switzerland), 11(19), 5145. https://doi.org/10.3390/su11195145

Almeida, F. C. R., & Klemm, A. J. (2018). Efficiency of internal curing by superabsorbent polymers (SAP) in PC-GGBS mortars. Cement and Concrete Composites, 88, 41–51. https://doi.org/10.1016/j.cemconcomp.2018.01.002

Almeida, F. C. R., Sales, A., Moretti, J. P., & Mendes, P. C. D. (2015). Sugarcane bagasse ash sand (SBAS): Brazilian agroindustrial by-product for use in mortar. Construction and Building Materials, 82, 31–38. https://doi.org/10.1016/j.conbuildmat.2015.02.039

American Concrete Institute ACI Committee 211. 2002. Standard Practice for Selecting Proportions for Normal, Heavyweight, and Mass Concrete (ACI 211.1-91). American Concrete Institute.

American Concrete Institute ACI Committee 222 (2001). Protection of Metals in Concrete Against Corrosion. [online] pp.3-7. Available at: http://civilwares.free.fr/ACI/MCP04/222r_01.pdf

American Society for Testing and Materials, ASTM C1556-(2011a). 2016 Standard Test Method for Determining the Apparent Chloride Diffusion Coefficient of Cementitious Mixtures by Bulk Diffusion.

Anandaraj, S., Rooby, J., Awoyera, P. O., & Gobinath, R. (2019). Structural distress in glass fibre-reinforced concrete under loading and exposure to aggressive environments. Construction and Building Materials, 197, 862–870.

Andrade, C. (2006). Advances in modeling of RILEM TC 178-TMC "Testing and modelling chloride penetration in concrete". https://doi.org/10.1617/2351580028.113

Arya, C., & Ofori-Darko, F. K. (1996). Influence of crack frequency on reinforcement corrosion in concrete. Cement and Concrete Research, 26(3), 345–353. https://doi.org/10.1016/S0008-8846(96)85022-8

Arya, C., & Xu, Y. (1995). Effect of cement type on chloride binding and corrosion of steel in concrete. Cement and Concrete Research, 25(4), 893–902. https://doi.org/10.1016/0008-8846(95)00080-V

Arya, C., Vassie, P., & Bioubakhsh, S. (2014). Chloride penetration in concrete subject to wet–dry cycling: influence of pore structure. Proceedings of the Institution of Civil Engineers-Structures and Buildings, 167(6), 343–354.

ASTM C 150, (2009). "Standard Specification for Portland Cement," Annual Book of ASTM Standards, Vol. 4.01, ASTM International.

ASTM C143/C 143M, (2005)." Standard Test Method for Slump of Hydraulic Cement Concrete", American Society for Testing and Materials.

ASTM C157/C157M, (2004). "Standard Test Method for Length, American Society for Testing and Materials", American Society for Testing and Materials

ASTM C490, (2004). "Standard Practice for Use of Apparatus for the Determination of Length Change of Hardened Cement Paste, Mortar, and Concrete", American Society for Testing and Materials.

ASTM C642, (2013). "Standard test method for density, absorption, and voids in hardened concrete", American Society for Testing and Materials.

Ballim, Y., & Reid, J. C. (2003). Reinforcement corrosion and the deflection of RC beams - An experimental critique of current test methods. Cement and Concrete Composites, 25(6), 625–632. https://doi.org/10.1016/S0958-9465(02)00076-8

Basheer, P. A. M., Gilleece, P. R. V., Long, A. E., & Mc Carter, W. J. (2002). Monitoring electrical resistance of concretes containing alternative cementitious materials to assess their resistance to chloride penetration. Cement and Concrete Composites, 24(5), 437–449.

BCA CSMA UKQAA. Embodied CO_2 of UK cement, additions and combinations. Information Sheet P1. November 2008.

Bentur, A., Diamond, S., & Berke, N. S. (1997). Steel corrosion in concrete: fundamentals and civil engineering practice (p. 201).

Bernal, J., Fenaux, M., Moragues, A., Reyes, E., & Gálvez, J. C., (2016). Study of chloride penetration in concretes exposed tohigh-mountain weather conditions with presence of deicing salts. Construction and Building Materials, 127, 971-983.

Bhattarai, P., Pavel, S., & Sherpa, P. (2019). Effect of Water Content on Workability of Concrete. International Journal of Civil Engineering Research, 1(January), 7.

Bouasker, M., Khalifa, N. E. H., Mounanga, P., & Ben Kahla, N. (2014). Early-age deformation and autogenous cracking risk of slag-limestone filler-cement blended binders. Construction and Building Materials, 55, 158–167.

Broomfield, J. P. (2006). Corrosion of Steel in Concrete: Understanding, Investigation and Repair, Second Edition. Crc Press.

Cabeza, L. F., Barreneche, C., Miró, L., Morera, J. M., Bartolí, E., & Inés Fernández, A. (2013). Low carbon and low embodied energy materials in buildings: A review. Renewable and Sustainable Energy Reviews, 23, 536–542.

Cement Association of Canada. (2004). "Concrete thinking for a sustainable future".

Chang, Z., & Goldfarb, R. (2019). Mineral deposits of China. Society of Economic Geologists.

Chen, C., Xu, R., Tong, D., Qin, X., Cheng, J., Liu, J., Zheng, B., Yan, L., & Zhang, Q. (2022). A striking growth of CO_2 emissions from the global cement industry driven by new facilities in emerging countries. Environmental Research Letters, 17(4), 44007.

Chen, J. J., & Kwan, A. K., (2012). Adding limestone fines to reduce heat generation of curing concrete. Magazine of Concrete Research, 64(12), 1101-1111.

Cheng, A., Huang, R., Wu, J. K., & Chen, C. H. (2005a). Influence of GGBS on durability and corrosion behavior of reinforced concrete. Materials Chemistry and Physics, 93(2–3), 404–411.

Cheung, M. M., Zhao, J., & Chan, Y. B. (2009). Service life prediction of RC bridge structures exposed to chloride environments. Journal of Bridge Engineering, 14(3), 164–178.

Collins, F., & Sanjayan, J. G. (2000). Numerical modeling of alkali-activated slag concrete beams subjected to restrained shrinkage. ACI Structural Journal, 97(5), 594–602.

Costa, A., & Appleton, J. (1999). Chloride penetration into concrete in marine environment—Part I: Main parameters affecting chloride penetration. Materials and Structures, 32, 252–259.

Daube, J., & Bakker, R. (1986). Portland blast-furnace slag cement: a review. Blended Cements.

Dhir, R. K., & Byars, E. A. (1993). PFA concrete: chloride diffusion rates. Magazine of Concrete Research, 45(162), 1–9.

Dhir, R. K., Paine, K. A., & O'Leary, S. (2003). Use of recycled concrete aggregate in concrete pavement construction: A case study. Sustainable Waste Management, Proceedings of the International Symposium, 373–382.

Divsholi, B. S., Lim, T. Y. D., & Teng, S. (2014). Durability Properties and Microstructure of Ground Granulated Blast Furnace Slag Cement Concrete. International Journal of Concrete Structures and Materials, 8(2), 157–164.

Duxson, P., Provis, J. L., Lukey, G. C., & van Deventer, J. S. J. (2007). The role of inorganic polymer technology in the development of "green concrete." Cement and Concrete Research, 37(12), 1590–1597.

El Maaddawy, T. A., & Soudki, K. A. (2003). Effectiveness of Impressed Current Technique to Simulate Corrosion of Steel Reinforcement in Concrete. Journal of Materials in Civil Engineering, 15(1), 41–47.

EUROFER (2013). A Steel Roadmap for a Low Carbon Concrete Europe 2050. [online] nocarbonnation.net, The European Steel Association, pp. 10-13.

European Committee for Standardization, BS EN 12390 part 2 :(2009). Testing hardened concrete –; Part 2: Making and curing specimens for strength tests. British Standard Institution.

European Committee for Standardization, BS EN 12390, part 3 :(2009). "Testing hardened Concrete Part 3: Compressive strength of test specimens". British Standard Institution.

European Committee for Standardization, BS EN 12390, part 6(2009). "Testing hardened Concrete. Tensile splitting strength of test specimens". British Standard Institution.

European Committee for Standardization, BS EN 12390, part 11(2015). "Testing hardened Concrete. Determination of the chloride resistance of concrete unidirectional diffusion. British Standard Institution.

European Committee for Standardization, BS EN 12504-2:2012, Testing concrete in structures Part 2: Non-destructive testing — Determination of rebound number. British Standard Institution.

European Committee for Standardization, BS EN 12504-4:(2012,). Testing concrete in structures Part 4: Determination of ultrasonic pulse velocity. British Standard Institution

European Committee for Standardization, BS EN 12620:2002+A1:2008 (2008). Aggregates for concrete. British Standard Institution.

European Committee for Standardization, BS EN 15167-1:(2006,). Ground granulated blast furnace slag for use in concrete, mortar and grout. Definitions, specifications and conformity criteria. British Standard Institution.

European Committee for Standardization, BS EN 197-part 1 (2011). Cement-part 1: Composition, specifications and conformity criteria for common cement. British Standard Institution.

European Committee for Standardization, BS EN 934-2:2009+A1:2012(2012). Admixture for concrete, mortar and grout, Part 2: Concrete admixtures - Definitions, requirements, conformity, marking and labelling. British Standard Institution.

European Committee for Standardization, BS EN 934-2:2009+A1:2012(2012). Admixture for concrete, mortar and grout, Part 2: Concrete admixtures - Definitions, requirements, conformity, marking and labelling. British Standard Institution.

Fan, F., Liu, Z., Xu, G., Peng, H., & Cai, C. S. (2018). Mechanical and thermal properties of fly ash based geopolymers. Construction and Building Materials, 160, 66–81.

Finland. (2008)."Finnish Road Administration, Winter Maintenance Policy", TIEH 1000199E-v-08. 1755-1315

Flower, D. J. M., & Sanjayan, J. G. (2007). Greenhouse gas emissions due to concrete manufacture. The International Journal of Life Cycle Assessment, 12, 282–288.

Flower, D. J. M., & Sanjayan, J. G. (2017). Greenhouse Gas Emissions Due to Concrete Manufacture. Handbook of Low Carbon Concrete, 12(5), 1–16.

Gartner, E. (2004). Industrially interesting approaches to "low-CO_2" cements. Cement and Concrete Research, 34(9), 1489–1498.

Ghodousi, P., Afshar, M. H., Ketabchi, H., & Rasa, E. (2009). Study of early-age creep and shrinkage of concrete containing Iranian pozzolans: An experimental comparative study. Scientia Iranica, 16(2 A), 126–137.

Ghourchian, S., Wyrzykowski, M., Baquerizo, L., & Lura, P. (2018). Susceptibility of Portland cement and blended cement concretes to plastic shrinkage cracking. Cement and Concrete Composites, 85, 44–55.

Glass, G. K., Reddy, B., & Buenfeld, N. R. (2000). The participation of bound chloride in passive film breakdown on steel in concrete. Corrosion Science, 42(11), 2013–2021.

Goggins, J., Keane, T., & Kelly, A. (2010). The assessment of embodied energy in typical reinforced concrete building structures in Ireland. Energy and Buildings, 42(5), 735–744.

Griffin, P. W., Hammond, G. P., & Norman, J. B. (2014). Prospects for emissions reduction in the UK cement sector. Proceedings of Institution of Civil Engineers: Energy, 167(3), 152–161.

GSG Systems (2010). Impressed Current Cathodic Protection.

Habert, G. (2013). Assessing the environmental impact of conventional and "green" cement production. In Eco-Efficient Construction and Building Materials: Life Cycle Assessment (LCA), Eco-Labelling and Case Studies (pp. 199–238). Elsevier.

Habert, G., Billard, C., Rossi, P., Chen, C., & Roussel, N. (2010). Cement production technology improvement compared to factor 4 objectives. Cement and Concrete Research, 40(5), 820–826.

Hachani, M. I., Kriker, A., & Seghiri, M. (2017). Experimental study and comparison between the use of natural and artificial coarse aggregate in concrete mixture. Energy Procedia, 119, 182–191.

G. P. Hammond, C. I. Jones (2008), Embodied energy and carbon in construction materials. *Proc. Inst. Civ. Eng. – Energ.* 161 (2), 2008, 87-98

Hansson, C. M. (1984). Comments on electrochemical measurements of the rate of corrosion of steel in concrete. Cement and Concrete Research, 14(4), 574–584.

Hausmann, D. A. (1967). Corrosion of steel in concrete. How does it occur. J Mater Prot, 6, 19–23.

Hemalatha, M. S., & Santhanam, M. (2018). Characterizing supplementary cementing materials in blended mortars. Construction and Building Materials, 191, 440–459.

Hewlett, P. C. (1999). The role of water in determining concrete performance. In Concrete Durability and Repair Technology (pp. 63–80). Thomas Telford Publishing.

Hilsdorf, H., & Kropp, J. (1995). Performance criteria for concrete durability. CRC Press.

Holt, E. (2005). Contribution of mixture design to chemical and autogenous shrinkage of concrete at early ages. Cement and Concrete Research, 35(3), 464–472.

Hong, K., & Hooton, R. D. (1999). Effects of cyclic chloride exposure on penetration of concrete cover. Cement and Concrete Research, 29(9), 1379–1386.

Huang, L., Krigsvoll, G., Johansen, F., Liu, Y., & Zhang, X. (2018). Carbon emission of global construction sector. Renewable and Sustainable Energy Reviews, 81, 1906–1916.

Iacovidou, E., Millward-Hopkins, J., Busch, J., Purnell, P., Velis, C. A., Hahladakis, J. N., Zwirner, O., & Brown, A. (2017). A pathway to circular economy: Developing a conceptual framework for complex value assessment of resources recovered from waste. Journal of Cleaner Production, 168, 1279–1288.

Ibn-Mohammed, T., Greenough, R., Taylor, S., Ozawa-Meida, L., & Acquaye, A. (2013). Operational vs. embodied emissions in buildings - A review of current trends. Energy and Buildings, 66, 232–245.

IPCC-2014, Pachauri, R. K., M. R. Allen, V. R. Barros, J. Broome, W. Cramer, R. Christ, J. A. Church, L. Clarke, Q. Dahe and P. Dasgupta (2014). Climate change 2014: synthesis report. Contribution of Working Groups I, II and III to the fifth assessment report of the Intergovernmental Panel on Climate Change,.

Iraqi specification IQ.S. No 5(2019), Portland cement. Central Organization for Standardization and Quality Control, 2019.

Iraqi Standard Specifications No. (45), 1984 for Aggregates of Natural Resources used for Concrete and Construction.

Iraqi Standard Specifications No. (5), 1984 for Portland Cement.

Irassar, E. F., González, M., & Rahhal, V. (2000). Sulphate resistance of type V cements with limestone filler and natural pozzolana. Cement and Concrete Composites, 22(5), 361–368.

Irvine, D. J. (2018). Bridging the Gap Between Research and Practice. Groundwater, 56(1), 1.

Ishida, T., T. Kishi and K. Maekawa (2014). " Multi-scale modeling of structural concrete ". Crc Press.

Isteita, M., & Xi, Y. (2017). The effect of temperature variation on chloride penetration in concrete. Construction and Building Materials, 156, 73–82.

Jiang, C., Yang, Y., Wang, Y., Zhou, Y., & Ma, C. (2014). Autogenous shrinkage of high performance concrete containing mineral admixtures under different curing temperatures. Construction and Building Materials, 61, 260–269.

Jones, A. E. K., Marsh, B. K., Clark, L. A., Seymour, B. P. A. M., & Long, A. M. (1997). Development of a holistic approach to ensure Cement, the durabilty of new concrete construction. In British Cement Association, Report C/21. British Cement Association.

Jönsson, Å., Björklund, T., & Tillman, A. M. (1998). LCA of concrete and steel building frames. International Journal of Life Cycle Assessment, 3(4), 216–224.

Joseph Davidovits. (1993). Geopolymer Cements to Minimise Carbon Dioxide Greenhouse Warming. Ceramic Transactions, 37(1), 165–182.

Journals, I., Suresh, D., & Nagaraju, K. (2015). Ground Granulated Blast Slag (GGBS) In Concrete – A Review.

Juenger, M. C. G., Snellings, R., & Bernal, S. A. (2019). Supplementary cementitious materials: New sources, characterization, and performance insights. Cement and Concrete Research, 122, 257–273.

Karthika, V., Awoyera, P. O., Akinwumi, I. I., Gobinath, R., Gunasekaran, R., & Lokesh, N. (2018). Structural properties of lightweight self-compacting concrete made with pumice stone and mineral admixtures. Revista Romana de Materiale, 48(2), 208–213.

Khan, M. N. N., Saha, A. K., & Sarker, P. K. (2020). Reuse of waste glass as a supplementary binder and aggregate for sustainable cement-based construction materials: A review. Journal of Building Engineering, 28, 101052.

Klemczak, B., & Batog, M. (2016). Heat of hydration of low-clinker cements. Journal of Thermal Analysis and Calorimetry, 123(2), 1351–1360.

Koroneos, C. J., & Dompros, A. T. (2009). Environmental assessment of the cement and concrete life cycle in Greece. International Journal of Environmental Technology and Management, 10(1), 71–88.

Krivenko, P., Drochytka, R., Gelevera, A., & Kavalerova, E. (2014). Mechanism of preventing the alkali-aggregate reaction in alkali activated cement concretes. Cement and Concrete Composites, 45, 157–165.

Kumar Karri, S., Rao, G. V. R., & Raju, P. M. (2015). Strength and Durability Studies on GGBS Concrete. International Journal of Civil Engineering, 2(10), 34–41.

Lee, C. L., Huang, R., Lin, W. T., & Weng, T. L. (2012). Establishment of the durability indices for cement-based composite containing supplementary cementitious materials. Materials and Design, 37, 28–39.

Lee, K. M., Lee, H. K., Lee, S. H., & Kim, G. Y. (2006). Autogenous shrinkage of concrete containing granulated blast-furnace slag. Cement and Concrete Research, 36(7), 1279–1285.

Li, L. G., & Kwan, A. K., (2015). Adding limestone fines as cementitious paste replacement to improve tensile strength, stiffness and durability of concrete, Cement and Concrete Composites, 60, 17-24.

Li, Q., & Zhang, Q. (2019). Experimental study on the compressive strength and shrinkage of concrete containing fly ash and ground granulated blast-furnace slag. Structural Concrete, 20(5), 1551–1560.

Li, S. (2016). Microstructure and composition characterisation of three 20-year-old GGBS-OPC blended pastes. Construction and Building Materials, 123, 226–234.

Li, S., & Roy, D. M. (1986). Investigation of relations between porosity, pore structure, and C1- diffusion of fly ash and blended cement pastes. Cement and Concrete Research, 16(5), 749–759.

Li, Z., Peng, J., & Ma, B. (1999). Investigation of chloride diffusion for high-performance concrete containing fly ash, microsilica, and chemical admixtures. Materials Journal, 96(3), 391–396.

Lindroos, N., Nysten, T., I Salpausselän pohjaveden kloridipitoisuuden muutokset ja niihin vaikuttavia tekijöitä, Liikenneviraston tutkimuksia ja selvityksiä 11/2015. Finland 2015. (in Finnish)

Liu, J., & Wang, D. (2017). Influence of steel slag-silica fume composite mineral admixture on the properties of concrete. Powder Technology, 320, 230–238.

Liu, J., Zhang, W., Li, Z., Jin, H., & Tang, L. (2021). Influence of deicing salt on the surface properties of concrete specimens after 20 years. Construction and Building Materials, 295, 123643.

Long, A. E., Henderson, G., Basheer, L., Sonebi, M., & Basheer, P. A. M. (2009). Chapter 19: Concrete mix design methods. In ICE manual of Construction Materials: Volume I: Fundamentals and theory; Concrete; Asphalts in road construction; Masonry (pp. 219–230). Thomas Telford Ltd.

Loser, R., Lothenbach, B., Leemann, A., & Tuchschmid, M. (2010). Chloride resistance of concrete and its binding capacity - Comparison between experimental results and thermodynamic modeling. Cement and Concrete Composites, 32(1), 34–42.

Lothenbach, B., Le Saout, G., Haha, M. Ben, Figi, R., & Wieland, E. (2012). Hydration of a low-alkali CEM III/B–SiO2 cement (LAC). Cement and Concrete Research, 42(2), 410–423.

Lothenbach, B., Scrivener, K., & Hooton, R. D. (2011). Supplementary cementitious materials. Cement and Concrete Research, 41(12), 1244–1256.

Lu, C., Yuan, S., Cheng, P., & Liu, R. (2016). Mechanical properties of corroded steel bars in pre-cracked concrete suffering from chloride attack. Construction and Building Materials, 123, 649–660.

Luo, L., & De Schutter, G. (2004). Study of the corrosion-inhibiting performance of corrosion inhibitors in reinforced concrete. 5th International PhD Symposium in Civil Engineering - Proceedings of the 5th International PhD Symposium in Civil Engineering, 1, 259–267.

Lura, P., Van Breugel, K., & Maruyama, I. (2001). Effect of curing temperature and type of cement on early-age shrinkage of high-performance concrete. Cement and Concrete Research, 31(12), 1867–1872.

Mahasenan, M., & Humphreys, K. (2002). Toward a Sustainable Cement Industry Substudy 8: Climate Change. World Business Council for Sustainable Development, 8.

Malhotra, V. M. (2004). Role of supplementary cementing materials and superplasticizers in reducing greenhouse gas emissions. Proceedings of ICFRC International Conference on Fiber Composites, High-Performance Concrete, and Smart Materials, Chennai, India, 489–499.

Martın-Pérez, B. (1999). Service life modelling of RC highway structures exposed to chlorides. University of Toronto Toronto, ON, Canada.

MASLI, A. (2011). *Interaction Between Cathodic Protection and MicrobiallyI Influenced Corrosion*. [online] University of Manchester, pp.29-35. Available at:

McCarthy, M. J., Robl, T., & Csetenyi, L. J. (2017). Recovery, processing, and usage of wet-stored fly ash. In Coal Combustion Products (CCPs): Characteristics, Utilization and Beneficiation (pp. 343–367). Elsevier.

Medina, J. M., Sáez del Bosque, I. F., Frías, M., Sánchez de Rojas, M. I., & Medina, C. (2019). Durability of new blended cements additioned with recycled biomass bottom ASH from electric power plants. Construction and Building Materials, 225, 429–440.

Mehta, P. K. (1983). Pozzolanic and cementitious byproducts as mineral admixtures for concrete - A critical review. American Concrete Institute, ACI Special Publication, SP-079, 1–46.

Mehta, P. K., & Monteiro, P. J. M. (2014). Concrete: microstructure, properties, and materials. McGraw-Hill Education.

Memon, A. H., Radin, S. S., Zain, M. F. M., & Trottier, J.-F. (2002). Effects of mineral and chemical admixtures on high-strength concrete in seawater. Cement and Concrete Research, 32(3), 373–377.

Metal Samples Company (2016). Corrosion Coupons & weight Loss Analysis. [online] Alabama Specialty Products.

Miller, S. A., John, V. M., Pacca, S. A., & Horvath, A. (2018). Carbon dioxide reduction potential in the global cement industry by 2050. Cement and Concrete Research, 114, 115–124.

Mineral Products Association MPA (2009). Mineral Products Association Sustainable Development Report 2009. [online] p.43.

Mohammed, T. U., Otsuki, N., & Hamada, H. (2001). Oxygen permeability in cracked concrete reinforced with plain and deformed bars. Cement and Concrete Research, 31(5), 829–834.

Moncaster, A. M., Pomponi, F., Symons, K. E., & Guthrie, P. M. (2018). Why method matters: Temporal, spatial and physical variations in LCA and their impact on choice of structural system. Energy and Buildings, 173, 389–398.

Moretti, J. P., Sales, A., Quarcioni, V. A., Silva, D. C. B., Oliveira, M. C. B., Pinto, N. S., & Ramos, L. W. S. L. (2018). Pore size distribution of mortars produced with agroindustrial waste. Journal of Cleaner Production, 187, 473–484.

Nemati, K. M. (2015). Concrete Technology: Strength of Concrete. University of Washington.

Neville, A. M. (2011). Properties of Concrete, 4th. London Pearson Education Limited, 443(846), 444.

Nilsson L, Ngo MH, Gjørv OE1998. High-performance repair materials for concrete structures in the port of Gothenburg. In: Second international conference on concrete under severe conditions: environment and loading, vol. 2; p. 1193–8.

Nilsson, L. O. (2019). Corrosion of steel in concrete. Developments in the Formulation and Reinforcement of Concrete, 115–129.

Nisbet, M., & Van Geem, M. G. (1997). Environmental life cycle inventory of Portland cement and concrete. World Cement, 28(4), 3.

NT BUILD 208 -3 (1996-11) Chloride Content by volhard titration.

NT Build 492. (1999). Concrete, mortar and cement-based repair materials: Chloride migration coefficient from non-steady-state migration experiments. Measurement, 1–8.

Nürnberg, H. W. (1984). The voltammetric approach in trace metal chemistry of natural waters and atmospheric precipitation. Analytica Chimica Acta, 164(C), 1–21.

Oh, B. H., Cha, S. W., Jang, B. S., & Jang, S. Y. (2002). Development of high-performance concrete having high resistance to chloride penetration. Nuclear Engineering and Design, 212(1–3), 221–231.

Okonkwo, V. O., & Arinze Emmanuel, E. (2018). A Study of the Effect of Aggregate Proportioning On Concrete Properties American Journal of Engineering Research (AJER). American Journal of Engineering Research, 7(4), 61–67.

Olivier, J. G. J. O., & Bakker, J. (2001). Good Practice Guidance and Uncertainty Management in National Greenhouse Gas Inventories. Intergovernmental Panel on Climate Change, 227–241.

Onuaguluchi, O., & Panesar, D. K., (2014). Hardened properties of concrete mixtures containing pre-coated crumb rubber and silica fume. Journal of Cleaner Production, 82, 125-131.

Osborne, G. J. (1999). Durability of Portland blast-furnace slag cement concrete. Cement and Concrete Composites, 21(1), 11–21.

P. Mukherjee, M. S., Vesmawala, D. G., & C Shah, M. S. (2016). Exploring GGBS Utilization in Construction of Residential Projects & Its Contribution toward Environment. IOSR Journal of Mechanical and Civil Engineering, 13(04), 01–11.

Papadakis, V. G., & Tsimas, S. (2002). Supplementary cementing materials in concrete: Part I: efficiency and design. Cement and Concrete Research, 32(10), 1525–1532.

Park, D. (2008). "Carbonation of concrete in relation to CO_2 permeability and degradation of coatings". Construction and building Materials 22(11): 2260-2268

Park, Y.-G., & Kim, J.-I. (2010). A Study on the Reduction of $ CO_2 $ Emission by the Application of Clean Technology in the Cement Industry. Clean Technology, 16(3), 182–190.

Patra, R. K., & Mukharjee, B. B. (2017). Influence of incorporation of granulated blast furnace slag as replacement of fine aggregate on properties of concrete. Journal of Cleaner Production, 165, 468–476.

Penttala, V. (2009). Causes and mechanisms of deterioration in reinforced concrete. In Failure, Distress and Repair of Concrete Structures (pp. 3–31). Elsevier.

Pittman, D. W., & Ragan, S. A. (1998). Drying shrinkage of roller-compacted concrete for pavement applications. Materials Journal, 95(1), 19–26.

Purnell, P., & Black, L. (2012). Embodied carbon dioxide in concrete: Variation with common mix design parameters. Cement and Concrete Research, 42(6), 874–877.

Ramezanianpour, A. A., & Bahrami Jovein, H. (2012). Influence of metakaolin as supplementary cementing material on strength and durability of concretes. Construction and Building Materials, 30, 470–479.

Ramezanianpour, A. A., & Malhotra, V. M. (1995). Effect of curing on the compressive strength, resistance to chloride-ion penetration and porosity of concretes incorporating slag, fly ash or silica fume. Cement and Concrete Composites, 17(2), 125–133.

Ramm, W., & Biscoping, M. (1998). Autogenous healing and reinforcement corrosion of water-penetrated separation cracks in reinforced concrete. Nuclear Engineering and Design, 179(2), 191–200.

Ritchie, H., & Roser, M. (2017). CO_2 and other greenhouse gas emissions. Our World in Data.

Rodrigues, R., Gaboreau, S., Gance, J., Ignatiadis, I., & Betelu, S. (2021). Reinforced concrete structures: A review of corrosion mechanisms and advances in electrical methods for corrosion monitoring. Construction and Building Materials, 269, 121240.

Rosales, J., Pérez, S. M., Cabrera, M., Gázquez, M. J., Bolivar, J. P., de Brito, J., & Agrela, F. (2020). Treated phosphogypsum as an alternative set regulator and mineral addition in cement production. Journal of Cleaner Production, 244, 118752.

Sanal, I., Sarialioglu, D., Pilgir, V., Turgut, T., & Akkaya, Y. (2016). Identification and Evaluation of CO_2 Emissions of Various Concretes Produced in Different Ready Mix Concrete Plants. 12th International Conference on Advances in Civil Engineering.

Sanjuán, M. Á., Rivera, R. A., Martín, D. A., & Estévez, E. (2022). Chloride Diffusion in Concrete Made with Coal Fly Ash Ternary and Ground Granulated Blast-Furnace Slag Portland Cements. Materials, 15(24), 8914.

Schöler, A., Lothenbach, B., Winnefeld, F., & Zajac, M. (2015). Hydration of quaternary Portland cement blends containing blast-furnace slag, siliceous fly ash and limestone powder. Cement and Concrete Composites, 55, 374–382.

Schuurmans, A., Rouwette, R., Vonk, N., Broers, J. W., Rijnsburger, H. A., & Pietersen, H. S. (2005). LCA of finer sand in concrete. International Journal of Life Cycle Assessment, 10(2), 131–135.

Scottish Water 2008, Scottish Water carbon footprint report 2007-2008. Scottish Water.

Scrivener, K. L., Lothenbach, B., De Belie, N., Gruyaert, E., Skibsted, J., Snellings, R., & Vollpracht, A. (2015). TC 238-SCM: hydration and microstructure of concrete with SCMs: State of the art on methods to determine degree of reaction of SCMs. Materials and Structures/Materiaux et Constructions, 48(4), 835–862.

Sear, L. K. a. (2001). Fly ash standards, market strategy and UK practice. International Ash Utilization Symposium, 38(7), Paper #36.

Shanks, W., Dunant, C. F., Drewniok, M. P., Lupton, R. C., Serrenho, A., & Allwood, J. M. (2019). How much cement can we do without? Lessons from cement material flows in the UK. Resources, Conservation and Recycling, 141, 441–454. https://doi.org/10.1016/j.resconrec.2018.11.002

Shehab, H. K., Eisa, A. S., & Wahba, A. M. (2016). Mechanical properties of fly ash based geopolymer concrete with full and partial cement replacement. Construction and Building Materials, 126, 560–565.

Shen, X., Liu, Q., Hu, Z., Jiang, W., Lin, X., Hou, D., & Hao, P. (2019). Combine ingress of chloride and carbonation in marine-exposed concrete under unsaturated environment: A numerical study. Ocean Engineering, 189, 106350.

Siddique, R. (2014). Utilization (recycling) of iron and steel industry by-product (GGBS) in concrete: Strength and durability properties. Journal of Material Cycles and Waste Management, 16(3), 460–467.

Siddique, R., & Bennacer, R. (2012). Use of iron and steel industry by-product (GGBS) in cement paste and mortar. Resources, Conservation and Recycling, 69, 29–34.

Silva, N. (2013). Chloride Induced Corrosion of Reinforcement Steel in Concrete Thershold Values and Ion Distribution at the Concrete-Steel Interface [online] p.10 fig 2.4.

Skibsted, J., & Snellings, R. (2019). Reactivity of supplementary cementitious materials (SCMs) in cement blends. Cement and Concrete Research, 124, 105799.

Snellings, R., Mertens, G., & Elsen, J. (2012). Supplementary cementitious materials. Reviews in Mineralogy and Geochemistry, 74(12), 211–278.

Statista. (2019). *Global cement production top countries 2017 /* Statistic.

Statistics 2016. EUROSLAG Survey European Steel. Available online:

Stratmann, M., & Müller, J. (1994). The mechanism of the oxygen reduction on rust-covered metal substrates. Corrosion Science, 36(2), 327–359.

Sturgis, S., & Roberts, G. (2010). Carbon Profiling as a solution to whole life carbon emmission measurement in buildings. RICS Research, May.

Summaries, M. C. (2021). Mineral commodity summaries. US Geological Survey: Reston, VA, USA, 200.

Szalay, A. Z.-Z. (2007). What is missing from the concept of the new European Building Directive? Building and Environment, 42(4), 1761–1769.

Tazawa, E. (2020). Temperature effects on early age autogenous shrinkage in high performance concretes. In Autogenous Shrinkage of Concrete (pp. 167–178). CRC Press.

Tazawa, E. ichi, & Miyazawa, S. (1995). Influence of cement and admixture on autogenous shrinkage of cement paste. Cement and Concrete Research, 25(2), 281–287.

Teychenne, D. C., Franklin, R. E., & Erntroy, H. C. (1997). Design of normal concrete mixes, amended by BK Marsh. Building Research Establishment, Garston, England.

Teychenné, D.C., E Franklin, R.E. and Erntroy, H. C., Design of normal concrete mixes. Second edition. Building Research Establishment. Garston, Watford, (1988).

Thangavel,K. and Rengaswamy, N.S. (1998). Relationship between chloride/hydroxide ratio and corrosion rate of steel in concrete. Cement and Concrete Composites, [online] 20(4), pp.283-292. Available at:

The European Union Euro-code 2: Design of concrete structures - Part 1-1(2011).: General rules and rules for buildings [Authority: The European Union Per Regulation 305/2011, Directive 98/34/EC, Directive 2004/18/EC]

Thomas, B. S. (2018). Green concrete partially comprised of rice husk ash as a supplementary cementitious material – A comprehensive review. Renewable and Sustainable Energy Reviews, 82, 3913–3923.

Thomas, M. (2011). The effect of supplementary cementing materials on alkali-silica reaction: A review. Cement and Concrete Research, 41(12), 1224–1231.

Thormark, C. (2002). A low energy building in a life cycle - Its embodied energy, energy need for operation and recycling potential. Building and Environment, 37(4), 429–435.

Toledo Filho, R. D., Ghavami, K., Sanjuán, M. A., & England, G. L. (2005). Free, restrained and drying shrinkage of cement mortar composites reinforced with vegetable fibres. Cement and Concrete Composites, 27(5), 537–546.

Torii, K., Sasatani, T., & Kawamura, M. (1995). Effects of fly ash, blast furnace slag, and silica fume on resistance of mortar to calcium chloride attack. American Concrete Institute, ACI Special Publication, SP-153, 931–949.

Tuutti, K. (1982). Corrosion of steel in concrete. Cement-och betonginst.

U.S., Geological, & Survey. (2019). Mineral Commodity Summaries 2019 [Internet].

Valcuende, M., Benito, F., Parra, C., & Miñano, I. (2015). Shrinkage of self-compacting concrete made with blast furnace slag as fine aggregate. Construction and Building Materials, 76, 1–9.

Venkatachalapathy, V. (2016). Effect of slag cement on drying shrinkage of concrete. ACI Materials Journal, 113(1), 121.

Vidal, T., Castel, A., & François, R. (2004). Analyzing crack width to predict corrosion in reinforced concrete. Cement and Concrete Research, 34(1), 165–174.

Vilane, B. R. T., & Sabelo, N. (2016). The effect of aggregate size on the compressive strength of concrete. Journal of Agricultural Science and Engineering, 2(6), 66–69.

Vold, M., & Ronning, A. (1995). LCA of Cement and Concrete. Stiftelsen ØstfoldforsKning.

Vollpracht, A., Lothenbach, B., Snellings, R., & Haufe, J. (2016). The pore solution of blended cements: a review. Materials and Structures/Materiaux et Constructions, 49(8), 3341–3367.

Wang, J., Basheer, P. A. M., Nanukuttan, S. V, Long, A. E., & Bai, Y. (2016). Influence of service loading and the resulting micro-cracks on chloride resistance of concrete. Construction and Building Materials, 108, 56–66.

WBCSD, I. E. A. (2009). Cement Technology Roadmap 2009. Carbon Emissions Reductions up To, 2050, 36.

Y. Liu, & R. E. Weyers. (1998). Modeling the Time to Corrosion Cracking in Chloride contaminated Reinforced Concrete Structures. In ACI Materials Journal (Vol. 95, Issue 6, pp. 675–680). Virginia Tech.

Yang, J., Wang, Q., & Zhou, Y. (2017). Influence of Curing Time on the Drying Shrinkage of Concretes with Different Binders and Water-to-Binder Ratios. Advances in Materials Science and Engineering, 2017.

Yang, K. H., Jung, Y. B., Cho, M. S., & Tae, S. H. (2017). Effect of Supplementary Cementitious Materials on Reduction of CO_2 Emissions from Concrete. Handbook of Low Carbon Concrete, 103, 89–110.

Yeo, D., & Gabbai, R. D. (2011). Sustainable design of reinforced concrete structures through embodied energy optimization. Energy and Buildings, 43(8), 2028–2033.

Yildirim, H., Ilica, T., & Sengul, O. (2011). Effect of cement type on the resistance of concrete against chloride penetration. Construction and Building Materials, 25(3), 1282–1288.

Yoon, Y. C., Kim, K. H., Lee, S. H., & Yeo, D. (2018). Sustainable design for reinforced concrete columns through embodied energy and CO_2 emission optimization. Energy and Buildings, 174, 44–53.

Yuan, J., Lindquist, W. D., Darwin, D., & Browning, J. (2015). Effect of slag cement on drying shrinkage of concrete.

Zevenhoven, R., Backman, R., Hupa, M., Oy, F., & Group, P. C. (2002). Modelling a Cement Manufacturing Process to Study Possible Impacts of Alternative Fuels. Fuel, 30, 1–9.

Zhang, J., Tan, H., He, X., Yang, W., & Deng, X. (2020). Utilization of carbide slag-granulated blast furnace slag system by wet grinding as low carbon cementitious materials. Construction and Building Materials, 249, 118763.

Zhang, S. P., & Zong, L. (2014). Evaluation of relationship between water absorption and durability of concrete materials. Advances in Materials Science and Engineering, 2014.

Zhang, W., Ye, Z., & Gu, X. (2017). Effects of stirrup corrosion on shear behaviour of reinforced concrete beams. Structure and Infrastructure Engineering, 13(8), 1081–1092.

Zhang, Y., Zhang, J., Lü, M., Wang, J., & Gao, Y. (2019). Considering uncertainty in life-cycle carbon dioxide emissions of fly ash concrete. Proceedings of the Institution of Civil Engineers: Engineering Sustainability, 172(4), 198–206.

Zhou, X. M., Slater, J. R., Wavell, S. E., & Oladiran, O. (2012). Effects of PFA and GGBS on early-ages engineering properties of Portland cement systems. Journal of Advanced Concrete Technology, 10(2), 74–85.

Živica, V. (2003). Corrosion of reinforcement induced by environment containing chloride and carbon dioxide. Bulletin of Materials Science, 26(6), 605–608.

Zou, D. J., Liu, T. J., & Qiao, G. F. (2014). Experimental investigation on the dynamic properties of RC structures affected by the reinforcement corrosion. Advances in Structural Engineering, 17(6), 851–86

Appendix-A1: Material safety datasheet

1. Data sheet of superplasticizer provided by the manufacturer

Hyperplast PC200

High performance concrete superplasticiser
(Formerly known as Flocrete PC200)

Description

Hyperplast PC200 is a high performance super plasticising admixture based on polycarboxylic ether polymers with long chains specially designed to enable the water content of the concrete to perform more effectively. This effect can be used in high strength concrete and flowable concrete mixes, to achieve highest concrete durability and performance.

Applications

- High strength and high performance concrete.
- Structures with congested reinforcement.
- Pre-cast concrete.
- Improved cohesion allow for use in mass concrete pours and piling.
- Self compacting concrete.

Advantages

- Optimises cement utilization.
- High density and impermeable concrete through very high water reduction.
- Improves shrinkage and creep behaviors.
- Minimizes segregation and bleeding problems by improving cohesion.
- Higher early and ultimate compressive strengths.
- Increases durability and resistance to aggressive atmospheric conditions thorough reduced permeability.

Compatibility

Hyperplast PC200 can be used with all types of Portland cement and cement replacement materials.

Hyperplast PC200 should not be used in conjunction with other admixtures unless DCP Technical Department approval is obtained.

Standards

Hyperplast PC200 complies with ASTM C494, Type A and G, depending on dosage used.

Method of Use

Hyperplast PC200 should be added to the concrete with the mixing water to achieve optimum performance.

Technical Properties @ 25°C:	
Color:	Light yellow liquid
Freezing point:	≈ -3°C
Specific gravity:	1.05 ± 0.02
Air entrainment:	Typically less than 2% additional air is entrained above control mix at normal dosages

Automatic dispenser should be used to dispense the correct quantity of Hyperplast PC200 to the concrete mix.

Dosage

The guidance dosage of Hyperplast PC200 is 0.75 - 2.50 liters/ 100 kg of cementitious
materials in the mix, including GGBFS, PFA or microsilica. Representative trials should be conducted to determine the optimum dosage of Hyperplast PC200 to meet the performance requirements by using the materials and conditions in actual use.

Effects of Over Dosage

Over dosing of Hyperplast PC200 will cause the following:

- Significant increase in retardation.
- Increase in workability.

Ultimate concrete strength will not be adversely affected and will generally be increased provided that proper concrete curing is maintained.

Cleaning

Hyperplast PC200 can be washed with fresh cold water.

Packaging

Hyperplast PC200 is available in 25 liters pails, 210 liters drums and 1000 liters bulks supply.

Storage

Hyperplast PC200 shelf life is 12 months if stored at temperatures between 2°C and 50°C.

APPENDIX-A1: MATERIALS SAFETY DATASHEET

Hyperplast PC200

If these conditions are exceeded, DCP Technical Department should be contacted for advice.

Cautions

Health and Safety

Hyperplast PC200 is not classified as hazardous material. Hyperplast PC200 should not come into contact with skin and eyes.

In case of contact with eyes wash immediately with plenty of water and seek medical advice promptly.

For further information refer to the Material Safety Data sheet.

Fire

Hyperplast PC200 is non-flammable.

More from Don Construction Products

A wide range of construction chemicals products are manufactured by DCP which include:

- Concrete admixtures.
- Grouts and chemical fixings.
- Concrete repairs.
- Industrial floorings.
- Structural protection.
- Waterproofing.

APPENDIX-A1: MATERIALS SAFETY DATASHEET

2. Data sheet of water proofing based (Setseal FLX) provided by the manufacturer

سيت سيل إف إل إكس
Setseal FLX

طلاء اسمنتي عازل للماء للأسقف معزز بالأكريليك المطاطي

الوصف

سيت سيل إف إل إكس طلاء اسمنتي عازل للماء معزز بالبوليمر المطاطي وذو مكونين لعزل الأسقف والمناطق الرطبة.

التطبيقات

- العزل المائي للأسقف والمناطق الرطبة.
- العزل المائي لمنشآت حفظ مياه والأحواض.
- حماية الأسطح الخرسانية ومواد البناء من ثاني أكسيد الكربون وأيونات الكلوريد والماء وأملاح إزالة الجليد.

الميزات

- عازل للماء، مناسب لعزل الأسقف ومنشآت حفظ مياه والأقبية.
- يتمتع بخاصية التنفس، فهو يسمح بخروج أبخرة الماء من خلاله.
- ذو ديمومة عالية ومقاومة ممتازة لأشعة UV.
- مقاومة ممتازة لثاني أكسيد الكربون وأيونات الكلوريد والماء.
- غير سام، يصلح لملامسة الماء الصالح للشرب.
- فعّال واقتصادي، يمكن تطبيقه بسرعة وسهولة بالفرشاة أو بالرش.
- مناسب للتطبيقات الداخلية والخارجية.
- قادر على تحمل حركة عبور مشاة.
- قادر على تحمل الضغوط العالية للماء الإيجابية والسلبية.

المعايير والمقاييس

سيت سيل إف إل إكس مناسب للاستخدام لملامسة الماء الصالح للشرب عند اختباره وفق المواصفة BS 6920.

طريقة الاستعمال

تحضير السطح

يجب أن تكون الأسطح سليمة ونظيفة وخالية من أي ملوثات قبل تطبيق سيت سيل سي. ويجب إزالة أي أثر لمركبات الإيداع وطبقات الخرسانة السطحية المفككة وأي أجسام عضوية أو غريبة وأفضل الطرق لتحقيق ذلك يتم باستخدام ضغط المياه العالي أو القذف الرملي الخفيف.

الخصائص الفنية عند 25 درجة مئوية:	
كثافة الخليط	1.75 ± 0.05 غم/سم³
زمن عمل الخليط	45 دقيقة
اللون	رمادي أو أبيض
نسبة الخلط	5.1 كغم من البوليمر السائل لكل 10.9 كغم بودرة.
أقل درجة حرارة للتطبيق	5 درجات مئوية
قوة الالتصاق ASTM D4541-02	> 1.6 ميغاباسكال
سعة تحمل الشقوق في حالة السكون	1 مم
النفوذية للماء (عند سماكة 2 مم) DIN 1048	ناجح عند ضغط إيجابي > 12 بار ناجح عند ضغط سلبي > 6 بار
الاستطالة عند القطع (من دون تدعيم عند سماكة 4 مم) ASTM D412	> 15% إيناع جاف بعد 28 يوم > 10% إيناع رطب بعد 28 يوم
الحدّ الأقصى لحجم الحصمة (الركام)	0.5 مم
زمن الشك الابتدائي	40 - 50 دقيقة
زمن الشك النهائي	2 - 3 ساعات

أوفي حال وجود تعشيش في الخرسانة أو أي أضرار أو أجزاء تالفة فيها يجب معالجتها باستخدام مونة اسمنتية مناسبة قليلة النفاذية للماء والمتوفرة ضمن أنظمة إصلاح DCP وذلك قبل البدء بتطبيق الطلاء.

APPENDIX-A1: MATERIALS SAFETY DATASHEET

سيت سيل إف إل إكس
Setseal FLX

طبقة التأسيس

لا يحتاج إلى طبقة تأسيس مستقلة لكن يجب إشباع الأسطح بالماء قبل تطبيق سيت سيل إف إل إكس.

الخلط

لضمان خلط مناسب، يجب استخدام خلاط ميكانيكي آلي أو مثقاب (دريل) مزود بريشة مناسبة.

يتم إضافة كامل محتوى مكون سيت سيل إف إل إكس السائل(5.1 كغم) إلى وعاء نظيف ثم يتم إضافة كامل مكون البودرة (10.9 كغم) ببطء مع استمرار الخلط باستخدام خلاط بطيء (دريل) بسرعة دوران تتراوح بين (400 و 600 دورة بالدقيقة) لمدة 3 دقائق لغاية الحصول على قوام متجانس.

التطبيق

يمكن تطبيق سيت سيل إف إل إكس باستخدام الفرشاة أو الرش. ويطبق الخليط بشكل جيد على السطح بالفرشاة باتجاه ثابت مع ضرورة الانتباه إلى عدم تنفيذ طبقات رقيقة جداً وعند ملاحظة بدء جفاف المادة وتكتلها لا تضف الماء ولكن رطب السطح مرة ثانية.

يجب ترك الطبقة الأولى لتجف لليوم التالي قبل تطبيق الطبقة الثانية. تنفذ الطبقة الثانية بالفرشاة وبنفس طريقة تنفيذ الطبقة الأولى لكن يفضل أن تكون بشكل عامودي عليها لضمان الحصول على التصاق أفضل وتغطية جيدة.

في المناطق المعرضة لحركة مرور مشاة يجب تركيب شبكة من الألياف الزجاجية (2*2) بين طبقتي سيت سيل إف إل إكس.

التنظيف

يجب تنظيف جميع التجهيزات مباشرة بعد الانتهاء من التطبيق بالماء النظيف. المواد المتصلبة تنظف ميكانيكياً.

التعبئة

سيت سيل إف إل إكس متوفر بعبوات 16 كغم (5.1 كغم البوليمر و 10.9 كغم بودرة).

التغطية

حوالي 9 م² عند تنفيذه على طبقة واحدة بسماكة 1 مم.

التخزين

سيت سيل إف إل إكس صالح لمدة 12 شهرا من تاريخ الانتاج مع مراعاة ضرورة تخزينه بدرجات حرارة تتراوح بين 5 و 35 درجة مئوية.

تجنب استخدام المنتج في حال لم تتحقق هذه الشروط إلا بعد استشارة القسم التقني في شركة DCP.

تحذيرات

الصحة والسلامة العامة

يحتوي سيت سيل إف إل إكس على الاسمنت والرمل لذلك قد يسبب تهيجاً للجلد والعين. في حال التلامس العرضي مع العين يلزم غسلها بالماء النظيف لمدة 10 دقائق على الأقل واطلب المشورة الطبية إذا لزم الأمر.

لمزيد من المعلومات راجع ورقة بيانات السلامة العامة للمادة.

الاشتعال

سيت سيل إف إل إكس مادة غير قابلة للاشتعال.

المزيد من منتجات شركة DCP

تنتج شركة DCP مجموعة واسعة من المنتجات الكيميائية في قطاع الإنشاءات تشتمل على:

- المضافات الخاصة بالخرسانة
- مواد معالجة الأسطح
- الجراوت ومواد زراعة قضبان التسليح
- مونة متخصصة لاصلاح الخرسانة
- أنظمة الأرضيات المتخصصة
- طلاءات التغطية لحماية الأسطح الخرسانية والمعدنية
- المعاجين (الماستيك) للفواصل ومواد ملء الفواصل
- المواد العازلة لتسرب المياه
- مواد التأسيس والمواد الرابطة
- لواصق وروبات البلاط
- القصارة الجاهزة ومواد التشطيب الخاصة
- مواد تقوية العناصر الانشائية

APPENDIX-A2: calculation of chloride diffusion rate (Da) and chloride accumulation on the concrete surface

This appendix contains the calculation of the rate of diffusion of chloride into concrete (Da) and the accumulation of chlorides on the concrete surface (Cs), the experimental results of the chloride concentration profile are compared to the non-linear best fitting of Fick's Second Law, as represented by **Equation (3-12)**

$$C(x,t) = C_i + (C_S - C_i)\left[1 - erf\left(\frac{x}{2\sqrt{D_a \cdot t}}\right)\right] \qquad \textbf{(3-12)}$$

C(x,t) represents the chloride concentration at a specific position *(x)* and time *(t)*, C_i is the initial chloride concentration, C_S is the surface concentration, *x* is the distance from the surface, *t* is the time duration, *erf* is the error function and *Da* is the apparent diffusion coefficient

Mixture	**C(25,0%)**					
Da	2.90E-11					
Cs	1.75	**Depth**	**Cl^-**	**Estimate from Eq. (3-12)**		**(Prid-Exper.)^2**
Ci	0.177	5	1.3	1.496		0.022113873
		15	1.1	1.028		0.001292337
		25	1.0	0.661		0.087462598
		35	0.5	0.418		0.012839573
		45	0.2	0.282		0.010940893
		55	0.2	0.216		0.001534869
					Summation	0.136184143

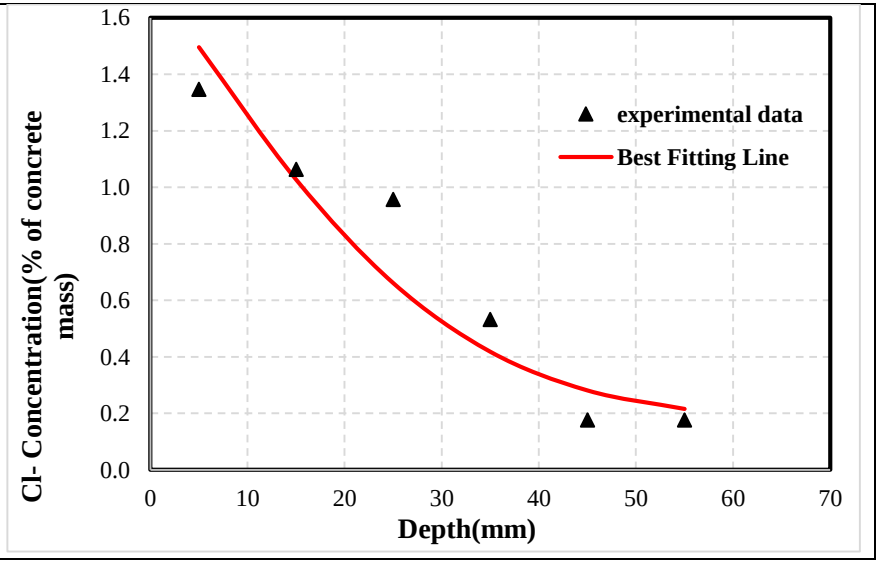

APPENDIX-A2: Calculation of Chloride diffusion rate (Da) and Chloride accumulation on the Concrete surface

Mixture	C(25,25%)					
Da	2.80E-11					
Cs	1.7	Depth	Cl^-	Estimate from Eq. (3-12)		(Prid-Exper.)^2
Ci	0.177	5	1.2	1.450		0.043616552
		15	1.0	0.990		8.75824E-06
		25	0.7	0.633		0.001636206
		35	0.4	0.400		0.002059548
		45	0.2	0.271		0.008866167
		55	0.2	0.211		0.001169738
					Summation	0.057356969

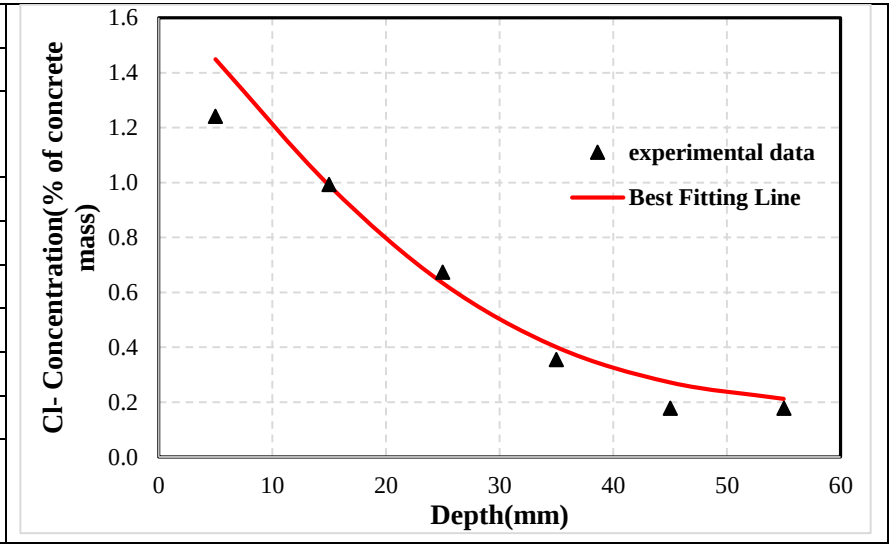

Mixture	C(25,50%)					
Da	2.7E-11					
Cs	1.52	Depth	Cl^-	Estimate from Eq. (3-12)		(Prid-Exper.)^2
Ci	0.177	5	1.1	1.295		0.02585575
		15	1.1	0.884		0.032385329
		25	0.7	0.567		0.02005114
		35	0.4	0.364		8.61978E-05
		45	0.2	0.254		0.005900306
		55	0.2	0.204		0.000728832
					Summation	0.085007554

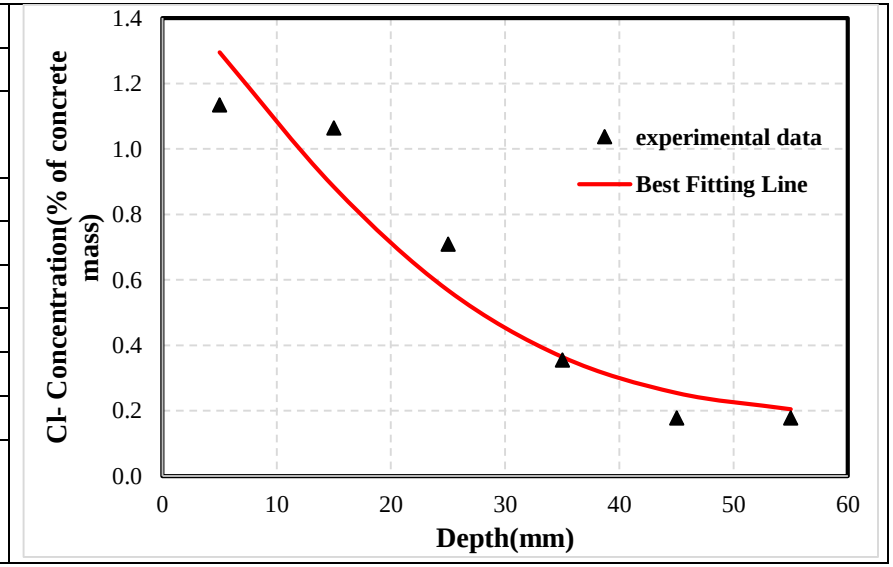

APPENDIX-A2: Calculation of Chloride diffusion rate (Da) and Chloride accumulation on the Concrete surface

Mixture	C(30,0%)					
Da	2.90E-11					
Cs	1.55	Depth	Cl^-	Estimate from Eq. (3-12)		(Prid-Exper.)^2
Ci	0.177	5	1.2	1.328		0.007642438
		15	1.0	0.919		0.005352088
		25	0.7	0.600		0.005431665
		35	0.4	0.388		4.80565E-06
		45	0.2	0.268		0.008335591
		55	0.2	0.211		0.001169378
					Summation	0.027935965

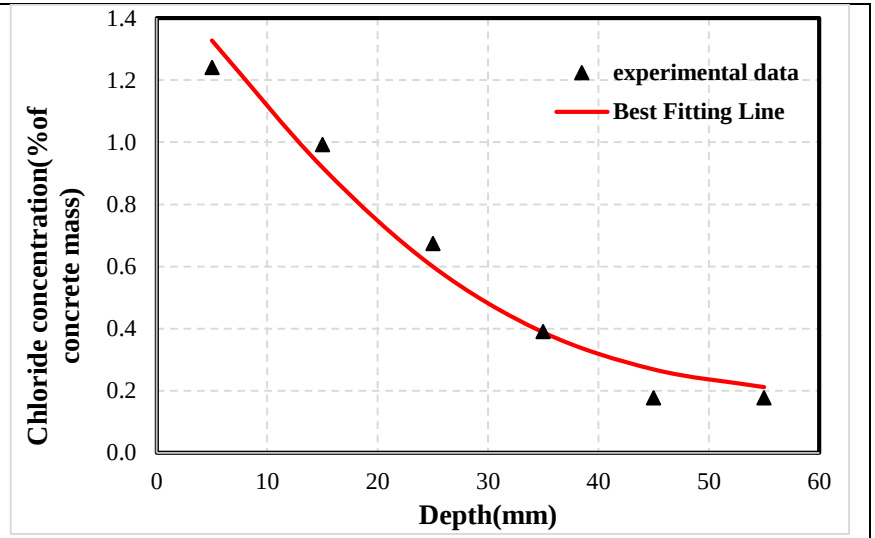

Mixture	C(30,25%)					
Da	2.60E-11					
Cs	1.44	Depth	Cl^-	Estimate from Eq. (3-12)		(Prid-Exper.)^2
Ci	0.177	5	1.2	1.225		0.000374935
		15	0.8	0.832		0.002670324
		25	0.7	0.533		0.019843148
		35	0.3	0.343		0.003571045
		45	0.2	0.243		0.004416473
		55	0.2	0.200		0.000508246
					Summation	0.03138417

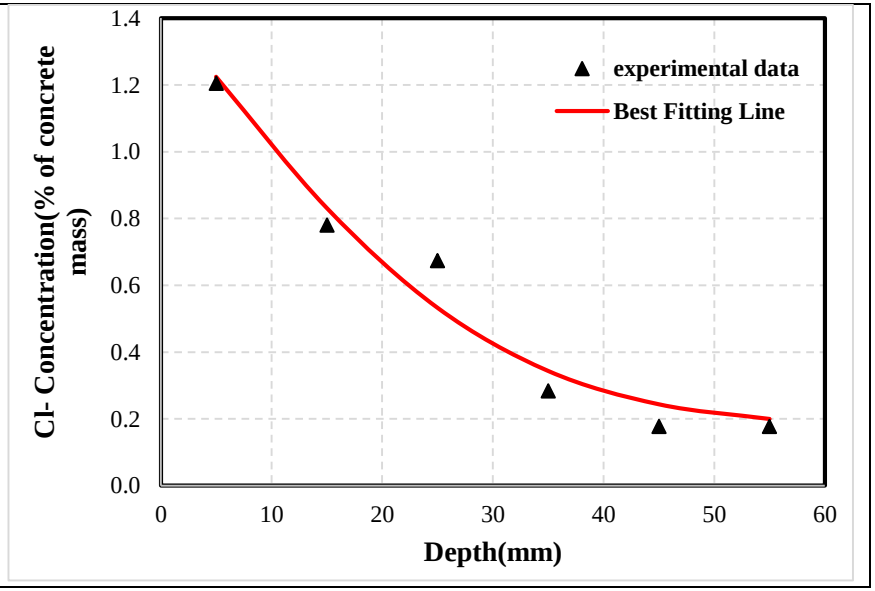

APPENDIX-A2: Calculation of Chloride diffusion rate (Da) and Chloride accumulation on the Concrete surface

Mixture	C(30,50%)					
Da	2.20E-11					
Cs	1.48	Depth	Cl^-	Estimate from Eq. (3-12)		(Prid-Exper.)^2
Ci	0.177	5	1.3	1.377		0.000917473
		15	1.1	0.918		0.021165055
		25	0.4	0.573		0.021635123
		35	0.4	0.358		9.04314E-06
		45	0.2	0.247		0.004885901
		55	0.2	0.200		0.000520927
					Summation	0.009775869

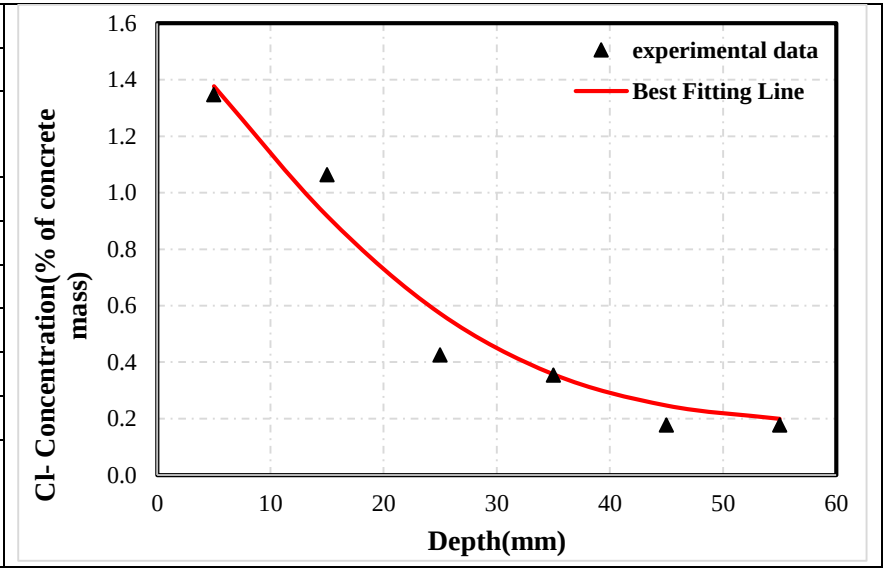

Mixture	C(35,0%)					
Da	2.8E-11					
Cs	1.58	Depth	Cl^-	Estimate from Eq. (3-12)		(Prid-Exper.)^2
Ci	0.177	5	1.2	1.349		0.020742692
		15	1.0	0.926		0.010494603
		25	0.8	0.597		0.033395004
		35	0.4	0.382		0.000773946
		45	0.2	0.264		0.007524046
		55	0.2	0.209		0.00097656
					Summation	0.073906851

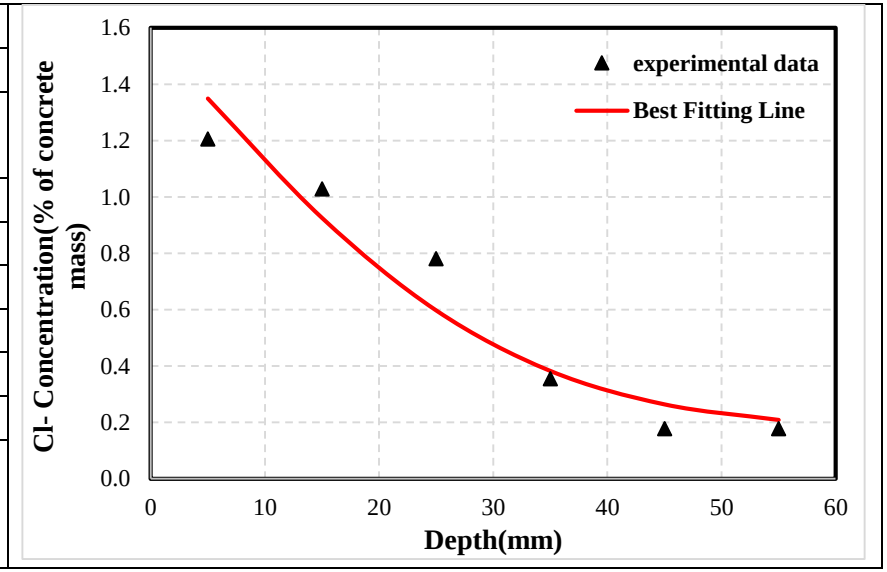

APPENDIX-A2: Calculation of Chloride diffusion rate (Da) and Chloride accumulation on the Concrete surface

Mixture	C(35,25%)					
Da	2.4E-11					
Cs	1.39	Depth	Cl^-	Estimate from Eq. (3-12)		(Prid-Exper.)^2
Ci	0.177	5	1.1	1.175		0.001635257
		15	0.9	0.785		0.0102345
		25	0.4	0.495		0.011102569
		35	0.3	0.319		1.21282E-05
		45	0.2	0.230		0.002806883
		55	0.2	0.194		0.000267081
					Summation	0.026058419

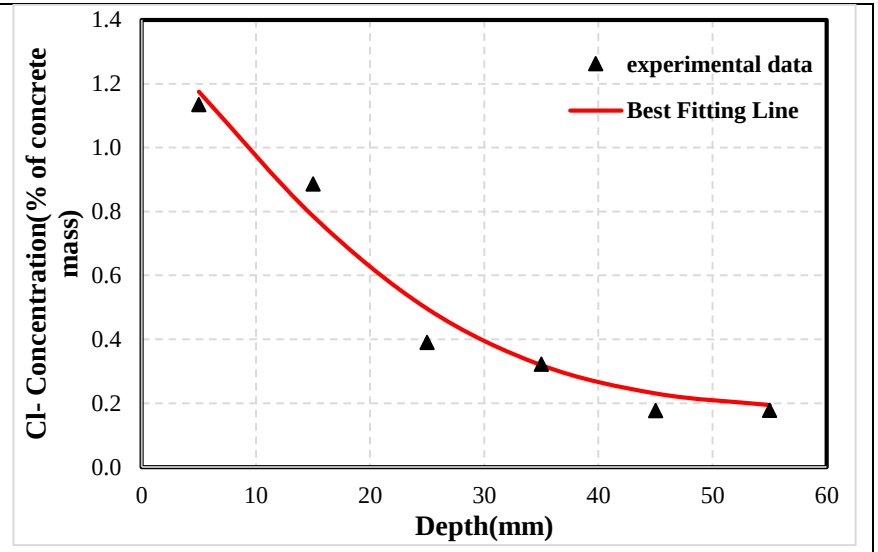

Mixture	C(35,50 %)					
Da	1.8E-11					
Cs	1.36	Depth	Cl^-	Estimate from Eq. (3-12)		(Prid-Exper.)^2
Ci	0.177	5	1.1	1.118		0.003011293
		15	0.8	0.695		0.007286391
		25	0.4	0.408		0.00291064
		35	0.3	0.260		0.003504701
		45	0.2	0.200		0.000551235
		55	0.2	0.182		2.46695E-05
					Summation	0.01728893

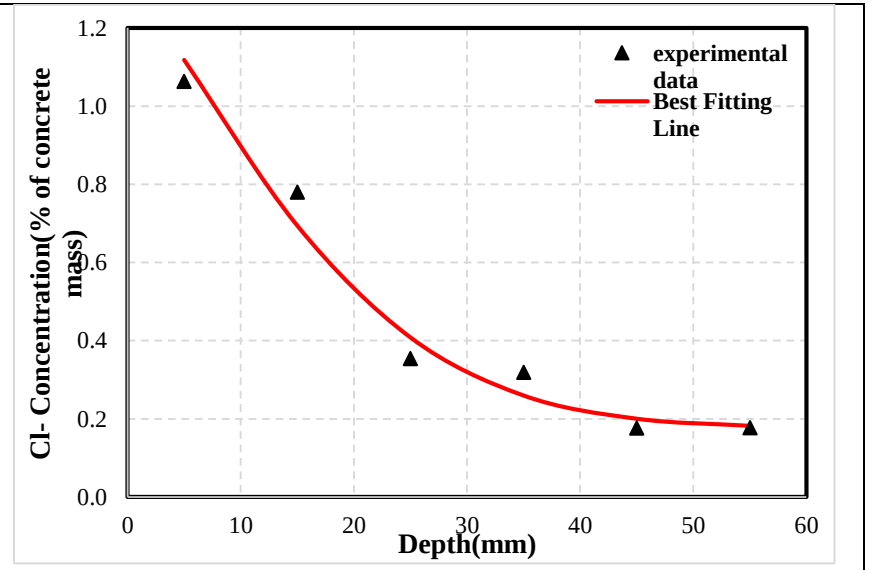

APPENDIX-A2: Calculation of Chloride diffusion rate (Da) and Chloride accumulation on the Concrete surface

Mixture	C(40,0%)					
Da	2.50E-11					
Cs	1.63	Depth	Cl^-	Estimate from Eq. (3-12)		(Prid-Exper.)^2
Ci	0.177	5	1.3	1.377		0.000917473
		15	1.1	0.918		0.021165055
		25	0.4	0.573		0.021635123
		35	0.4	0.358		9.04314E-06
		45	0.2	0.247		0.004885901
		55	0.2	0.200		0.000520927
					Summation	0.049133523

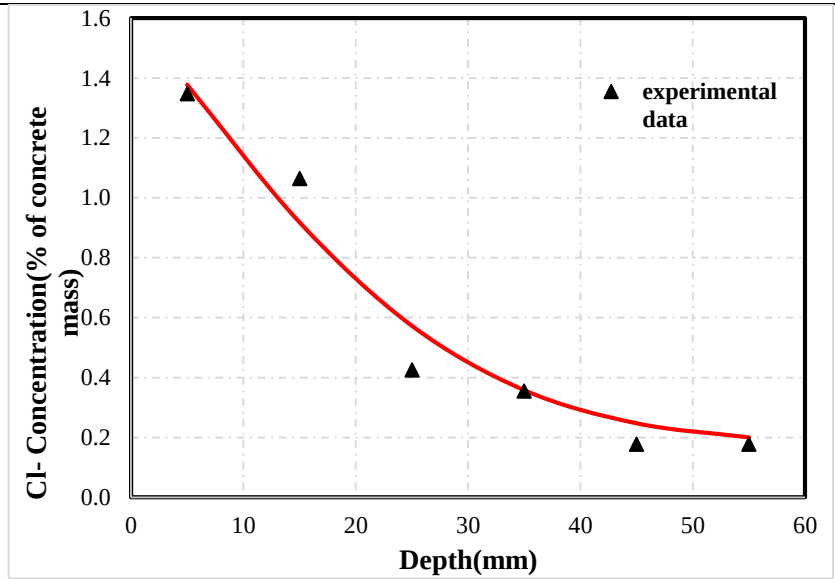

Mixture	C(40,25%)					
Da	2.40E-11					
Cs	1.48	Depth	Cl^-	Estimate from Eq. (3-12)		(Prid-Exper.)^2
Ci	0.177	5	1.1	1.249		0.022478596
		15	1.0	0.830		0.016115884
		25	0.5	0.519		0.000164288
		35	0.4	0.329		0.000528195
		45	0.2	0.234		0.003238855
		55	0.2	0.195		0.00031794
					Summation	0.007140626

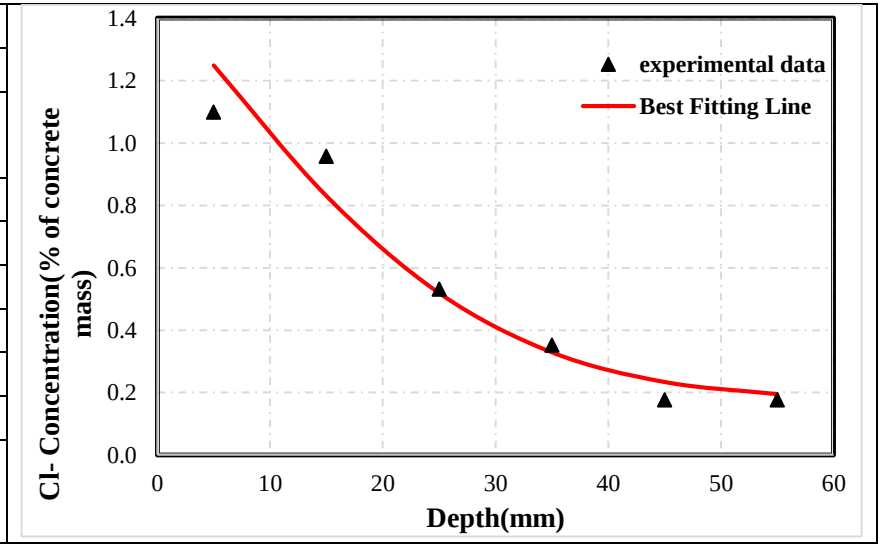

APPENDIX-A2: Calculation of Chloride diffusion rate (Da) and Chloride accumulation on the Concrete surface

Mixture	C(40,50%)					
Da	1.70E-11					
Cs	1.32	Depth	Cl^-	Estimate from Eq. (3-12)		$(Prid-Exper.)^2$
Ci	0.177	5	1.0	1.080		0.007627506
		15	0.9	0.662		0.050295958
		25	0.2	0.386		0.019050632
		35	0.3	0.248		0.001253245
		45	0.2	0.196		0.000357429
		55	0.2	0.181		1.50705E-05
					Summation	0.013099973

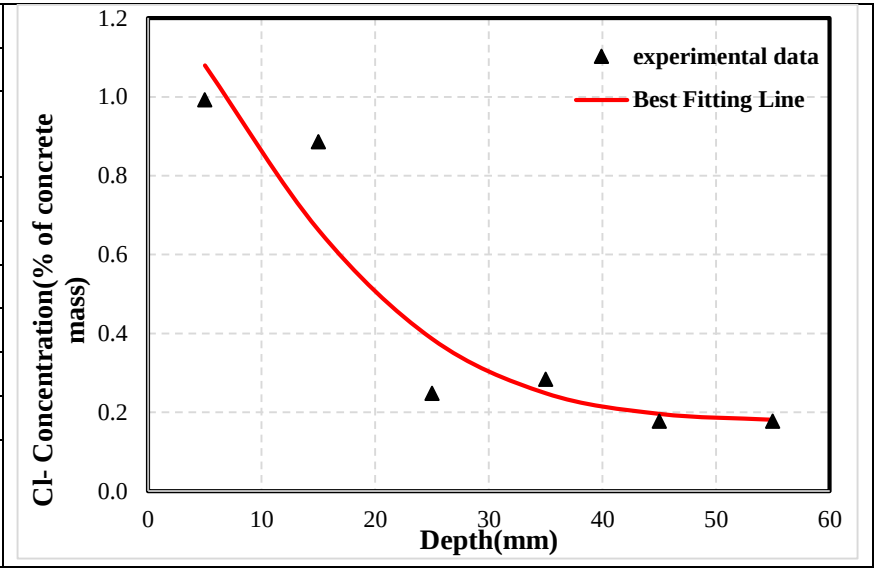

Mixture	C(55,0%)					
Da	2.3E-11					
Cs	1.3	Depth	Cl^-	Estimate from Eq. (3-12)		$(Prid-Exper.)^2$
Ci	0.177	5	1.0	1.097		0.004698199
		15	0.9	0.730		0.036872796
		25	0.3	0.460		0.031234524
		35	0.4	0.299		0.003035527
		45	0.2	0.221		0.00195223
		55	0.2	0.190		0.000175204
					Summation	0.07796848

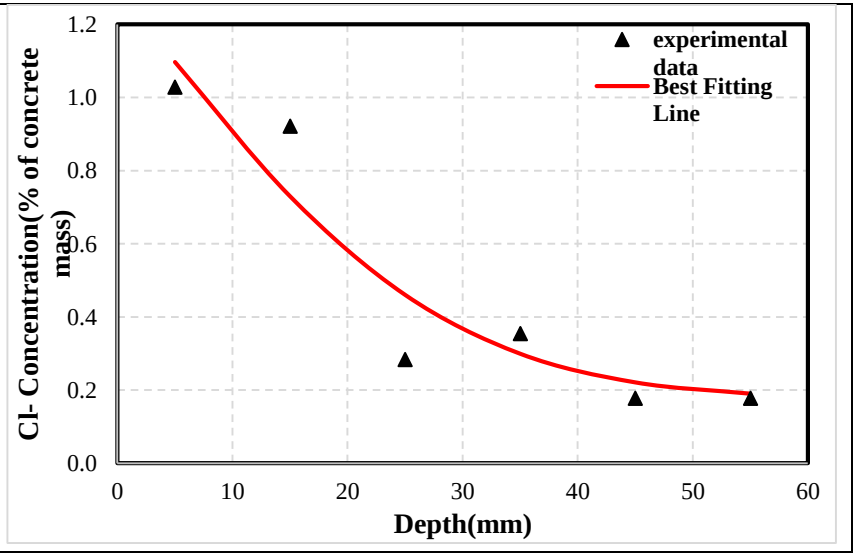

APPENDIX-A2: Calculation of Chloride diffusion rate (Da) and Chloride accumulation on the Concrete surface

Mixture	C(55,25%)					
Da	1.8E-11					
Cs	1.28	Depth	Cl^-	Estimate from Eq. (3-12)		$(Prid-Exper.)^2$
Ci	0.177	5	1.0	1.055		0.00951919
		15	0.9	0.660		0.036581713
		25	0.4	0.393		0.001466713
		35	0.3	0.254		0.000861579
		45	0.2	0.199		0.000479202
		55	0.2	0.182		2.37195E-05
					Summation	0.048932117

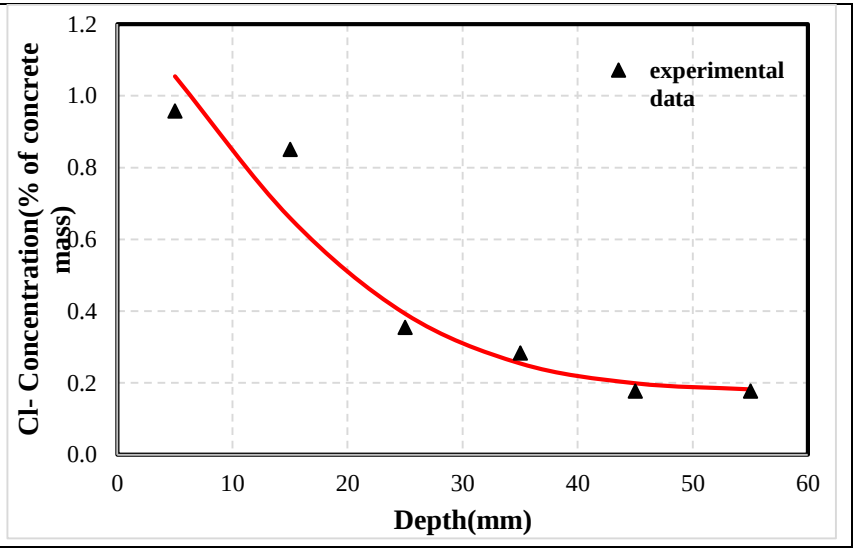

Mixture	C(55,50%)					
Da	1.8E-11					
Cs	1.16	Depth	Cl^-	Estimate from Eq. (3-12)		$(Prid-Exper.)^2$
Ci	0.177	5	0.9	0.959		0.005325299
		15	0.7	0.607		0.018881542
		25	0.3	0.369		0.007348154
		35	0.2	0.246		5.3202E-06
		45	0.2	0.197		0.000380605
		55	0.2	0.181		1.88392E-05
					Summation	0.031959758

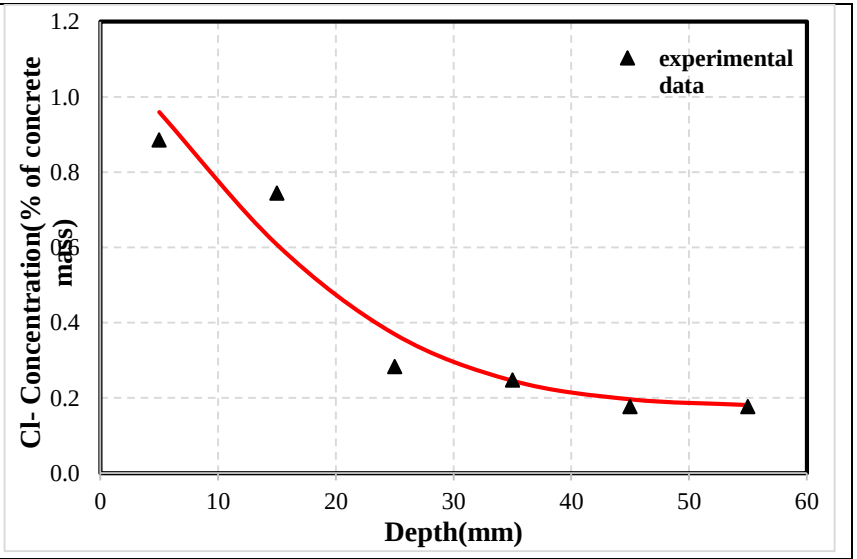

الخلاصة

يعتبر الاحتباس الحراري مشكلة خطيرة تهدد العالم ومستقبل الحياة البشرية. يعتبر قطاع البناء من بين المصادر الرئيسية لانبعاثات الكاربون، وتساهم صناعة السمنت بشكل كبير في هذه الانبعاثات. لذلك، تُعَدُّ الخرسانة منخفضة الكربون (LCC) حلاً لتقليل انبعاثات ثاني أكسيد الكربون خلال عملية تصنيعها.

تقوم الصناعة العالمية لمواد البناء بتطوير أدوات وقواعد بيانات ومنهجيات لتقدير كمية الانبعاثات المتجسدة من ثاني أكسيد الكربون (eCO_2) في المباني وتطوير استراتيجيات للحد منها. حيث يستهلك قطاع البناء حوالي 40٪ من الطاقة العالمية ويُسهم بحوالي 30٪ من انبعاثات الغازات الدفيئة (GHG) .

تمت دراسة مقاومة الانضغاط وسرعة الذبذبات فوق الصوتية وانكماش الجفاف لمختلف الخلطات الخرسانية في أعمار مختلفة (28، 56 و90 يومًا) لتقييم تأثير استبدال السمنت بخبث افران الصهر العالية (GGBS) على الخواص الفيزيائية والميكانيكية للخرسانة. تمت دراسة خصائص الخرسانة المتصلدة مثل امتصاص الماء والمسامية وعمق اختراق الكلوريد وتركيز الكلوريد وتآكل حديد التسليح لتقييم ديمومة ومتانة هذه الأنواع من الخرسانة وتحديد العلاقة بين مقاومة اختراق أيون الكلوريد ومقاومة التآكل والنسبة المثلى للخلطات الخرسانية.

في هذه الدراسة، تم اختيار خمسة عشر خلطة مختلفة من خلال صب مكعبات 100 ملم ، واسطوانة بقطر100 ملم وارتفاع 200 ملم لقياس مقاومة الانشطار ، واسطوانة قصيرة (100 × 50) ملم لاختبار مقاومة هجرة ايون الكلوريدات ، وقوالب موشورية (100 × 100 × 400) ملم مسلحة بحديد تسليح قطر 10 ملم لاختبار التآكل المعجل باستخدام التيار الكهربائي.

أظهرت النتائج أن الخلطة ذات المقاومة 35 ميجا باسكال تستهلك الحد الأدنى من ثاني أكسيد الكربون المتجسد (eCO_2) مقارنةً بالخلطات الأخرى. أيضًا، أظهرت النتائج انخفاضًا في خصائص الخرسانة الطرية، مثل قابلية التشغيل، مع زيادة نسبة GGBS في الخلطة. تم اختبار خصائص الخرسانة المتصلدة مثل مقاومة الانضغاط والانشطار وسرعة انتقال الموجات فوق الصوتية وانكماش التجفيف. بشكل عام، زيادة نسبة استبدال GGBS تحسن

معظم الخصائص باستثناء انكماش الجفاف، حيث سجلت الخلطات التي تحتوي على نسبة عالية من GGBS قيمًا أعلى لهذا الفحص.

أما بالنسبة لخصائص الديمومة، مثل امتصاص الماء والمسامية وهجوم الكلوريد وعمق اختراق الكلوريد وتركيز الكلوريد وتآكل حديد التسليح، فكانت النتائج غير متساوية. وجد أن مقاومة اختراق الكلوريد تزداد مع زيادة مقاومة الانضغاط ونسبة GGBS بشكل عام، ولكن هذا العلاقة لم تنطبق على جميع الخلطات الأخرى. على سبيل المثال، وجد أن العينات ذات المقاومة 35 ميجا باسكال التي تحتوي على نسبة 50٪ من GGBS تظهر نفس مقاومة اختراق الكلوريد للعينات ذات المقاومة 55 ميجا باسكال التي تحتوي على نفس نسبةGGBS . وعمومًا، ترتفع مقاومة التآكل عادةً مع زيادة مقاومة الانضغاط ونسبة GGBS . ولكن هذا لم يكن صحيحًا بالنسبة لجميع العينات، حيث وجد أن العينات التي تحتوي على 35 ميجا باسكال ونسبة 25٪ من GGBS كانت أكثر مقاومة لاختراق أيون الكلوريد من العينات التي تحتوي على 55 ميجا باسكال ونفس نسبة.GGBS

تشير نتائج هذه الدراسة إلى إن الديمومة الجيدة يمكن تحقيقها ليس فقط بزيادة المقاومة بل ممكن الحصول على ديمومة عالية من خلال زيادة فعالية الخبث مع السمنت من خلال تحقيق بنية عالية ومقاومة لاختراق العناصر العدائية مثل الكلوريدات.

جمهورية العراق
وزارة التعليم العالي والبحث العلمي
جامعة بابل
كلية الهندسة
قسم الهندسة المدنية

الخصائص الميكانيكية والديمومة للخرسانة منخفضة الكاربون الحاوية على مسحوق خبث الافران العالية

رسالة مقدمة الى كلية الهندسة في جامعة بابل كجزء من متطلبات نيل درجة الماجستير في الهندسة – الهندسة المدنية – المواد الانشائية

من قبل:

شهد صباح عبد الله جابر

إشراف

أ.د. عباس سالم عباس الاميري

أ.د. سهيلة غازي مطر

2023م **1444ه**